THE NATURE OF BONDING OF SOLUTES ON MONTMORILLONITE SURFACES

by KENNETH SHYAN-ELL SU

(Under the supervision of Associate Professor
Jens Thurø Carstensen)

Adsorption of drugs on solids is an important subject in the pharmaceutical areas both as a technique (taste masking, stability) and a phenomenon (physiological availability, compression characteristics). In the capacity of taste masking, it is unusual that several very bitter substances can be rendered practically tasteless and yet remain biologically available upon oral ingestion. It appears that the bonding force is sufficiently strong and of such a nature that taste is masked; nevertheless desorption takes place in the stomach.

The study reported here deals with the possible nature of bonding in such adsorbates. Montmorillonite is a layer like aluminum magnesium silicate allowing ion or molecule attachment either by surface, edge or intercalation adsorption. Preliminary investigations along this line have shown that benzoic acid is adsorbed from anhydrous solvents onto montmorillonite surface (and does not penetrate the crystal lattice of the clay); it was found that the number of sites on the surface for such adsorption was of the order $10^{19} \sim 10^{20}$ per gm of montmorillonite.

With this knowledge it is possible to further study the nature of the interaction. In order not to confound the overall approach, substances have been selected which are not ionized in aqueous (or other) solutions, so that the adsorption will not be possible via ion exchange. Isotherms of diazepam in several solvents and isotherms of a series of benzodiazepine derivatives in one solvent were conducted and Langmuir isotherms prevailed for solvents with dielectric constants of less than 20. It has shown that the number of sites on the surface are of comparable magnitude (of the order of 10^{19} sites per gram) with results from B.E.T. measurements. Adsorption isotherms were also determined from solvents with dielectric constants higher than 25. Linear isotherms are, here, achieved when adjustment for solvent intercalation is made.

At an early point in the investigation, it became clear that the adsorption from anhydrous solvents was the stronger the smaller the dielectric constant. The higher the dielectric constant of a solvent the larger the extent of its intercalation. The general trend, therefore, is indicative of forces of electrical nature being of significance, the dielectric constant being one of the main parameters. The benzodiazepine derivatives under investigation possess dipole moments, and if the forces involved in the adsorption are electrical forces between

surface ions and the solute dipoles, then the forces can be formulated mathematically and the pertinent relations can be tested experimentally in a systematic fashion.

Consistent values have been arrived at by two different procedures with respect to the types of isotherms and the equilibrium value at infinite dielectric constant. A consistent relation has been found between dipole moment and equilibrium distance. All these facts are based on a model whereby the solute molecule, which is not ionized, but which possess a dipole moment, is bound to the surface oxygen ions by an ion dipole interaction, and it seems reasonable to postulate that the data support such a model.

APPROVED ~~[illegible]~~ Jesse Thomas Carteman

DATE 6/2 - 1971

THE NATURE OF BONDING OF SOLUTES ON MONTMORILLONITE SURFACES

by

KENNETH SHYAN-ELL SU

A thesis submitted in partial fulfillment of the requirements for the degree of

DOCTOR OF PHILOSOPHY
(Pharmaceutics)

at the

UNIVERSITY OF WISCONSIN

1971

ACKNOWLEDGEMENTS

I wish to take the liberty to express my very sincere appreciation to Professor Jens T. Carstensen for his untiring efforts on my behalf during the course of this study as well as in the preparation of this manuscript. His inspiration and encouragement and his genuine interest have been crucial from the very inception of my graduate career. In addition, I have been enriched from my close association with him both as a person and as a scholar.

I also gratefully acknowledge the financial support rendered by the Wisconsin Alumni Research Foundation and partially by Hoffmann-La Roche, Inc., N.J. and R. T. Vanderbilt Company, Inc., N.Y.

TO

My wife, Chu-Chu,

and

my parents,

for their love,

encouragement and

understanding.

TABLE OF CONTENTS

TABLE OF CONTENTS - Cont.

LIST OF TABLES

LIST OF FIGURES

LIST OF FIGURES - Cont.

LIST OF FIGURES - Cont.

Table IV—Value of A_1, A_2, ω_1, and ω_2 as a Function of Viscosity and Tube Diameter

Glycerin, % v/v	Viscosity, poises	Radius, cm.	A_1, cm. ±10%	ω_1, hr.$^{-1}$ ±10%	A_2, cm. ±6%	ω_2, hr.$^{-1}$ ±1%
0	0.0089	1.23	4.9	0.42	24.1	0.0276
0	—	1.86	10.3	0.38	16.0	0.0260
0	—	2.30	10.2	0.29	18.7	0.0242
0	—	2.77	8.2	0.13	20.0	0.0229
5	0.0105	1.23	6.0	0.41	31.2	0.0248
5	—	1.86	9.3	0.38	31.3	0.0230
5	—	2.30	10.0	0.31	20.5	0.0220
5	—	2.77	9.8	0.29	18.6	0.0202
10	0.0120	1.23	7.1	0.38	41.0	0.0216
10	—	1.86	9.6	0.30	19.3	0.0197
10	—	2.30	8.6	0.33	17.4	0.0190
10	—	2.77	8.8	0.15	20.0	0.0175

Table V—Slopes and Intercepts from Figs. 6 and 7

Line	Fig.	Slope (ζ/2.3), cps.$^{-1}$	Slope (μ/2.3), cm.$^{-1}$	Intercept	log [θ/Γ]
R = 1.23 cm.	7	−0.36		0.77	0.84–2[a]
R = 1.86 cm.	7	−0.40		0.78	0.88–2[a]
R = 2.30 cm.	7	−0.35		0.70	0.82–2[a]
T = 2.77 cm.	7	−0.39		0.71	0.86–2[a]
η = 0.89 cps.	6		−0.054	0.51	0.88–2[b]
η = 1.05 cps.	6		−0.057	0.46	0.85–2[b]
η = 1.20 cps.	6		−0.057	0.40	0.84–2[b]

[a] Based on an average value of μ/2.3 = 0.055. [b] Based on an average value of ζ/2.3 = 0.37.

two figures show acceptably good agreement, especially considering that they have been obtained from extrapolated figures (intercepts).

This fact in combination with the linearity of the plots in Figs. 6 and 7, the closeness of the values of the slopes, and the adherence of all the data to an equation of the type of Eq. 8 lends credence to the views presented here.

It should be mentioned, qualitatively, that increasing concentrations tend to decrease (or mask) the values of A_1, and that this parameter eventually is of such small magnitude that it can no longer be detected within experimental error. In the same vein, H_0 becomes larger with increasing solids content and, eventually, at a critical concentration the initial constant-density plug phase will disappear, and at a second critical concentration, the A_1-term will disappear. The entire sedimentation pattern will then be a simple logarithmic decay curve. The critical concentration for kaolin in 10% v/v glycerin in a tube of 2.5-cm. i.d. is 8–10 w/v percent. Data of this nature have been reported occasionally in literature in the past, the data by Haines and Martin (6) being a notable example.

The final height, H_u, as reported here, may still be subject to some decrease by consolidation processes such as described by Ratcliff (23, 24). This phase has not been a subject of this investigation.

SUMMARY

The sedimentation of flocculated suspensions takes place in successive stages; the sedimentation phase following the initial phase has been studied and found, based on consideration of the forces involved, to be confined to follow the following equation: $[x - H_u] = A_1e^{-\omega_1\tau} + A_2e^{-\omega_2\tau}$. Experimental data have supported the presented concepts and suggest that the frictional term in the equation of motion is of the form $B(\eta,R) = \Gamma \cdot e^{\mu R}e^{\zeta\eta}$.

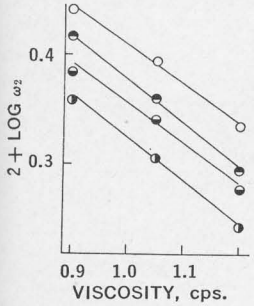

Figure 7—*Plot of the logarithm of the smaller characteristic root, ω_2, as a function of viscosity. Key: ○, 2.46-cm. i.d. tube; ◓, 3.72-cm. i.d. tube; ◒, 4.60-cm i.d. tube; and ◑, 5.54-cm. i.d. tube.*

NOMENCLATURE

A, A_1, A_2, A_1', A_2'	= preexponential factors in descent of sedimentation boundary
$B(\eta,R)$	= viscosity dependent component of frictional force
C^*	= preexponential factor for radial dependence of ω_2
g	= gravitational acceleration
H_0	= critical height
M	= mass of sediment
r	= radius of floc
R	= radius of tube
t	= time measured from start of sedimentation
t_0	= critical time
x	= height of sedimentation boundary above bottom of tube
y	= distance of sedimentation boundary from critical height (= $H_0 - x/2$)
y_∞,y^*	= y-value at infinite time (= $H_0 - H_u/2$)
$\psi(R)$	= viscosity independent component of frictional force
ρ_0	= density of fluid
ρ	= density of suspended solid
τ	= time measured from critical time (= $t - t_0$)
μ	= exponential factor to radial dependence of ω_2
Γ	= preexponential factor to radial dependence of ω_2
θ	= dimensional factor in electrical repulsion term
ζ	= exponential factor to viscosity dependence of ω_2
ω, ω_1, ω_2	= exponential decay constants in descent of sedimentation boundary

REFERENCES

(1) J. T. Carstensen and K. Su, *J. Pharm. Sci.*, **59,** 666(1970).
(2) R. Stokes, *Proc. Cambridge Phil. Soc.*, **9,** 5(1856).
(3) G. Kynch, *Trans. Faraday Soc.*, **48,** 166(1952).
(4) H. Steinour, *Ind. Eng. Chem.*, **36,** 840(1944).
(5) *Ibid.*, **35,** 901(1944).
(6) B. A. Haines, Jr., and A. N. Martin, *J. Pharm. Sci.*, **50,** 228 (1961).
(7) C. S. Robinson, *Ind. Eng. Chem.*, **18,** 869(1926).

[Reprinted from the Journal of Pharmaceutical Sciences,
Vol. 59, No. 5, May, 1970. ©1970 by the American Pharmaceutical Association]

Sedimentation Kinetics of Flocculated Suspensions I: Initial Sedimentation Region

J. THURØ CARSTENSEN* and KENNETH S. E. SU

Abstract □ Depending on the concentration of a suspension, it will exhibit one of three sedimentation patterns pertaining to low, intermediate, and high concentrations of solids, respectively. Of these, only the dilute region has been thoroughly investigated in the past from a theoretical and experimental standpoint. Pharmaceutical suspensions are mostly of the intermediate type. It is shown here that if the models by Kynch, Michaels, and Bolger pertain, and if the sedimented cake experiences an exponential compaction from the onset, experimental data are consistent with theory and lead to the relation: $x = x_0 \exp[-kt] + C \cdot [1 - \exp(-kt)] \cdot \exp[-\omega t]$, where k is a sedimentation rate constant pertaining to a constant density plug, and ω is a sedimentation rate constant pertaining to the cake. It has also been found that, empirically, the sedimentation heights in the initial stage may be presented by the relation: $[x_0^2 - x^2] = \beta t$, where x denotes height, and t time.

Keyphrases □ Sedimentation kinetics—flocculated suspensions □ Kinetic equations—suspension sedimentation □ Suspensions, flocculated—sedimentation cakes □ Viscosity effect—suspension cake concentrations

Stokes's law has been known for over a century (1) but, nevertheless, as pointed out by Kynch (2), a satisfactory theory of sedimentation of multiparticle, coarse suspensions has never been put forth. Although it might appear that sedimentation should follow Stokes's law, Higuchi (3) and Hiestand (4) have shown that both in peptized and flocculated systems such a simple point of view is in agreement with neither theory nor fact. In most of the investigations reported in the past, attempts have been made to modify Stokes's law in some way (5–9) to account for sedimentation behaviors. The more dilute a suspension is, the more closely should the fall of each particle or floc adhere to Stokes's law. Pharmaceutical suspensions are, however, rarely very dilute, and their behavior would not be expected to fall in this category.

Michaels and Bolger (10) have reported a linear pattern for sedimentation rates for dilute suspensions (<1%). These authors, as well as Haines and Martin (7), point to the fact that very concentrated suspensions follow yet another pattern, a fact that will not be a point of discussion here but will be reserved for a subsequent study (11). Suspensions of "intermediate" concentration, however, have a downward curvature, *i.e.*, the sedimentation boundary moves downward with greater and greater velocity until a certain critical height, H_0, is reached, at which time (t_0) the rate decreases abruptly.

Examples of this pattern may be found described occasionally in pharmaceutical literature, the work by Benedict *et al.* (12) being an example. Pharmaceutical suspensions are mostly of the intermediate type. They, also, are of the floc-aggregate type described by Michaels and Bolger (10), and the considerations in the following apply to this type system.

Robinson (8) considered the sediment to be of uniformly increasing concentration during the descent of the boundary; Ward and Kammermeyer (9) showed that the ensuing equations apply only to special systems. Michaels and Bolger (10) and Gaudin and Fuerstenau (13, 14) have, furthermore, demonstrated that the density of the sediment remains constant at and for some (time-dependent) distance below the boundary, with a cake of higher density building up at the bottom, and that, therefore, the system is uniform at time zero only. The terms cake and sediment will be used for these two phases in the following. These views correlate with the simplest of the models proposed by Kynch (2).

From a pharmaceutical point of view, it is important to determine the pattern (and predict ultimate heights) of suspension sedimentation. It is one of the objectives of this communication to establish graphical means of describing the descent of the sedimentation boundary in the initial stage, *i.e.*, prior to the critical height, H_0. Another objective is to attempt to correlate the initial sedimentation pattern with existing views on the sedimentation process and arrive at a general equation for the initial sedimentation of flocculated suspensions in the intermediate concentration range.

EXPERIMENTAL

The system used here is the same as that employed by Michaels and Bolger (10) except that concentrations are higher. At higher concentrations, air entrapment might be a source of variation, and an apparatus such as shown in Fig. 1 was used. Previous investigators of dilute suspensions (8) have pointed out that initial turbulence was a source of variation, without spelling out the extent of this variation. The method of providing a uniform starting suspension used here was the same as that employed by Michaels and Bolger (10) (turning the tube end-over-end 10 times). This, of course, causes initial turbulence; the extent to which this affected results was gauged by performing each experiment at least three times.

The size of aggregates is a dynamic property and forming the aggregate under high shear (Waring blender) will not necessarily give a representative floc-aggregate (10) in the sense that the size will subsequently remain constant during settling. Some experiments were, therefore, conducted by allowing a mildly agitated suspension to equilibrate. The sedimentation experiment was repeated until the curves were reproducible. This appeared to require about 24 hr. Reproducible curves all show the convexity noted in the top curve of Fig. 2. Where suspensions were made in a blender, they were also checked on succesive days until the sedimentation rates had changed to a constant value.

The general procedure used, then, was as follows: 25 g. of colloidal kaolin NF[1] was rinsed with 500 ml. of water which had previously been distilled over potassium permanganate. The volume was then adjusted to 500 ml. and the suspension transferred to a tube of the type shown in Fig. 1. The suspension was thoroughly deaerated by applying aspirator vacuum to one of the outlets of the two-way stopcock. The tube was occasionally turned end-over-end, and finally after no more visible escape of air, the tube was turned end-over-end 10 times, then opened to the atmosphere and placed vertically; the movement of the interface was followed by use of a high precision cathetometer[2] and an electric timer. After 24 hr., the

[1] Merck and Co., Log No. 781603-62325, Rahway, N. J.
[2] Gaertner Scientific Corp., Chicago, Ill.

(9) A. S. Michaels and J. C. Bolger, *Ind. Eng. Chem. Fundam.*, **1,** 24(1962).

(10) A. M. Gaudin and M. C. Fuerstenau, *Eng. Mining J.*, **159,** 110(1958).

(11) A. M. Gaudin and M. C. Fuerstenau, *Int. Mining Proc. Congr.*, London, England, Apr. 1960.

(12) A. M. Gaudin, M. C. Fuerstenau, and S. R. Mitchell, *Mining Eng. (London)*, **11,** 613(1959).

(13) C. B. Egolf and W. L. McCabe, *Trans. Amer. Inst. Chem. Eng.*, **33,** 620(1937).

(14) J. deBoer, *Advan. Colloid Interface Sci.*, **3,** 21(1950).

(15) F. London, *Z. Phys.*, **63,** 245(1930).

(16) B. Deryagin, A. Titijevskaia, I. Abriscova, and E. Lifshitz, *Discuss. Faraday Soc.*, **18,** 24(1954).

(17) B. Deryagin, I. Abriscova, and E. Lifshitz, *Quart. Rev. (London)*, **10,** 295(1956).

(18) E. Verway and J. Overbeek, "Theory of the Stability of Lyophobic Colloids," Elsevier, Amsterdam, The Netherlands, 1948.

(19) V. Vand, *J. Phys. Colloid Chem.*, **52,** 277(1948).

(20) C. R. Wylie, Jr., "Advanced Engineering Mathematics," McGraw-Hill, New York, N. Y., 1960, p. 177.

(21) C. M. Metzler, APhA Academy of Pharmaceutical Sciences, 5th National Meeting, Washington, D. C., November 20, 1968.

(22) J. T. Carstensen, J. B. Johnson, D. C. Spera, and M. J. Frank, *J. Pharm. Sci.*, **57,** 23(1968).

(23) G. A. Ratcliff, D. A. Blackader, and D. N. Sutherland, *Chem. Eng. Sci.*, **22,** 201(1967).

(24) G. A. Ratcliff, *J. Colloid Interface Sci.*, **25,** 586(1967).

(25) W. Higuchi and R. G. Stehle, *J. Pharm. Sci.*, **54,** 265(1965).

(26) T. Gillespie, *J. Phys. Chem.*, **66,** 1077(1962).

(27) T. Gillespie, *J. Colloid Sci.*, **15,** 219(1960).

(28) C. F. Goodeve, *Trans. Faraday Soc.*, **35,** 342(1939).

ACKNOWLEDGMENTS AND ADDRESSES

Received August 21, 1969, from the *School of Pharmacy and Extension Services in Pharmacy, University Extension, University of Wisconsin, Madison, WI 53706*

Accepted for publication November 14, 1969.

This investigation was supported by grants from R. T. Vanderbilt Co., New York, NY 10017 and Hoffmann-La Roche, Inc., Nutley, NJ 07110

* To whom requests for reprints should be addressed.

Nature of Bonding in Montmorillonite Adsorbates I: Surface Adsorption

J. THURØ CARSTENSEN* and KENNETH S. E. SU

Abstract □ It has been shown that organic solutes that do not have groups which are cation exchangeable adsorb on the surface of neutralized montmorillonite and do not (unlike several solvents such as alkanols and water) penetrate to the interior of the crystal. The number of available sites on the surface is of the order 10^{18}–10^{19} sites per m.^{2} of surface area. The number of interior sites available is about 600 times as high. The fact that surface adsorption is the process involved explains in part the fact that such adsorbates are physiologically available when used in pharmaceutical preparations.

Keyphrases □ Montmorillonite adsorbates—bonding nature □ Bonding nature—montmorillonite adsorbates □ Benzoic acid adsorption—montmorillonite □ Moisture isotherm—montmorillonite □ Particle-size determination—montmorillonite

MacEwan (1) showed by X-ray studies that some clays, including montmorillonite, have a micalike structure, being built up in layers; the interlaminar distance is large, and layers are held together by second-order forces. The interlaminar distance in montmorillonite can vary from 10 to 20 Å or even more, depending on its water content. Bradley *et al.* (2) showed that these water molecules form layers about 3 Å thick, whereas the thickness of the aluminum silicate framework is 9.6 Å (3). The distance in dehydrated montmorillonite can be more than 9.6 Å, due to the presence of various cations; according to Hendricks (4), these cations place themselves in the same fashion as do the water molecules. Mering (5) showed that the structure of montmorillonite (Fig. 1) is one of a repeating unit of $[Al_{2-x}Mg_x, Si_{4-y}Al_y, O_{10}(OH)_2]$ where $(x + y)$ represents the negative charge; this is compensated for by cations which position themselves on the crystal surface and, hence, are exchangable. In "neutralized" species[1], this cation is H^+.

MacEwan (1) pointed out that water can be replaced by organic molecules. He showed that the number of layers of organic solvent molecules present between silicate layers is zero for heptane; one for heptanol, ethylenediamine, and 1-propanol; two for 1,2-propanediol, ethanol, ethylene glycol, methanol, and acetone; and three for acetonitrile. This type of work has been extended and verified in many subsequent publications (6–10). Studies of this type have most frequently been conducted by exposing the montmorillonite to the organic vapor and measuring the change in crystal spacing.

MacEwan and Talib-Uddin (11), in the case of α-zinc hydroxide, showed that the sodium salt of 1-hydroxy-2,4-dinitro-7-naphthalenesulfonic acid "adsorbed" by placing itself in the interlaminar positions. Wai and Banker (12) showed that, for many organic

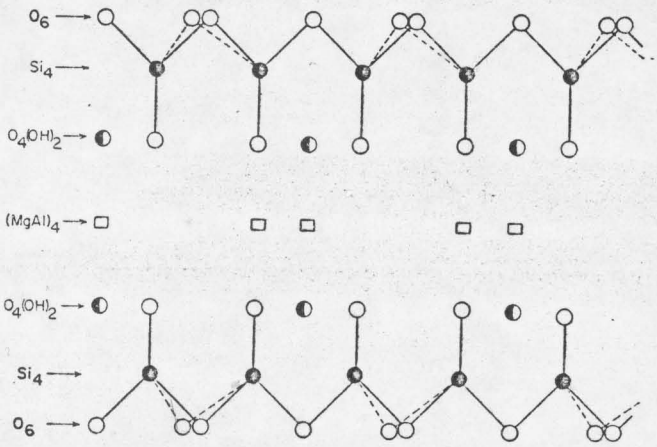

Figure 1—*Structure of montmorillonite according to Mering (5).*

compounds, adsorption on montmorillonite, which is not neutralized, is one of ion exchange. Zentner (13) showed that "neutralized" montmorillonite may be employed to make adsorbates which serve the purpose of taste-masking of bitter compounds. These adsorbates are physiologically available (14); it would, therefore, appear that they could not be too strongly adsorbed (*e.g.*, could not be chemisorbed).

In the case of protonized substituted amines (and other protonized compounds), the adsorbates on neutralized montmorillonite are presumably of an ion-exchange nature. In the case of uncharged species, however, this cannot be the process. From the description given, the adsorbates could be either a surface adsorption or they could be brought about by an adsorption of the type described for α-zinc hydroxide, where the organic molecule actually penetrates the crystal.

An investigation of the nature of the bonding involved is presently being conducted by the authors. This preliminary publication directs itself to the question whether, in the case of neutralized montmorillonite, solutes adsorb on the surface only or whether adsorption in the interlaminar space is also taking place.

EXPERIMENTAL AND RESULTS

Mering (5) pointed out that treatment of montmorillonite with mineral acids may give rise to structural changes of the surface. Micronized neutralized montmorillonite[2] was, therefore, used as received from the supplier; the entire study refers to one single lot[2], except where noted. Drying by heat also may cause structural alterations (5), so the montmorillonite was dried by exposure (on a vacuum rack with high vacuum capability) to less than 0.5-μ pressure. After exposure for 7 days, the samples had equilibrium pressures of less than 1 μ Hg. Nevertheless, the samples contained 5.6% structural water, as determined by Karl Fischer titrations.

[1] Veegum Neutral, marketed by R. T. Vanderbilt Co., Inc., New York, NY 10017

[2] Micronized Veegum Neutral, Type S-6814, Lot FX 329, marketed by R. T. Vanderbilt Co., Inc., New York, NY 10017

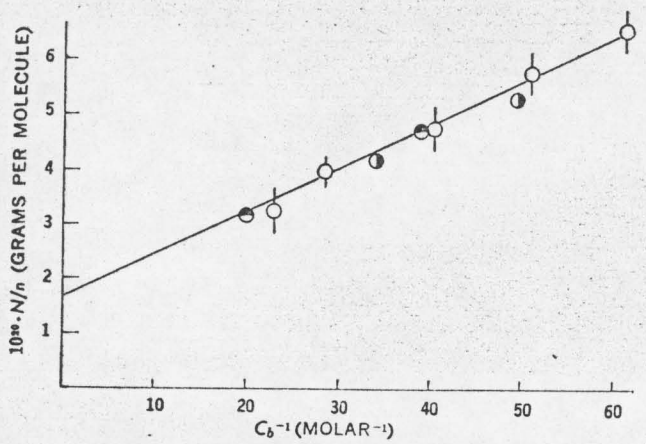

Figure 2—*Benzoic acid isotherm from anhydrous isopropanol. Ordinate represents grams of montmorillonite per molecule of benzoic acid, and abscissa is reciprocal molarity of benzoic acid. Key:* ○, *represents the procedure described in the text;* ◓, *represents pre-extracted montmorillonite (see text); and* ◑, *represents a log of montmorillonite different from the lot used in the main portion of the study. The equation for the line is:* $1/n = 1.67 \cdot 10^{-20} + [8.31 \cdot 10^{-22}/C_b]$.

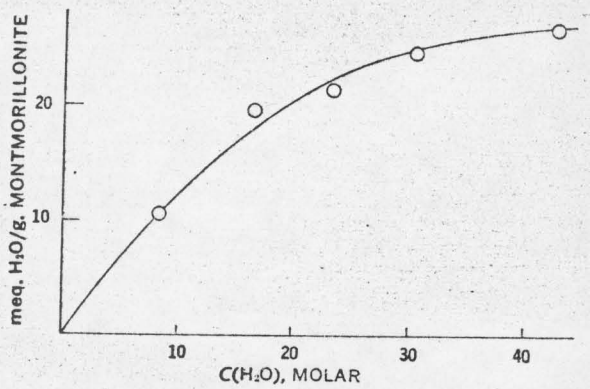

Figure 3—*Moisture isotherm of montmorillonite from aqueous solutions of isopropanol.*

Benzoic acid isotherms were determined by dissolving a weighed amount of benzoic acid in the appropriate solvent. An aliquot was titrated with 0.02 *N* NaOH; another aliquot was exposed to a weighed amount of dried montmorillonite in a sealed conical flask and shaken mechanically at 25° for 48 hr. The sample was then centrifuged, and an aliquot of the supernatant was titrated; the amount adsorbed was determined by difference. A blank sample, containing no benzoic acid, was prepared in a similar fashion and showed zero titer.

Reciprocal plotting of the data yields straight lines, as exemplified in Fig. 2. Since anhydrous solvents (*e.g.*, methanol) have been reported to (and were found to) extract and replace the structural water, the solvent after equlibration contains small amounts of water. One to six grams of montmorillonite was used per 100 ml. of solvent, so the moisture content of the solvent, in reality, would be 60–360 mg./100 ml. To ascertain that this small amount did not affect the results, two runs were made with montmorillonite pre-extracted with solvent. Results from these fall in line with the remaining results (Fig. 2); hence, the effect of the small amount of water is within experimental error. Two runs were made with a different lot of montmorillonite, also giving consistent results (Fig. 2).

Moisture isotherms were performed by exposing 5 g. of montmorillonite to 100 ml. of water–isopropanol mixtures for 3 weeks in sedimentation tubes of 4.2-cm. i.d., of the type described elsewhere (16). The water content of the solvent was determined before and after equilibration by means of Karl Fischer titrations; a plot of moisture content of the montmorillonite as a function of water content of solvent is shown in Fig. 3.

The cross-sectional area of benzoic acid was estimated by molecular model to be 7 Å^2 from a lengthwise direction and 14 Å^2 from the side.

Microscopic examination of the lot of montmorillonite used revealed the majority of particles to be of a 1-2-μ dimension. A few (less than 0.05% by number) were 5–10 μ. A 2-μ cube, employing a density figure obtained by displacement in hexane, results in a calculated surface area of 1 m.^{2}/g. B.E.T. nitrogen isotherms give higher results but may involve not only external, but also internal, laminar surfaces. It is, furthermore, to be expected that the experimental figure is larger than geometrically expected, since the latter is predicated on smooth surfaces and on monodispersity.

Table I—Benzoic Acid Isotherms in Various Solvents

Solvent	Intercept	Sites per Gram
Isopropanol	$1.67 \cdot 10^{-20}$	$6.0 \cdot 10^{19}$
Water–isopropanol (50% w/w)	$2.07 \cdot 10^{-20}$	$4.6 \cdot 10^{19}$
Ethanol	$2.51 \cdot 10^{-20}$	$4.0 \cdot 10^{19}$
Butanol	$2.34 \cdot 10^{-20}$	$4.3 \cdot 10^{19}$
Methanol	$2.01 \cdot 10^{-20}$	$5.0 \cdot 10^{19}$
Average		$4.8 \cdot 10^{19}$
Standard deviation		$0.8 \cdot 10^{19}$

DISCUSSION

Isotherms of benzoic acid and of water on neutral montmorillonite were determined since they give information relative to the number of adsorption sites. If the adsorption of benzoic acid is a competition between solvent (*o*) and benzoic acid (*b*), then the surface fraction covered (θ) is given in terms of the concentrations in solution (C) by (15):

$$\theta_b = \frac{K_b C_b}{1 + K_b C_b + K_o C_o} \qquad \text{(Eq. 1)}$$

If $K_o C_o$ is negligible compared to unity, then (taking reciprocals) this equation becomes:

$$\frac{1}{\theta_b} = 1 + \frac{1}{K_b C_b} \qquad \text{(Eq. 2)}$$

If 1 g. of montmorillonite contains N sites in total, and the number of sites occupied per gram is n (*i.e.*, there are n molecules adsorbed per gram), then $\theta_b = n/N$ is the fractional coverage. If (as is conventionally assumed) the number of sites N equals the saturation value of n for high values of C_b, then $N = n_\infty$ and $\theta_b = n/n_\infty$ is a dimensionless quantity. Equation 2 may be written:

$$\frac{N}{n} = 1 + \frac{1}{K_b C_b} \qquad \text{(Eq. 3)}$$

Since this equation is dimensionless, K_b is in reciprocal concentration units; molarity is used here so this unit is M^{-1}. Equation 3 may be written:

$$\frac{1}{n} = \frac{1}{N} + \frac{1}{K_b N} \cdot \frac{1}{C_b} \qquad \text{(Eq. 4)}$$

so that a plot of the reciprocal of the number of molecules adsorbed per gram of montmorillonite *versus* reciprocal concentration yields an intercept of $1/N$ and an intercept/slope ratio of K_b. These considerations assume that $K_o C_o$ is negligible compared to unity. If $K_o C_o$ is not negligible, then Eq. 4 becomes:

$$\frac{1}{n} = \frac{1}{N} + \frac{[K_o C_o + 1]}{K_b N} \cdot \frac{1}{C_b} \qquad \text{(Eq. 5)}$$

For the benzoic acid isotherms, the concentration of benzoic acid is low, so C_o is practically invariant; reciprocal plotting, therefore, still yields a straight line (Fig. 2) and the intercept still reflects the reciprocal of the number of sites (Eq. 5). However, the intercept-to-slope ratio only yields the value for K_b if the value of $K_o C_o$ is negligible compared to unity.

Figure 2 shows that in the case of isopropanol, the intercept is $1.67 \cdot 10^{-20}$; hence, $N = 6.0 \cdot 10^{19}$. Intercept and N-values for other

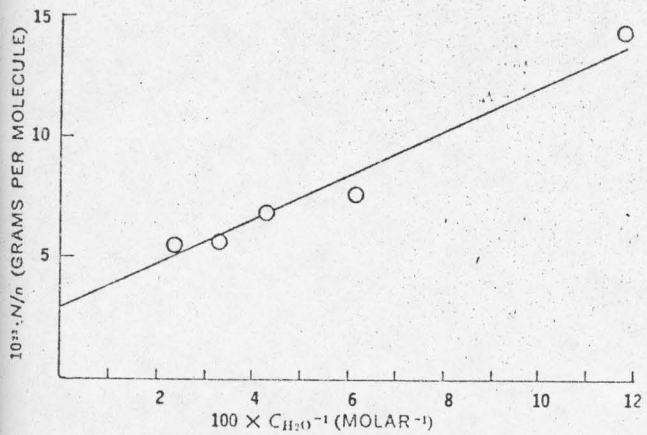

Figure 4—*Langmuir plot of data from Fig. 3. The equation of the line is:* $1/n = 2.86 \cdot 10^{-23} + [9.4 \cdot 10^{-22}/C_{H_2O}]$.

solvents are listed in Table I, and it is seen that these do not differ greatly from solvent to solvent; $N = 4.8 \cdot 10^{19}$ is the average value. From Fig. 2, it is seen (from intercept-to-slope ratio) that, provided $K_o C_o$ is negligible compared to unity, $K_b = 20\ M^{-1}$.

The adherence to a Langmuir plot should preclude multiple-layer adsorption, and estimates of surface area should be possible from saturation data. The benzoic acid molecule has a cross-sectional area of about 10 Å^2, so the surface of the neutral montmorillonite in contact with solution may be estimated at 5 m.^{2}/g., *i.e.*, there are about 10^{19} sites per m.^{2} of surface.

As mentioned in the introduction, solvent (and water) molecules migrate into the crystal space in the montmorillonite. It is, *a priori*, possible that the solute molecules behave likewise (11). If so, then the total number of interstitial and surface sites should be available for adsorption, and the number of sites obtained from a water isotherm should equal that from a benzoic acid isotherm. For this reason, the amount of water removed by montmorillonite from hydroisopropanolic solutions was determined. In this case, the concentration of water in Eq. 5 is represented by C_b, and C_o is concentration of isopropanol. Since C_b in this case is not small and is varied over a large range, C_o is not invariant. If, however, $K_o C_o$ is negligible (compared to unity), Eq. 4 should be obeyed.

A plot of the data is shown in Fig. 3, and plotting according to Eq. 4 is shown in Fig. 4. The linearity of the data in Fig. 4 is good, and the number of sites calculated is $N = 3.5 \cdot 10^{22}$. This is about 600 times larger than the number of sites available for benzoic acid adsorption, and it may be concluded that the adsorption of the latter is strictly a surface phenomenon on the neutralized montmorillonite.

It is important to note that the number of sites available to benzoic acid adsorption does not change appreciably with water content, as seen from Table I; the number of sites calculated from the benzoic acid isotherm in 50% isopropanol equals those obtained in anhydrous isopropanol and other solvents.

Mering (5) showed that three to four monolayers of water are introduced per silicate layer in the intercalation process. He showed that the thickness of these is 3 Å each; the thickness of the silicate layer, as mentioned, is 9.6 Å. If four molecular layers of water exist between each layer of silicate and if there are n layers, the interior sites should amount to approximately $4 \cdot n \cdot A \cdot \gamma$, and the platelet surface sites should number $2 \cdot A \cdot \gamma$, where γ is a proportionality constant related to area, and A is the site density on the platelet. The ratio of internal to surface sites (assuming A to be constant) should then be $2 \cdot n = 600$, *i.e.*, n should be approximately 300. The average thickness of the montmorillonite particles in contact with hydrous solvent should then be $300 \cdot [9.6 + 12] = 6500$ Å $= 0.7\ \mu$, which is not in conflict with the microscopically found dimensions. In this description the adsorption energies of the different layers cannot differ greatly, since the adsorption isotherm, otherwise, would not be of the Langmuir type.

Regarding the assumption that $K_o C_o \ll 1$, it is seen from Fig. 4 that reciprocal plotting yields a straight line; for linearity to prevail in the water isotherm, it is necessary that $K_o C_o \ll 1$ (Eq. 5). The value of $K_b = 20\ M^{-1}$, therefore, represents a realistic figure. In the benzoic acid isotherms, C_b is in the range $0.02 \cdot 0.05\ M$ so $K_b C_b = 0.4$–1; since $K_b C_b$, therefore, is of the order of unity and $K_o C_o$ is much smaller than unity, it can also be stated with acceptable credibility that $K_b C_b \gg K_o C_o$.

SUMMARY

Benzoic acid adsorbs from alkanolic solutions on the surface of neutralized montmorillonite by Langmuir isotherms.

The number of surface sites estimated from the benzoic acid isotherms is much less than that of water (which adsorbs by intercalation), showing that the benzoic acid does not penetrate the crystal.

REFERENCES

(1) D. M. C. MacEwan, *Colloq. Int. Centre Nat. Rech. Sci.*, **10**, 21(1948).

(2) W. F. Bradley, R. E. Grim, and G. L. Clark, *Z. Kristallogr., Kristallgeometrie, Kristallphys., Kristallchem.*, **97**, 216(1937).

(3) J. W. Jordan, *J. Phys. Chem.*, **53**, 294(1949).

(4) S. B. Hendricks, *Amer. Mineral.*, **23**, 295(1938).

(5) J. Mering, *Colloq. Int. Centre Nat. Rech. Sci.*, **10**, 189(1948).

(6) W. H. Slabaugh and P. A. Hiltner, *J. Phys. Chem.*, **72**, 4295 (1969).

(7) W. T. Granquist and J. L. McAtee, Jr., *J. Colloid Sci.*, **18**, 409(1963).

(8) S. Weiss, *Proc. Nat. Conf. Clays Clay Miner.*, **10**, 191(1963).

(9) C. T. Cowan and D. White, *ibid.*, **9**, 459(1962).

(10) R. M. Barrer and K. E. Kelsey, *Trans. Faraday Soc.*, **57**, 625 (1961).

(11) D. M. C. MacEwan and O. Talib-Uddin, *Colloq. Int. Centre Nat. Rech. Sci.*, **10**, 24(1948).

(12) K. Wai and G. S. Banker, *J. Pharm. Sci.*, **55**, 1215(1966).

(13) M. R. Zentner, U. S. pat. 3,337,402 (1967).

(14) S. H. Rubin, private communication.

(15) J. T. Carstensen, M. Osadca, and S. H. Rubin, *J. Pharm. Sci.*, **58**, 549(1969).

(16) J. T. Carstensen and K. S. E. Su, *ibid.*, **59**, 666(1970); **59**, 671(1970).

ACKNOWLEDGMENTS AND ADDRESSES

Received March 30, 1970, from the *School of Pharmacy, University of Wisconsin, Madison, WI 53706*

Accepted for publication January 7, 1971.

This work was supported by grants from Hoffmann-La Roche, Inc., Nutley, N. J.; and R. T. Vanderbilt Company, Inc., New York, NY 10017

* To whom requests for reprints should be directed.

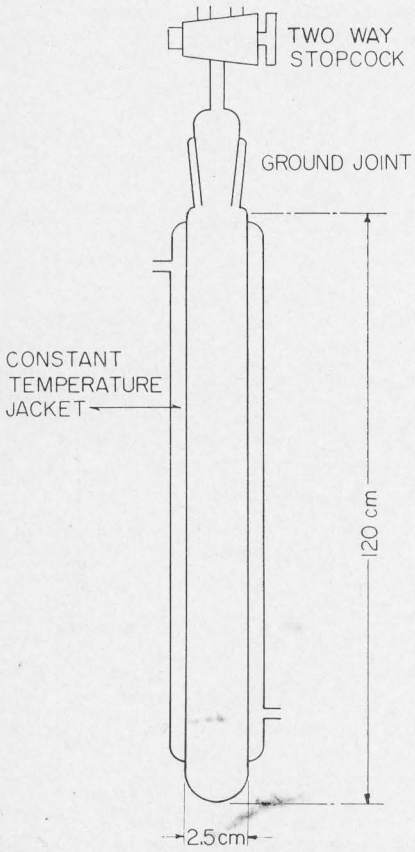

Figure 1—*Apparatus set-up for sedimentation studies.*

tube was again evacuated, turned end-over-end 10 times, opened to the atmosphere, and the procedure carried out again. This was then repeated until three successive, reproducible curves were obtained.

Part of the supernatant was then replaced by an equal volume of glycerin and the procedure repeated. Data were obtained at four glycerin concentrations; at each point where supernatant was replaced by glycerin, the viscosity of the supernatant was checked by means of an Ostwald-Fenske viscometer. All experiments were carried out in a constant-temperature room (25 ± 0.3°). In one set of experiments, lower (constant) temperatures were obtained by circulating constant temperature water through the jacket of the tube. It should be noted that the apparatus cannot be insulated and that good temperature control throughout the length of the tube is only possible at temperatures less than 5° above or below the temperature of the surrounding area.

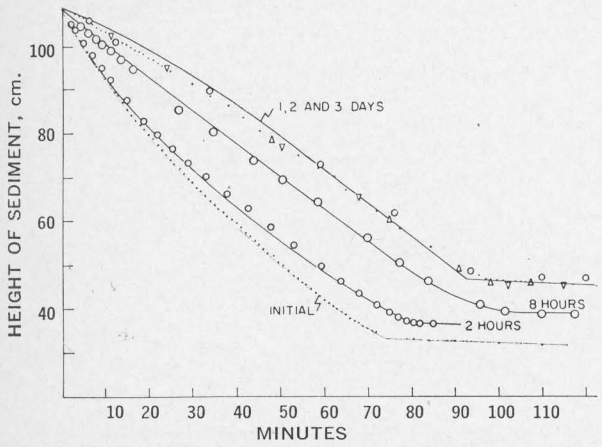

Figure 2—*Sedimentation curves in water as a function of time of a suspension made at low shear. Triangles and small circles by the upper curve are points from different runs.*

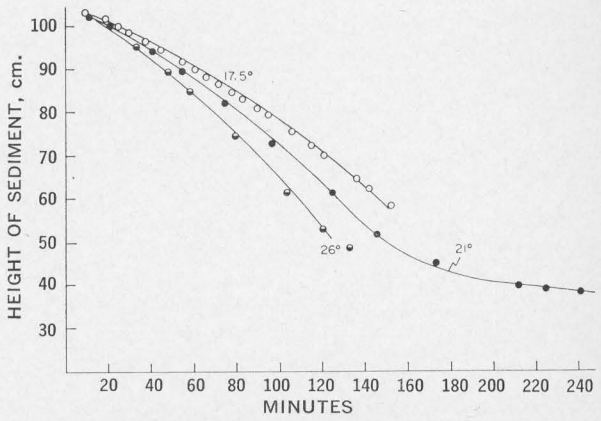

Figure 3—*Sedimentation curves in 10% v/v glycerin in water at various temperatures. The temperature was varied from experiment to experiment as a means of varying the viscosity.*

A note on some visual manifestations may be in order here. The interface is well defined and horizontal during the free-fall period. When the point of transition into the second, slower phase of the sedimentation is approached, a fairly heavy concentration of fine particles appears above the interface for a short while. At the critical time t_0, which is reproducible to within 5%, the surface suddenly becomes ragged, and at that particular time the second phase starts. The patterns associated with the second phase are the subject of a separately reported study (11). A set of runs was performed at 7, 9, and 11% by weight of kaolin in water as well.

RESULTS AND DISCUSSION

All of the tested systems showed convex curvature in the initial phase, such as shown in Figs. 2 and 3. This evidently differs from the linearity exhibited by more dilute systems.

If the sedimentation patterns found here for flocculated suspensions in the intermediate concentration range are analogous to those suggested for dilute systems by Kynch (2), Michaels and Bolger (10), and Gaudin and Fuerstenau (13–15), then, at time t, there will be a-centimeters of suspension containing the initial volume fraction ϕ_0 of solids, and b-centimeters of suspension containing the volume fraction in the cake (ϕ). The height of the sediment will be $x = a + b$. As time progresses, a will diminish at the expense of b. The a-values deduced from the data by Michaels and Bolger (Fig. 6, *Reference 10*) are reproduced in Fig. 4, and it is seen that an equation of the form $a = x_0 \exp[-kt]$ is a good fit. The decrease in a may, therefore, be considered to be of the form:

$$a = x_0 \exp[-kt] \qquad \text{(Eq. 1)}$$

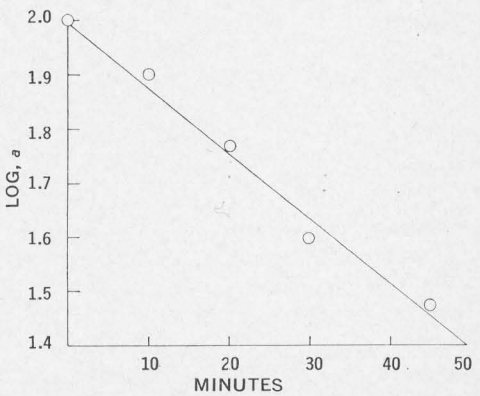

Figure 4—*The graph shows the result of logarithmic treatment of data reported by Michaels and Bolger (10). If the logarithm of the length of the constant-density plug is plotted as a function of time, then a straight line results, as shown in the plotting used here. The data refer to a 1.9% calcium oxide suspension.*

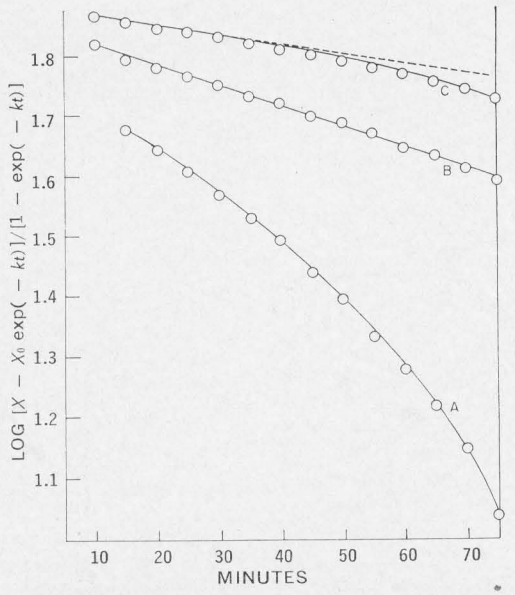

Figure 5—*Sedimentation data from a 7% by weight kaolin suspension plotted according to Eq. 7, using three values of* k. *Key: Curve A, $k = 0.005$ min.$^{-1}$; Curve B,* k *= 0.01 min.$^{-1}$; Curve C,* k *= 0.025 min.$^{-1}$. Temperature: 28°.*

To describe the time dependence of x, it is necessary to know how b changes with time. It has been shown (11, 16) that the cake (in the final phase) experiences an exponential decay, so $db/dt = -\omega \cdot b$. In the initial phase, it also experiences a build-up from the temporal contribution of the sediment. If the cross-sectional area is denoted Q, then the amount of solids in the cake at time t is $b \cdot Q \cdot \phi$; the amount of solids in the suspension above the cake is $Q \cdot a \cdot \phi_0$ (since it contains the initial volume fraction of solids). The original amount of solids was $x_0 \cdot Q \cdot \phi_0$, so material balance dictates that $Q \cdot a \cdot \phi_0 + b \cdot Q \cdot \phi = x_0 \cdot \phi_0 \cdot Q$, or $a \cdot \phi_0 + b \cdot \phi = x_0 \cdot \phi_0$. This may be rewritten:

$$\phi = \frac{[x_0 - a] \cdot \phi_0}{b} \qquad \text{(Eq. 2)}$$

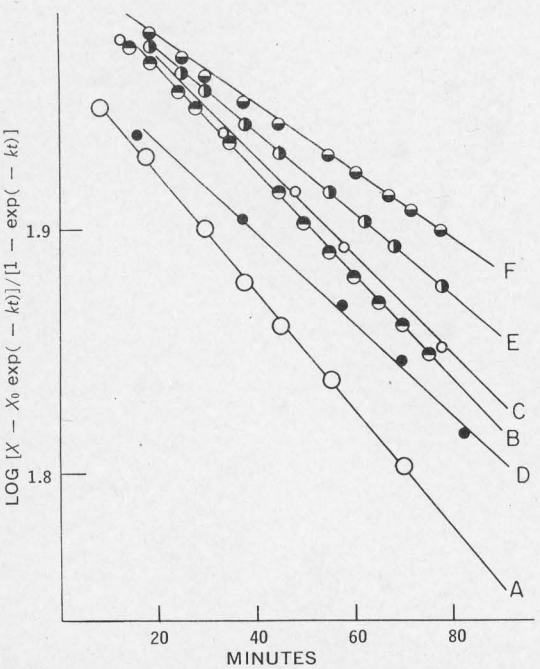

Figure 6—*Sedimentation data from 5% kaolin suspensions in aqueous glycerin vehicles, plotted according to Eq. 7. Curve notations are shown in Table I, indicating the employed* k*-values and the viscosity corresponding to each line.*

Table I—k- and ω-Values at Various Viscosities

Curve in Fig. 6	Viscosity, cps.	Rate Constant k, min.$^{-1}$, $\pm 10^{-3}$	Compaction Constant ω, min.$^{-1}$, $\pm 10^{-4}$
A	0.87	0.035	0.0055
B	0.96	0.032	0.0049
C	1.12	0.028	0.0046
D	1.19	0.024	0.0046
E	1.35	0.023	0.0039
F	1.40	0.022	0.0032
	2.40	0.013	0.0023

The total change of b with time, then, is:

$$\frac{db}{dt} = \frac{k \cdot \phi_0 \cdot a}{\phi} - \omega \cdot b \qquad \text{(Eq. 3)}$$

Inserting Eqs. 1 and 2 into Eq. 3 yields:

$$\frac{db}{dt} = k \cdot \frac{\exp[-kt]}{1 - \exp[-kt]} \cdot b - \omega \cdot b \qquad \text{(Eq. 4)}$$

which has the solution:

$$b = C \cdot \{1 - \exp[-kt]\} \cdot \exp[-\omega t] \qquad \text{(Eq. 5)}$$

The expression for $x = a + b$, then is:

$$x = x_0 \exp[-kt] + C \cdot \{1 - \exp[-kt]\} \cdot \exp[-\omega t] \qquad \text{(Eq. 6)}$$

For the purpose of plotting, this is rearranged:

$$\log\left(\frac{x - x_0 \exp[-kt]}{1 - \exp[-kt]}\right) = -\frac{\omega}{2.3} \cdot t + \log C \qquad \text{(Eq. 7)}$$

The data may now be plotted using estimates of k,[3] and by applying successive values of k, a best k-value (*i.e.*, the k-value that imparts linearity[4] to the data when treated according to Eq. 7) can be arrived at. An example of this is shown in Fig. 5. If done manually, two or three k-values are arrived at (*e.g.*, 0.034, 0.035, and 0.036 min.$^{-1}$) which produce lines without apparent curvature. The value giving the best statistical fit (17, 18) is then chosen. With the aid of a computer, the iteration procedure can be accomplished rapidly. Figure 6 and Table I show data at various viscosities plotted according to Eq. 7. With the proper k-value, linearity prevails to within 15 cm. of the critical height.

The dependency of k on the viscosity is of interest, and Fig. 7 shows that the logarithm of the rate constant is linearly related to the logarithm of the viscosity. The slope is reasonably close to minus unity, so that k is inversely proportional to viscosity. This type behavior might suggest that Stokes's law, with some modification, applies, since the stokes velocity is also inversely proportional to viscosity. In a suspension, the forces involved are both of van der Waals and electrical nature (15, 19–23). In causing flocculation they might be playing a part directly in the sedimentation process, *i.e.*, the rate constant might be associated with a flocculation rate. By such a visualization, the initial perturbance causes an equilibrium floc, A_j (containing on the average j single particles) to be broken up into smaller flocs, A_i. This, of course, is a highly simplified picture, because $A_j \rightarrow A_i$ could not be a single-step process. Furthermore, both i and j would present averages of a population of numbers.

It would also have to be assumed that A_j, once formed, would appear immediately in the cake; in spite of these shortcomings, the viewpoint explains the inverse relationship between rate constant and viscosity, and can not be eliminated as a possibility. W. Higuchi *et al.* (24, 25) have shown that k_{ij} approaches some factor times k_{11}, the rate constant for combination of single particles, and have also shown that $k_{11} = 8k_0T/3\eta$. It is not possible to test this hypothesis on more concentrated systems with the data presented here;

[3] First estimates of k (and ω) can be obtained from Eq. 6 by feathering technique if k and ω are not of the same order of magnitude.

[4] The value giving the best statistical fit (17, 18), *i.e.*, the one producing the least residual sum of squares.

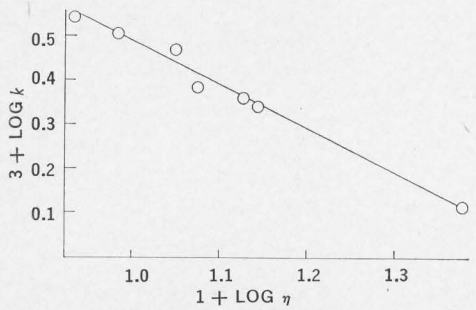

Figure 7—*A plot of the logarithm of the rate constant* k versus *the logarithm of the viscosity. The drawn line has a slope of minus unity:* k *is in units min.*$^{-1}$ *and viscosity is in cps.*

to such an end it would be necessary to perform experiments where the initial perturbance (deflocculation) could be varied in a quantitative way. Experimental procedures in previous publications as well as this work have simply been designed to achieve a reproducible perturbance, so that data are comparable; it may be, for the reasons quoted, that data may not be comparable from author to author.

The values of ω are obtained from the slopes in Fig. 6 and are listed in Table I. The values are plotted as a function of viscosity in Fig. 8. The general range of the ω-values is in good agreement with data on cake contraction reported by Carstensen and Su (11) who found ω_1-values in the range of 0.2–0.4 hr.$^{-1}$ (*i.e.*, 0.003–0.007 min.$^{-1}$). It would appear from Fig. 8 that ω is inversely proportional to the viscosity.

At higher concentrations the critical height, H_0, increases and the curves show less distinct breaks. Evaluation of data by Eq. 7 becomes less exacting, and k values are at best ±20%. The k-values seem to taper off at a value of 0.01 hr.$^{-1}$ as shown in Fig. 9, but ω-values decrease with increasing concentration.

As a last comment on the treatment of the preceding, attention should be called to the fact that an obvious approximation is made in assuming the cake to be of uniform concentration along the entire length b. However, attempts to present ϕ as a function of x lead to forms of Eq. 3 that cannot be solved analytically. That the approximation is not unrealistic is apparent both from the X-ray data by Gaudin and Fuerstenau (13, 14) and by the linearity which can be achieved by inserting proper k-values in Eq. 7. On the other hand, deviation from linearity close to the critical height undoubtedly reflects the effect of the approximation.

It is often convenient, in the laboratory, to have a rapid method available for plotting; the treatment just outlined, clearly, is not rapid. For routine plotting, the initial convex portion of the curve may be approximated by a parabola, *i.e.*, $x_0^2 - x^2 = \beta t$, where x_0 is the initial height. Data are plotted in this fashion in Figs. 10 and 11, and, with exception of the initial turbulent period (8), the data fit such a relationship well. It should be noted that this means of presentation is purely empirical, and that the comments to follow may not have general applicability but may merely apply to the kaolin–glycerin–water system. The value of this type of practical approach

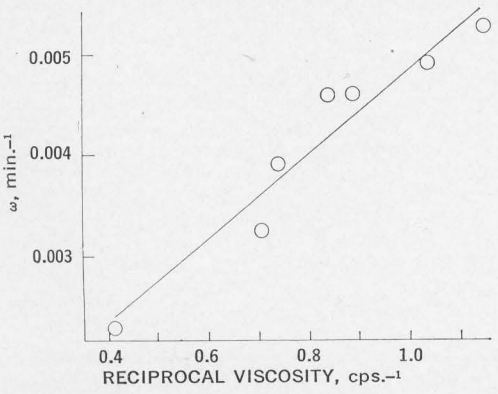

Figure 8—*A plot of the compaction-rate constant,* ω, versus *reciprocal viscosity.*

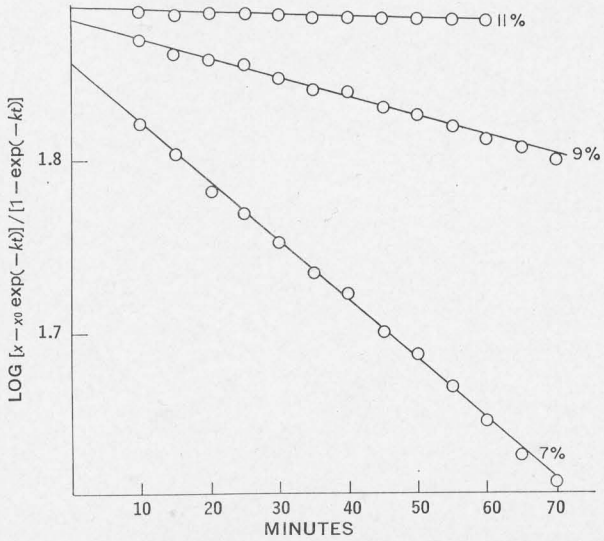

Figure 9—*Sedimentation data from 7, 9, and 11% kaolin suspensions in water, plotted according to Eq. 7, all using a* k*-estimate of 0.01 min.*$^{-1}$.

is that it allows rapid extrapolation and implies at what time the critical height is being approached.

Analogies have been made in the past (26) between the fall of the boundary to the flow of liquid through a porous plug in an infinitely long medium. By applying the Poiseiuille equation[5] such a view would require that $V/t = \pi Pr^4/8L\eta$, where V/t is volume flow per unit time, P is pressure head, r is a capillary radius parameter, and L is the length of the plug. Since each milliliter flowing through the plug is associated with a height decrease of $1/\pi R^2$, the velocity of the interface would be: $V/(t\pi R^2) = (Pr^4)/(8L\eta R^2) = \beta/(2.L) = (dx)/(dt)$, where R is the radius of the tube and the sedimentation constant $\beta = Pr^4/4\eta R^2$. If L approximately equals x, a formal integration would yield $x^2 - x_0^2 = -\beta t$, assuming the pressure head to be constant. This is not theoretically justifiable. Although, as required by the treatment, the sedimentation constant appears to be inversely proportional to the viscosity, it should also be inversely proportional to R^2; data reported elsewhere (11) show this not to be the case. The squared-heights fitting is, therefore, only empirical.

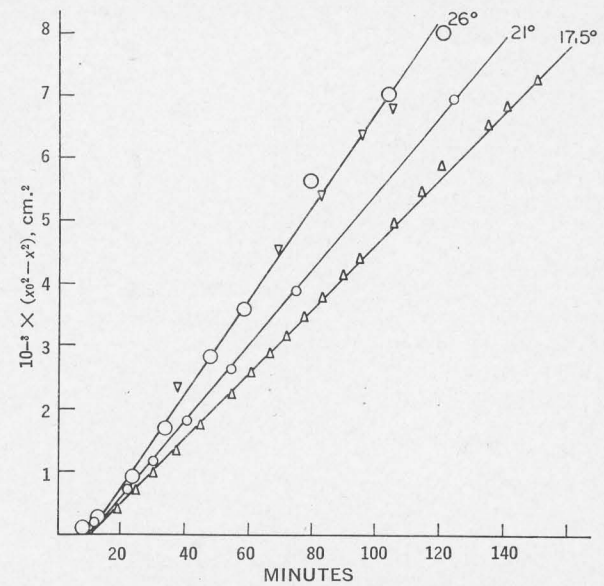

Figure 10—*Squared-heights curves for 5% kaolin suspensions in 10% v/v glycerin in water at three temperatures.*

[5] Use of the Kozeny-Carmen equation (27, 28) does not change the consequences of the arguments outlined.

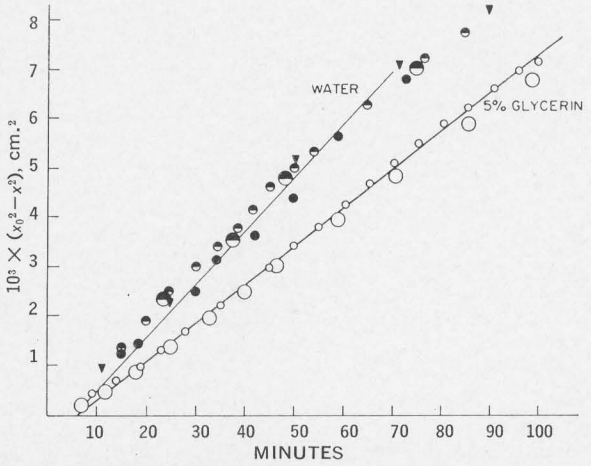

Figure 11—*Squared-heights curves for 5% kaolin suspensions in water and 5% v/v glycerin in water.*

SUMMARY

By assuming the sedimentation process to consist of the descent of a constant density plug and simultaneous build-up of a higher density cake, it has been shown that sedimentation data are consistent with theory, if it is assumed that the exponential contraction of the cake is initiated at zero time. The point in time, t_0, the critical time, where the boundary of the sediment and the cake coincide, denotes the end of the initial stage of sedimentation.

Empirically, sedimentation data in the initial stage are amenable to plotting by graphing the square of the height as a function of time. The slope of these lines appears to be proportional to the ratio of density difference to viscosity.

NOMENCLATURE

a = length of sediment (cm.) (constant-density plug).
b = height of cake (cm.).
C = preexponential factor for cake contraction (cm.).
H_0 = critical height (cm.) at which point the first phase of sedimentation ends and the second phase starts.
k = rate constant for sediment (min.$^{-1}$).
L = length of constant-density plug falling through infinitely long column of liquid (cm.).
P = pressure head (dynes/cm.^{2}).
R = radius of tube (cm.).
t_0 = time at which H_0 occurs; critical time (min.).
V = volume (cm.^{3}).
x = height of sediment interface above bottom of tube (cm.).
x_0 = initial height (cm.).
β = sedimentation constant (cm.^{2}/min.).
η = viscosity, centipoise or poise, as indicated.
ϕ = volume fraction of suspended matter in cake.
ϕ_0 = volume fraction of suspended matter in sediment.
ω = compaction rate constant (min.$^{-1}$), *i.e.*, exponential decay constant for cake height.

REFERENCES

(1) R. Stokes, *Proc. Cambridge Phil. Soc.*, **9,** 5(1856).
(2) G. Kynch, *Trans. Faraday Soc.*, **48,** 166(1952).
(3) T. Higuchi, *J. Amer. Pharm. Ass., Sci. Ed.*, **47,** 657(1958).
(4) E. N. Hiestand, *J. Pharm. Sci.*, **53,** 1(1964).
(5) H. Steinour, *Ind. Eng. Chem.*, **36,** 840(1944).
(6) *Ibid.*, **35,** 901(1944).
(7) B. A. Haines, Jr., and A. N. Martin, *J. Pharm. Sci.*, **50,** 228(1961).
(8) C. S. Robinson, *Ind. Eng. Chem.*, **18,** 869(1926).
(9) H. Ward and K. Kammermeyer, *ibid.*, **32,** 622(1940).
(10) A. S. Michaels and J. C. Bolger, *Ind. Eng. Chem. Fundam.*, **1,** 24(1962).
(11) J. T. Carstensen and K. Su, to be published.
(12) L. K. Benedict, G. S. Banker, and W. V. Kessler, *J. Pharm. Sci.*, **54,** 1659(1965).
(13) A. M. Gaudin and M. C. Fuerstenau, *Eng. Mining J.*, **159,** 110(1958).
(14) A. M. Gaudin and M. C. Fuerstenau, *Int. Mining Proc. Congr.*, London, England, Apr. 1960.
(15) A. M. Gaudin, M. C. Fuerstenau, and S. R. Mitchell, *Mining Eng. (London)*, **11,** 613(1959).
(16) C. B. Egolf and W. L. McCabe, *Trans. Amer. Inst. Chem. Eng.*, **33,** 620(1937).
(17) C. R. Wylie, Jr., "Advanced Engineering Mathematics," McGraw-Hill, New York, N. Y., 1960.
(18) J. T. Carstensen, J. B. Johnson, D. C. Spera, and M. J. Frank, *J. Pharm. Sci.*, **57,** 23(1968).
(19) J. deBoer, *Advan. Colloid Interface Sci.*, **3,** 21(1950).
(20) F. London, *Z. Phys.*, **63,** 245(1930).
(21) B. Deryagin, A. Titijevskaia, I. Abriscova, and E. Lifshitz, *Discuss. Faraday Soc.*, **18,** 24(1954).
(22) B. Deryagin, I. Abriscova, and E. Lifshitz, *Quart. Rev. (London)*, **10,** 295(1956).
(23) E. Verway and J. Overbeek, "Theory of the Stability of Lyophobic Colloids," Elsevier, Amsterdam, The Netherlands, 1948.
(24) W. Higuchi, R. Okada, G. Stelter, and A. Lemberger, *J. Pharm. Sci.*, **52,** 49(1963).
(25) W. Higuchi, R. Okada, and A. Lemberger, *ibid.*, **51,** 683 (1962).
(26) P. G. W. Hawksley, "Some Aspects of Fluid Flow," Arnold, London, England, 1951, p. 114.
(27) J. Kozeny, *S. B. Akad. Wiss. Wien. Abh. Math. Naturwiss. Kl. IIa*, **136,** 271(1927).
(28) P. C. Carman, *Trans. Inst. Chem. Eng.*, **15,** 150(1937).

ACKNOWLEDGMENTS AND ADDRESSES

Received February 12, 1969, from the *School of Pharmacy and Extension Services in Pharmacy, University Extension, University of Wisconsin, Madison, WI 53706*

Accepted for publication December 11, 1969.

This work was supported in part by grants from Hoffmann-La Roche, Nutley, N. J., and R. T. Vanderbilt Co., Inc., New York, NY 10017

* To whom requests for reprints should be directed.

[Reprinted from the Journal of Pharmaceutical Sciences,
Vol. 59, No. 5, May, 1970. ©1970 by the American Pharmaceutical Association]

Sedimentation Kinetics of Flocculated Suspensions II: Sedimentation below the Critical Height

J. THURÖ CARSTENSEN* and KENNETH S. E. SU

Abstract □ Aside from the phenomenological equation by Egolf and McCabe and by Robinson, no attempts have appeared in literature in the past to quantitate terminal sedimentation characteristics of flocculated suspensions. The physical factors involved are suggested here, taking into account electrical effects and geometric factors contributing to friction. The equation of settling emerges as a linear combination of exponential decays—*viz.*, $[x - H_u] = A_1e^{-\omega_1\tau} + A_2e^{-\omega_2\tau}$, where x is the height of the sediment at time τ, H_u is the final height, and A and ω are constants. From the data it would appear that the friction, B, exerted is both viscosity (η) and dimension (R) dependent and of the form $B(\eta,R) = \Gamma \cdot e^{\xi\eta}e^{\mu R}$, where μ, ξ, and Γ are system-dependent constants.

Keyphrases □ Sedimentation kinetics—flocculated suspensions, equations □ Kinetics, sedimentation, flocculated suspensions—critical height, equations derived □ Suspensions, flocculated—sedimentation kinetics, equations

Sedimentation of flocculated suspensions has been the subject of several publications in the past (1–12); such systems have been shown (1, 7, 9–13) to sediment first at a rapid rate, primarily governed by gravitational and frictional forces. At a particular, well-reproducible point, the rate changes abruptly, and further sedimentation appears to be governed by forces over and above those just mentioned. With a few exceptions (1, 3, 13), all of the cited references attempt to modify Stokes's law to explain experimental data. In no case [except indirectly by Robinson (7)] has cognizance been taken of interparticle forces in relation to sedimentation rates.[1]

The treatment to follow deals with the second phase of sedimentation of flocculated suspensions of intermediate concentration, and attempts to account for the effect of such forces.

As shall be shown the final sedimentation pattern follows a linear combination of exponential decays. No previous treatment has led to such a pattern for the second stage of sedimentation or to the type plot encountered in concentrated suspensions, although the data in several examples in literature (2, 6, 7, 9) imply such a relationship.

THEORETICAL

London-van der Waals forces (14, 15) are responsible for the stability of the flocculated state, and in general, at small separations, the potential energy between two particles will be negative. At intermediate distances (16–19), however, the potential energy becomes positive because of the repulsion of double layers. Since the true charge of the particle surface cannot be determined by experiment, quantitation of such forces is difficult, and the upper limit for distances over which these forces will be effective cannot be stated *a priori*.

[1] A sizable amount of information regarding interparticle forces has been obtained by rheological approaches, notably the studies by Higuchi and Stehle (25), Gillespie (26, 27), Goodeve (28), and Vand (19).

Since the authors are dealing with the phase of sedimentation which occurs at a critical height, H_0, it may be advantageous, at the onset, to use a coordinate system slightly different from the one customarily used. Usually the position of the boundary is measured from the bottom of the tube and denoted x; time, t, is measured from the time sedimentation starts. Here, if the height H_0 occurs at time t_0, the position and time axes are chosen with the points t_0 and H_0 as the origin. Distance is now denoted y ($y = H_0 - x$), *i.e.*, positive in downward direction and positive for the times τ ($\tau = t - t_0$) in question. It shall be assumed that the center of gravity of the sediment is at one-half the height of the boundary of the sediment, *i.e.*, its position is $y = H_0/2$ originally, and at time τ it is $H_0 - x + x/2 = H_0 - x/2 = y$.

The forces exerted on the sediment are gravitational forces, frictional and reactional forces, and forces that are electrical in nature. The gravitational force is in the y-direction and of magnitude $M[1 - (\rho_0/\rho)]g$, where ρ and ρ_0 are the densities of solid and liquid, M is the mass of the sediment, and g is the gravitational acceleration. The frictional and reactional forces are in a direction opposite to y and must be related to viscosity and to wall and bottom effects, *i.e.*, to the geometry of the vessel. The functional relationship is not equated to $6\pi\eta r$, nor is an attempt made at this particular point in the development to formulate the diameter dependency, but the force is described as a velocity-dependent $[-B(\eta,R)dy/d\tau]$ and a velocity-independent $[-\psi(R)]$ component. The electrical force is assumed to be a repulsion (*i.e.*, in a direction opposite to the direction of the y-axis) and with regard to magnitude it is assumed to increase the closer the floc-aggregates are to one another; they are related to distance between flocs which in turn is related to the liquid volume of the cake, *i.e.*, $\pi R^2(x) - 4\pi r^3 n/3$, where R is the radius of the tube, and where n is the number and r the "radius" of the floc-aggregates. These forces are assumed to be of the form θy. The sum of all the forces then equals the mass of the sediment times its acceleration, *i.e.*,

$$M[1 - \rho_0/\rho]g - B(\eta,R)\frac{dy}{d\tau} - \psi(R) - \theta y = M\frac{d^2y}{d\tau^2} \quad \text{(Eq. 1)}$$

This may be rewritten

$$\frac{d^2y}{d\tau^2} + \frac{B(\eta,R)}{M}\frac{dy}{d\tau} + \frac{\theta}{M}y = [1 - \rho_0/\rho]g - \frac{\psi(R)}{M} \quad \text{(Eq. 2)}$$

It is apparent from inspection of Eqs. 1 and 2 that

$$y^* = \frac{M[1 - \rho_0/\rho]g - \psi(R)}{\theta}$$

is a particular solution to the differential equation. The remaining solutions are obtained by inserting an expected solution of the form $y = -A \cdot e^{-\omega\tau}$ into the homogeneous equation corresponding to Eq. 2. This yields:

$$-A \cdot e^{-\omega\tau}\left[\omega^2 - \frac{B(\eta,R)}{M}\omega + \frac{\theta}{M}\right] = 0 \quad \text{(Eq. 3)}$$

When the expression in brackets is equated to zero, Eq. 3 is satisfied; the characteristic roots are:

$$\omega = \frac{B(\eta,R)}{2M} \pm \sqrt{\left[\frac{B(\eta,R)}{2M}\right]^2 - \frac{\theta}{M}} \quad \text{(Eq. 4)}$$

The roots shown in Eq. 4 may be simplified if $B(\eta,R)/M \gg \theta/B(\eta,R)$ in which case they are:

$$\omega_1 = \frac{B(\eta,R)}{M} \quad \text{(Eq. 5)}$$

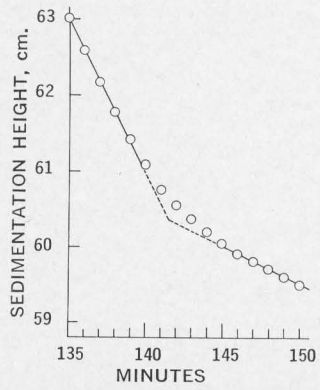

Figure 1—*Graph showing the method for determining the critical height* (H_0) *in a 5.54-cm. i.d. tube, 10% v/v glycerin and 11% w/v kaolin, and the critical time* (t_0).

and

$$\omega_2 = \frac{\theta}{B(\eta,R)} \qquad \text{(Eq. 6)}$$

The complete solution, in terms of y, is:

$$y = \frac{M[1 - \rho_0/\rho]g - \psi(R)}{\theta} - A_1' \cdot e^{-\omega_1 \tau} - A_2' \cdot e^{-\omega_2 \tau} \qquad \text{(Eq. 7)}$$

where the exponents in Eq. 7 have the meaning denoted in Eqs. 5 and 6. It is noted that $y^* = M[1 - \rho_0/\rho]g - \psi(R)/\theta$ corresponds to y_∞ by virtue of Eq. 7, and, therefore, is related to H_u, the ultimate height, by the relation $y_\infty = y^* = H_0 - H_u/2$. Inserting this into Eq. 7 and rearranging, yields:

$$x - H_u = A_1 e^{-\omega_1 \tau} + A_2 e^{-\omega_2 \tau} \qquad \text{(Eq. 8)}$$

where $A_1 = 2A_1'$ and $A_2 = 2A_2'$.

It is apparent from Eq. 8 that the terminal sedimentation pattern should be characterized by a linear combination of two exponential decays. By the assumption leading to Eqs. 5 and 6, $\omega_1 \gg \omega_2$ and the first term on the right hand side of Eq. 8 should be predominant at small values of τ and the last term should predominate at high values of τ.

EXPERIMENTAL

A previously described setup and methodology (1) were used: tubes 1.25 m. high, and of inside diameter 2.46, 2.72, 4.60, or 5.54 cm. were used as sedimentation vessels. The exact inside dimension was determined for each tube by introducing known amounts of water and checking heights with a precision cathetometer. The system studied was an 11% weight per volume kaolin[2] suspension

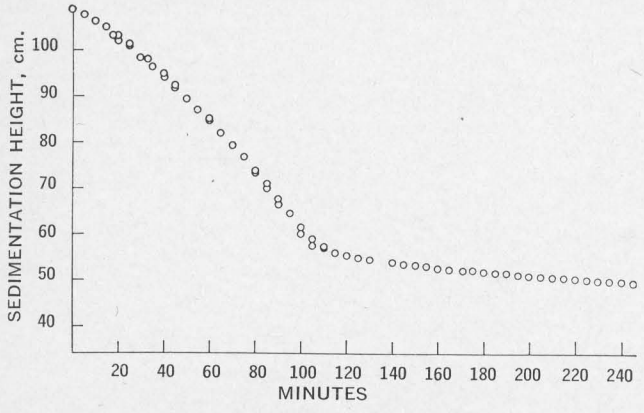

Figure 2—*Sedimentation curve of 11% w/v of kaolin in water in a tube of 5.54-cm. i.d. Duplicate points are shown.*

[2] Colloidal kaolin NF, lot No. 781603, Merck and Co., Rahway, N. J.

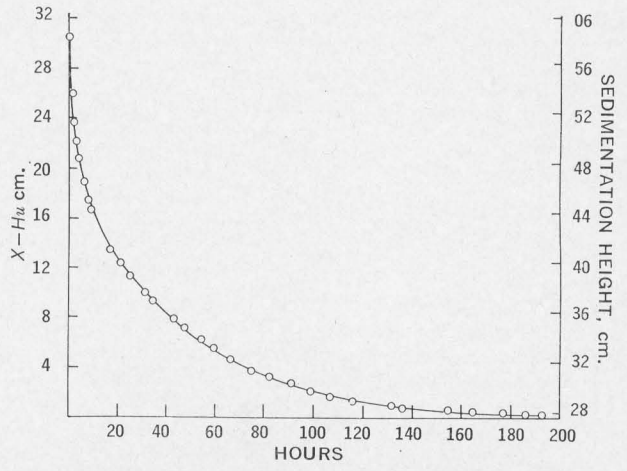

Figure 3—*Sedimentation pattern in a tube of 4.60-cm. i.d. of an 11% w/v suspension of kaolin in 5% v/v glycerin solution at heights below the critical height,* H_0. *The left ordinate is adjusted for final height,* H_u; *the right ordinate axis shows the actual heights* (x). *The curve shown in full is the theoretical curve;* $10 \cdot e^{-0.31\tau} + 20 \cdot e^{-0.0233\tau}$. *The points shown are experimental points.*

in water, 5% v/v glycerin, or 10% v/v glycerin. The suspensions were made in a Waring blender and transferred to the sedimentation tubes. The tops of the tubes were connected by means of a 24/40 ground joint to a stopcock, and after transfer, the stopcock was attached to the tube, and the suspension thoroughly deaerated by means of aspirator vacuum. Once deaerated, the tubes were turned end-over-end 10 times, the stopcock opened, the tube placed vertically and securely on a stand, and the position of the sedimentation boundary noted every 5 min.; timing intervals were made shorter when the critical height, H_0, was approached. This height, as well as the critical time, t_0, was then determined by graphical interpolation as shown in Fig. 1. Following this the position of the boundary was noted every 5 min. for 0.5 hr., and then hourly for 50 hr. (except for necessary schedule interruptions). Subsequently, the sedimentation height was recorded twice daily until a point in time had been reached where less than 0.2 mm. change occurred in a 24-hr. period; this usually required 7–13 days. Each set was obtained in duplicate. All sedimentation heights were determined by means of a cathetometer, and readings were accurate to 0.1 mm. The tubes used were not jacketed, but the experiments were carried out in a constant-temperature room at 25 ± 0.6°. The viscosity of the super-

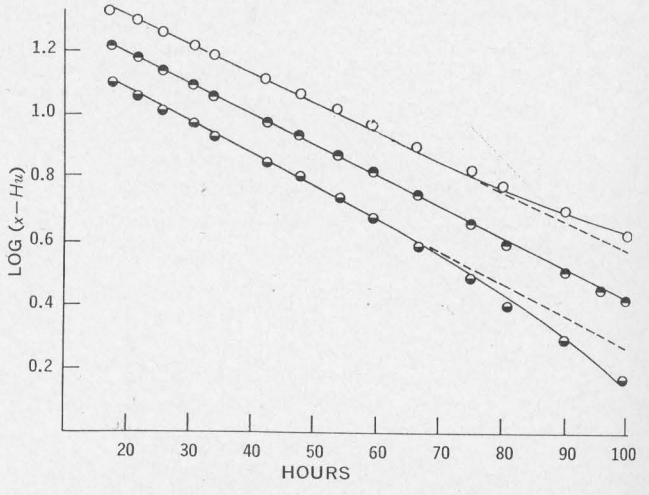

Figure 4—*Decay pattern of 11% w/v kaolin suspension in 5% v/v glycerin solution at high time values where* ω_2 *and* A_2 *predominate. Test was performed in a tube of 4.60-cm. i.d. The curves are separated by 0.1 and 0.2 logarithmic units as indicated. The plots demonstrate estimation of final sedimentation height prior to the time when it is reached. Key:* ○, H_u = *27.3 cm. (scale minus 0.2);* ◓, H_u = *27.8 cm. (scale minus 0.1), and* ◒, H_u = *28.4 cm.*

Table I—Theoretical Sedimentation Curve for 11% w/v Kaolin in 5% v/v Aqueous Glycerin in 4.6-cm. i.d. Tube[a]

Hr.	-0.137τ	$e^{-0.31\tau}$	$10e^{-0.31\tau}$	-0.097τ	$e^{-0.0223\tau}$	$20e^{-0.0223\tau}$	$10e^{-0.31\tau} + 20e^{-0.0223\tau}$
1	0.8630–1	0.730	7.30	0.9903–1	0.9780	19.56	26.86
2	0.7260–1	0.532	5.32	0.9806–1	0.9563	19.13	24.45
3	0.5890–1	0.388	3.88	0.9709–1	0.9352	18.70	22.58
4	0.4520–1	0.283	2.83	0.9612–1	0.9146	18.29	21.12
5	0.3150–1	0.207	2.07	0.9515–1	0.8944	17.89	19.96
6	0.1780–1	0.151	1.51	0.9418–1	0.8746	17.49	19.00
8	0.9280–2	0.085	0.85	0.9224–1	0.8361	16.72	17.57
10	0.6300–2	0.043	0.42	0.9030–1	0.8000	16.00	16.43
12	0.3560–2	0.023	0.23	0.8836–1	0.7649	15.30	15.53
14	0.2600–2	0.018	0.18	0.8642–1	0.7315	14.63	14.81
15	0.9450–3	0.009	0.09	0.8545–1	0.7164	14.33	14.42
20	0.260 –3	0.002	0.02	0.8060–1	0.6398	12.80	12.82
40				0.6120–1	0.4093	8.19	8.19
80				0.224 –1	0.1675	3.35	3.35
160				0.448 –2	0.0281	0.56	0.56

[a] $A_1 = 10$ cm., $\omega_1 = 0.31$ hr.$^{-1}$, $A_2 = 20$ cm., $\omega_2 = 0.0223$ hr.$^{-1}$.

natant was checked after each experiment by means of an Ostwald-Fenske viscometer.

RESULTS

A typical sedimentation curve is shown in Fig. 2; the shape is of the same nature as the one described elsewhere (1); the scale is selected so as to show both the initial and the beginning of the second phases of sedimentation, and the characteristic point separating the two curves. Even with the scale used it is apparent that some slight curvature exists in the second phase. In proper scale, all of the sedimentation curves have the shape shown in Fig. 3 when x is plotted as a function of τ.

Once the ultimate height, H_u, is attained, a first estimate of the parameters ω_2 and A_2 can be made, by using values of τ higher than 15 hr. In this case (as seen in Table I) $A_2e^{-\omega_2\tau} \gg A_1e^{-\omega_1\tau}$ and Eq. 8 becomes $[x - H_u] = A_2e^{-\omega_2\tau}$. The logarithmic form of this is

$$\log [x - H_u] = -\frac{\omega_2}{2.3}\tau + \log A_2 \quad (\tau > 15 \text{ hr.}) \quad \text{(Eq. 9)}$$

An example of this is shown in Table II and Fig. 4. It should be noted that the final height may be estimated well in advance of its actual occurrence from linearity as opposed to curvature of this type plot. Estimated values were always within 0.5 mm. of the actual, experimentally determined, final height.

By means of the estimates of A_2 and ω_2 the value of $[x - H_u] - A_2e^{-\omega_2\tau}$ can be determined at values of τ less than 15 hr., so the two other parameters may be estimated by rearrangement of Eq. 8:

$$\log \{[x - H_u] - A_2e^{-\omega_2\tau}\} = -\frac{\omega_1}{2.3}\tau + \log A_1 \quad \text{(Eq. 10)}$$

An example of this is shown in Table III and Fig. 5. By this plotting a better estimate of A_2 is obtained as shown in Fig. 5. The difference between this estimate and the original estimate was always within error of the graphical estimate in Fig. 4. With the estimates of A_1, ω_1, A_2, and ω_2, statistically best values may be obtained by computer, using iteration techniques (20–22). It should be noted, however, that graphical and manually generated estimates are quite good. Construction of the theoretical curve from the parameter estimates arrived at in Tables II and III and Figs. 4 and 5 is shown in Table I, and the curve drawn in full in Fig. 3 is taken from this table. It is quite obvious from the figure that the data fit the curve well. Averages of duplicate determinations of A_1, ω_1, A_2, and ω_2 from all the sedimentation tests are listed in Table IV.

DISCUSSION

In not too concentrated suspensions the sedimentation pattern is characterized first by a settling pattern which is linear (9) or parabolic with time (1) caused, respectively, by free fall or constant-density plug descent (1, 9). Attempts to describe mathematically the phase that follows the initial settling have been made by Robinson (7) and by Egolf and McCabe (13). Robinson found the dependency of the initial settling rates on concentration and then

Table II—Sedimentation Data for High Values of τ when ω_2 and A_2 Are the Predominant Terms

Hr.	Height, x, cm.	$x - 28.4$, cm.	log $[x - 28.4]$	$x - 27.8$, cm.	log $[x - 27.8]$	$x - 27.3$, cm.	log $[x - 27.3]$
17.67	41.06	12.76	1.1059	13.36	1.1258	13.86	1.1318
21.50	40.02	11.62	1.0652	12.22	1.0871	12.72	1.1045
25.65	38.96	10.56	1.0237	11.16	1.0477	11.66	1.0630
30.42	37.88	9.48	0.9768	10.08	1.0035	10.58	1.0245
34.20	37.12	8.72	0.9405	9.32	0.9694	9.82	0.9921
42.70	35.56	7.16	0.8549	7.76	0.8899	8.26	0.9170
47.22	34.87	6.47	0.8109	7.07	0.8494	7.57	0.8791
53.98	33.90	5.50	0.7404	6.10	0.7853	6.60	0.8195
59.30	33.23	4.83	0.6840	5.43	0.7348	5.93	0.7731
66.70	32.32	3.92	0.5933	4.52	0.6551	5.02	0.7007
75.23	31.51	3.11	0.4928	3.71	0.5694	4.21	0.6243
82.30	30.93	2.53	0.4031	3.13	0.4955	3.63	0.5599
90.18	30.39	1.99	0.2989	2.59	0.4133	3.09	0.4900
98.90	39.90	1.50	0.1761	2.10	0.3222	2.60	0.4150
107.12				1.70			
115.55				1.34			
132.23				0.92			
136.70				0.70			
155.12				0.52			
165.17				0.41			
176.93				0.32			
186.00				0.20			
193.50				0.19			

Table III—Sedimentation Data at Low Values of τ[a]

Hr.	Height, x, cm.	$[x - 27.8]$, cm.	0.0097τ	$Q = e^{-0.0223\tau}$	$[x-27.8-19.2Q]$, cm.	$[x-27.8-20Q]$, cm.	$[x-27.8-20.5Q]$, cm.
0	58.3	30.5	0	1	11.3	10.5	10.0
0.27	56.55	28.75	0.9974–1	0.9940	9.67	8.87	8.37
0.52	55.33	27.53	0.9950–1	0.9885	8.55	7.76	7.27
1.30	52.87	25.07	0.9874–1	0.9714	6.42	5.64	5.16
1.97	51.41	23.61	0.9809–1	0.9570	5.24	4.47	3.99
2.47	50.56	22.76	0.9760–1	0.9463	4.59	3.83	3.36
2.92	49.85	22.05	0.9717–1	0.9369	4.06	3.31	2.84
3.48	49.15	21.35	0.9662–1	0.9252	3.59	2.85	2.38
4.05	48.49	20.69	0.9607–1	0.9135	3.15	2.42	1.96
4.52	48.01	20.21	0.9562–1	0.9040	2.85	2.13	1.68
5.02	47.54	19.74	0.9513–1	0.8939	2.58	1.86	1.42
5.52	47.12	19.32	0.9465–1	0.8840	2.35	1.64	1.20
6.03	46.68	18.88	0.9415–1	0.8740	2.10	1.40	0.96
6.50	46.33	18.53	0.9370–1	0.8648	1.93	1.23	0.80
7.02	45.96	18.16	0.9319–1	0.8549	1.75	1.06	0.63
7.45	45.66	17.88	0.9277–1	0.8466	1.63	0.95	0.52
8.03	45.32	17.52	0.9221–1	0.8358	1.47	0.80	0.39
8.62	44.97	17.17	0.9164–1	0.8249	1.33	0.67	0.20
9.45	44.50	16.70	0.9083–1	0.9097	1.15	0.51	0.10

[a] Eleven percent w/v of kaolin in 5% v/v glycerin in a tube of 4.60-cm. i.d.

applied these findings to experimental data; since in that context, the sedimentation volume represents a suspension of time-dependent concentration (disregarding the supernatant) the settling rates should constantly change in a predictable fashion.

Egolf and McCabe suggested a phenomenological log–log relationship between absolute height and time for the phase following the initial settling. Ward and Kammermeyer (8) tested both models in different type systems (carbonates, silica, and magnesium oxide), and found fair agreement with regard to the shape of the curves, but large (20–40%) quantitative deviations in the second phase of sedimentation. These authors concluded that the application of the approaches of Robinson (7) and Egolf and McCabe (13) is limited to prediction of settling of only such systems that are closely related to the ones used to develop the appropriate equations and factors. Reflecting on the later findings that the initial settling is in the form of a constant-density plug (1, 9–11), it would appear that it may be erroneous to assume that the sediment may be viewed as a uniform suspension of constantly changing concentration; this may be the source of the cited quantitative deviations.

The approach taken here is to account for the forces involved (even though all of them cannot be expressed explicitly *a priori*) and then to try to gain insight into them, quantitatively and qualitatively, by way of experimental results. Experimental variation limits the number of conclusions that may be drawn from the A_1- and ω_1-values. It will be noted from Table IV that the coefficient of variation for these two parameters is 5%; this prohibits any conclusions that may be drawn regarding the viscosity dependency of ω_1 (and, therefore, also of $B[\eta,R]$). The data would imply that either ω_1 does not vary with changing R, or, possibly, it decreases with increasing R.

On the other hand, ω_2 is quite reproducible (±1%); it appears from the results in Table IV that $\omega_2\{\omega_2 = \theta \cdot [B(\eta,R)]^{-1}\}$ decreases with both increasing R- and η-values, and suggest the radial dependence of $B(\eta,R)$ to be of the form $e^{\mu R}$; in this case Eq. 6 takes the form:

$$\log \omega_2 = \log \theta - \log C^* - \frac{\mu}{2.3} R \qquad \text{(Eq. 11)}$$

where C^* is a constant. Figure 6 shows the data plotted in this fashion, and the plots are fairly linear; the slopes (calculated by least-squares fit of the data in Table IV) are shown in Table V, and are, as seen, fairly close to one another.

The data in Table IV would also suggest the dependence of ω_2 on viscosity to be an exponential decay; if this is the case, then $B(\eta,R) = \Gamma \cdot e^{\mu R} e^{\xi\eta}$; inserting this in Eq. 6 yields:

$$\log \omega_2 = \log \frac{\theta}{\Gamma} - \frac{\mu}{2.3} R - \frac{\xi}{2.3}\eta \qquad \text{(Eq. 12)}$$

If $\log \omega_2$ is plotted as a function of viscosity, four straight lines should result, one for each tube. The data plotted in this fashion are shown in Fig. 7. It is seen that fairly good linearity is exhibited, and the values of the slopes as shown in Table V are close to each other. Least-squares values of the intercepts from Figs. 6 and 7 are also shown in this table. The intercepts in Fig. 6 should be $[2 + \log \theta/\Gamma - (\mu \cdot R/2.3)]$ and the intercepts in Fig. 7 should be $[2 + \log \theta/\Gamma - (\xi \cdot \eta/2.3)]$. It is, therefore, possible to get a crude estimate of $\log [\theta/\Gamma]$ by means of the intercept values. Results of this type calculation are shown in Table V and values derived from the

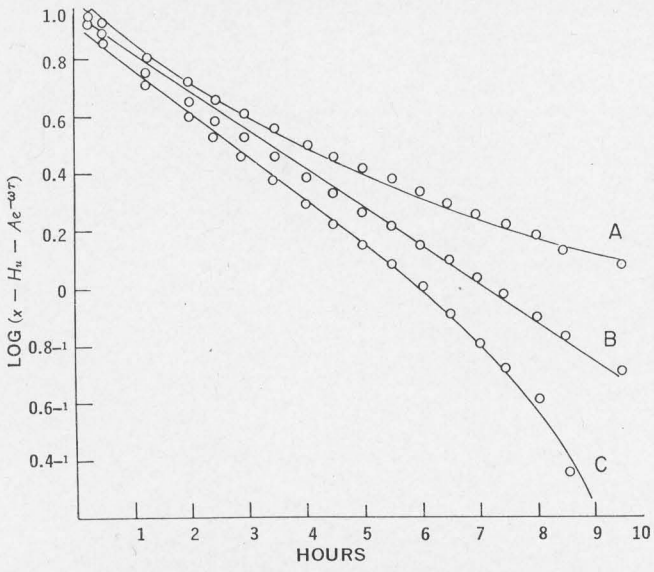

Figure 5—*Decay pattern of 11% w/v kaolin suspension in 5% v/v glycerin solution at low time values where ω_1 and A_1 predominate. Data pertain to 4.60-cm. i.d. tube. The plots demonstrate refinement of the estimate of A_2. Key: A, A_2 = 19.2 cm.; B, A_2 = 20.0 cm.; and C, A_2 = 20.5 cm.*

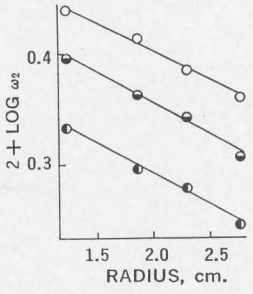

Figure 6—*Plot of the logarithm of the smaller characteristic root, ω_2, as a function of the tube diameter. ○, 0.89 cps.; ◒, 1.05 cps.; ◐, 1.20 cps.*

I. INTRODUCTION

A. General Background

The manner in which gaseous or solute molecules adsorb onto solid surfaces has been of long standing interest. It has, in the past, been the subject of considerable research efforts (1-18). The interest it has attracted in pharmacy has been in many fields; granules, powders and solid dosage forms, for instance, adsorb atmospheric moisture and this may effect such properties as flow, dissolution and stability. Whereas these effects are (mostly) unwanted, technological use has been made of adsorption phenomena at times. Purifications (mostly by charcoal) during recrystallization is one example of this.

A rather recent utilization of adsorption is the taste masking of bitter drugs by adsorption, described by Zentner (19-22). In this application montmorillonite is used as adsorbent. In practice, the drug in question is dissolved in a hydro-alcoholic medium which is added to the montmorillonite at 50-60°C. The solvent is then removed by evaporation. The (so-called) adsorbate formed in this manner is suspended in a suitable pharmaceutical medium and administered as a suspension. Although a solution is a more elegant dosage form, the advantage, tastewise,

outweighs the disadvantage, appearancewise, in many cases. Montmorillonite is superior to other adsorbents for this use.

It is remarkable that adsorbates of this type are sufficiently strong to allow masking of the taste of even extremely bitter substances, and yet allow the drug to be biologically available (23). It appears that the bonding force is sufficiently strong, or of such a nature, that taste is masked; nevertheless desorption takes place in the stomach. It might be worthwhile to elaborate, at the onset, on some of the forces that apply in such an adsorbate situation.

The bonding forces between an atom or molecule and a solid surface are electromagnetic in origin, involving the electrons and nuclei of the system. Generally, the forces can be classified into two categories: intermolecular forces and valence bonds. When the equilibrium charge distribution is such that there is no transfer or sharing of electrons among the participating atoms and the individuality of the interacting species is thus maintained, the forces are said to be intermolecular forces. Such forces are, conventionally, attractive van der Waals' forces balanced by repulsive forces originating in the proximity of neighboring electron clouds (24). The attractive forces may be further divided into several categories. If the adsorbed atom or molecule possesses no

permanent dipole or multipole moment, then the attractive interaction with the solid surface is due to non-polar dispersion forces only, unless the solid itself has an external electric field, as, for instance, in the case of an ionic crystal. In this latter case the field of the adsorbent will induce electric moments in the adsorbed atom, producing an interaction in addition to the dispersion forces. If the adsorbed atom or molecule has a dipole (or multipole) moment of its own there will be additional electrical interactions between adsorbed molecule and adsorbent of the nature usually referred to as dipole interaction. If the adsorbing surface is ionic in nature, this would be an ion-dipole interaction; if it is dipolar in nature it would be a dipole-dipole interaction. Finally if it were neither, the adsorbing molecule would induce a dipole in the surface and the interaction would be a dipole-induced dipole interaction.

Valence bonds may, of course, also be visualized as being the attractive component between adsorbing and adsorbed species. These could be hydrogen bonds (having a strength of 5-20 kcal/mole), or covalent (being about ten times as strong as hydrogen bonds). In reality this type of bond is a chemical adsorption (chemisorption); it is usually distinguished experimentally from physical adsorption by the energy of activation involved. Values as high as 20 kcal per mole have been used to define the

upper limit of physical adsorption; higher values can only arise from a chemical bond between adsorbate and surface. It is, however, not always possible to draw such a conclusion merely on energy of activation values (25), and the general question as to what constitutes a chemical, what a physical bond is, to a large measure, a matter of interpretation. To gain a full understanding of the adsorption, it is necessary to elucidate the actual forces in each case. In general, one would, a priori, discard the possibility of chemical bonding in adsorbates that mask taste but are biologically available on the grounds that the latter point is not compatible with such strong bonding.

Adsorption from solution is the means by which the adsorbates by Zentner are produced, and this manner of accomplishing adsorption is complicated by (a) polymerization, (b) competition from solvent and (c) adsorption on sites other than surface sites. It is in particular the latter two points which are of significance with regard to montmorillonite since it swells in contact with many solvents; this is due to solvent molecules penetrating the lattice and forming layers between the silicate layers, and the process is known as intercalation (26). This poses the question whether organic solutes are only adsorbed on the surface or whether they, too, are capable of intercalation. The process of swelling, therefore, may be of significance

in the mode of adsorbate formation, and for this reason, a short review of the general properties of montmorillonite is in order.

B. General Properties of Montmorillonite

(1) Composition and Structure

Montmorillonite is the common name for a group of clays of the saponite type and its general structure is shown in Figure 1. It is a complex form of magnesium aluminum silicate containing varying amounts of other metal oxides. In composition it is intermediate between aluminum silicate and magnesium silicate (saponite); these are plate-like and rod-like, respectively (27). The distortion of the plate to a rolled-up tube or rod takes place wherever magnesium has substantially replaced aluminum in the crystal lattice. The greater size of the magnesium ion causes a crystal strain resulting in this change. These views have been confirmed by electron microscopy and X-ray diffraction studies (28). The chemical composition and crystal structure of montmorillonite is similar to that of pyrophyllite (29-32). It, however, differs from pyrophyllite in that it possesses high base exchange capacity and a variable crystal spacing along the c-axis. Marshall (32) has suggested that the silicate structure has a permanent negative charge due, as in mica, to the replacement of Si^{4+} by Al^{3+} or Al^{3+} by Mg^{2+} and that the

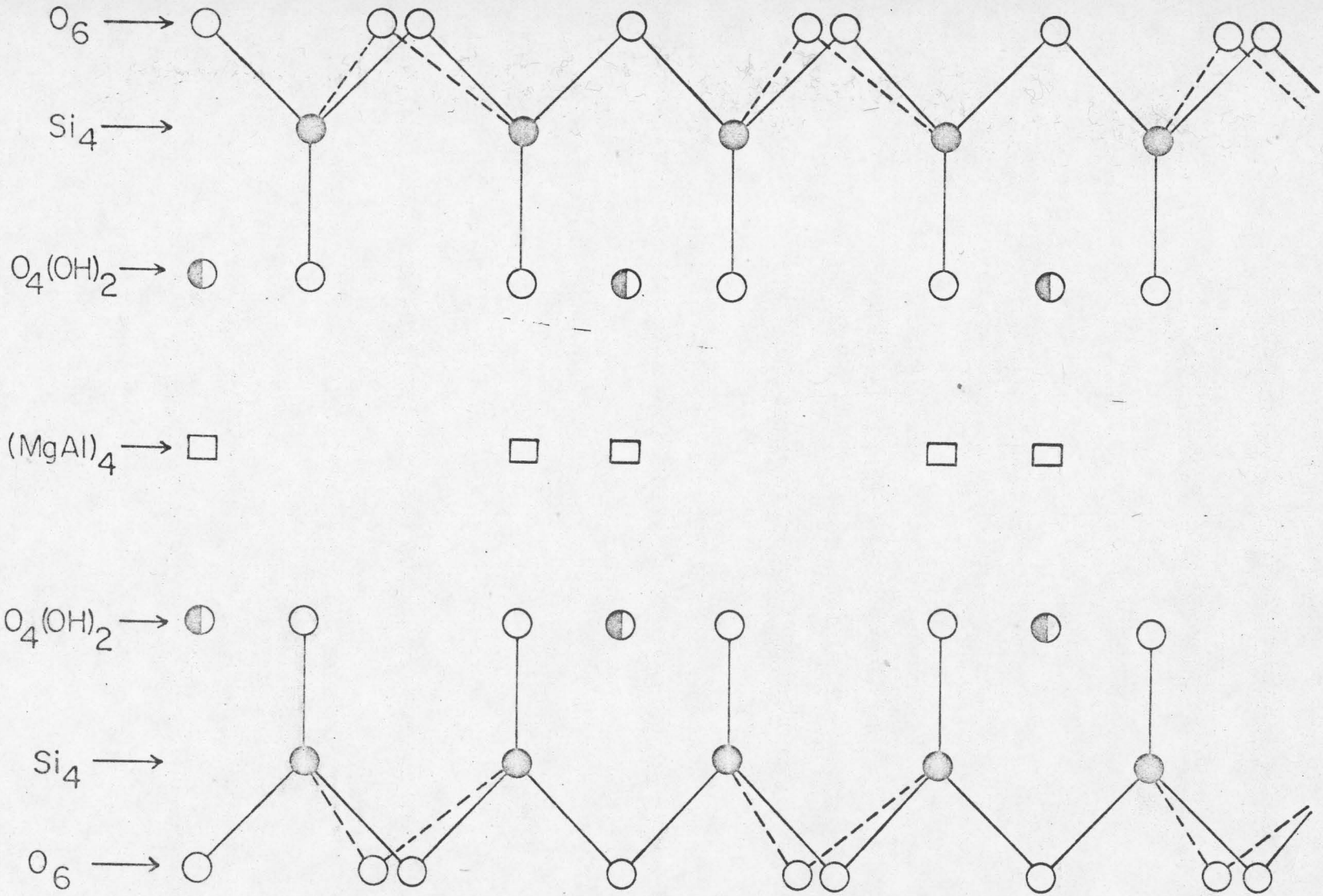

Figure 1. Structure of montmorillonite according to Mering (26).

exchangeable cations are situated on the surface or between the silicate layers neutralizing the excess charge. This is in accord with the structure proposed by Mering (26); this is shown in Figure 1; it is noted that the repeating unit is $[Al_{2-x}Mg_x,Si_{4-y}Al_y,O_{10}(OH)_2]$ so that it represents a negative charge of (x+y) per unit. Mering visualized this to be compensated for by cations which position themselves on the crystal surface, and, hence to be a measure of the exchange capacity. The ions are primarily sodium in the mined mineral, but in the "neutralized" species consist of H^+. Some of the sodium ion present in mined montmorillonite is "free" (and apparently has its origin in the processing of the crude clay) and some of the sodium is exchangeable, typical figures being: 13 mg (as Na_2O) per gram of free sodium and 19 mg (as Na_2O) per gram of exchangeable sodium (33). A typical analysis of montmorillonite will, therefore, reveal the presence of the metal ions which balance the charge, as well as magnesium, aluminum and silicate. A typical analysis of a commercially available montmorillonite would be (28): 61% of silicon dioxide, 14% of magnesium oxide, 9% of aluminum oxide, 7.2% of water and about 9% oxides of calcium, sodium, iron (III), potassium, titanium and carbon.

"Neutralized" montmorillonite is made (commercially) by mild acid treatment of the mined clay. More severe

acid treatments lead to conversion to kaolinite (34-36) which is structurally quite close; the repeating unit is $[Al_{2-x}Mg_xSi_{2-y}Al_yO_5(OH)_4]$. The special configuration is shown in Figure 2.

Bentonite U.S.P. is a mineral composed of 90% montmorillonite (37) and some of the work referred to in this introduction actually deals with bentonite purified in various ways on a laboratory scale (for example, successive centrifugation) (38,39). Wurster (40), for instance, has studied the benzoic acid-bentonite system extensively.

(2) Swellability

Montmorillonite is capable of absorbing large amounts of water; when dispersed in water, the molecules of water are adsorbed by the clay platelets and subsequent penetration of water then causes swelling. Norrish (41) has shown that the swelling phenomenon, indeed, occurs in two stages. Wai and Banker (33) have shown that increasing the concentration of electrolyte (sodium chloride) causes an 80% decrease in the swelling of the clay. The remaining 20% are then attributed to the first, adsorptive phase. The mechanism has been substantiated by vapor phase adsorption isotherms and X-ray diffraction analysis of the c-spacing (42). The swelling property is reversible, i.e., the clay can be dispersed in water, dried (at low

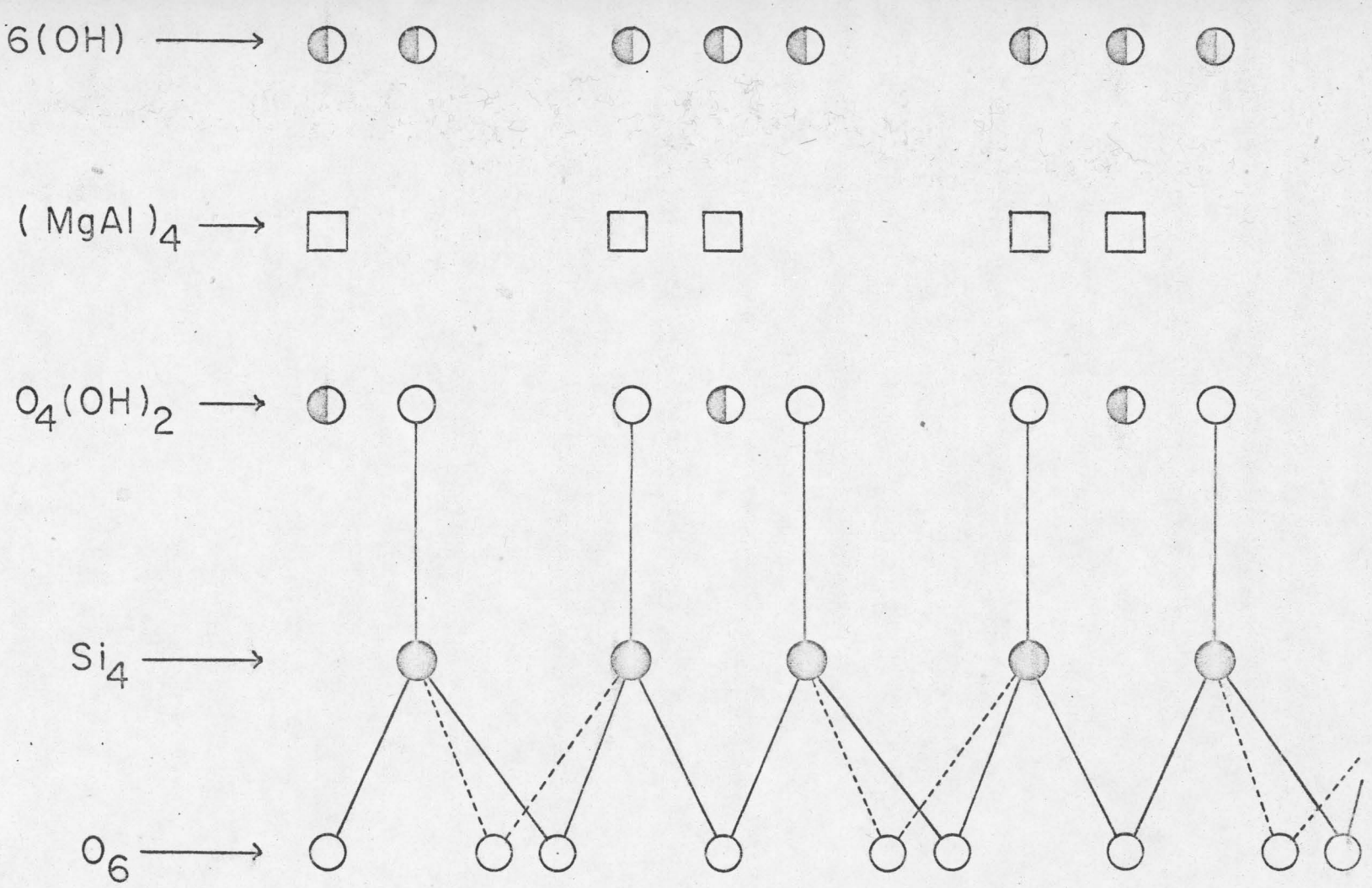

Figure 2. Structure of kaolinite according to Hoffmann (31).

temperature) and rehydrated any number of times. The process of swelling and contraction is tied in with the ability of water to penetrate in between the silicate layers of the lattice (and thereby increasing the lattice spacing) when hydrating. The spacing between the silicate layers thereby may increase from 10 Å to 20 Å.

C. Rheology, Gelation and Hydration

Due to the structural network, montmorillonite imparts viscosity to aqueous systems. The network is one of plate-to-plate, but whether this is edge-to-edge (38) or surface-to-surface (43) in a point not yet resolved. A model of positively charged edges to negatively charged surfaces has been proposed and seems consistent with experimental data (44); the gel strength depends on the number of contact points and the force between platelets is of the order of 10^{-4} dynes (45). The rate of gelation is first order with an activation energy of 14-17 kcal/mole, and the rate varies with the sixth power of the total solids content (44).

In practice the hydration is exceedingly slow (46,47); the viscosity of a dispersion, will furthermore change with time since the original structure is a random mesh (48), and rearrangements to more stable configurations will occur in time. The suspensions are thixotropic (46,49,50).

D. General Approach and Research Goal

The interlaminar distance in montmorillonite is large and the layers are held together by second order forces (51); it can vary from 10 to 20 Å or more depending upon the water content. These water molecules form layers about 3 Å thick (52), whereas the thickness of the aluminum silicate framework is 9.6 Å (53). The distance in dehydrated montmorillonite can be more than 9.6 Å, due to the presence of various cations; according to Hendrick (54) these cations place themselves in the same fashion as do the water molecules. These results have been substantiated by using small angle X-ray scattering techniques to compute the equilibrium distances between parallel clay layers in water with different electrolyte concentration. It has been suggested that the interlaminar spacing depends primarily on the sodium ion concentration and not on the concentration of anion (55). Regarding the force involved, the data obtained by means of infrared absorption spectroscopy for the sorption of water at 490°C have demonstrated that the sorbed water molecules at high temperatures no longer adsorb by intercalation but are for the most part hydrogen-bonded to the surface of montmorillonite (56-58).

MacEwan (51) pointed out that water molecules can be replaced by organic molecules and has shown that the number

of layers of organic solvent molecule present between silicate layers of the montmorillonite is as follows: heptane, none; heptanol, ethanediamine and propanol-1, one; propanediol-1,3, ethanol, ethylene glycol, nitrobenzene, methanol and acetone, two; nitromethane and acetonitrile, three.

The mode in which the organic molecules enter the layers between the clay crystals was studied by exposing the montmorillonite either to the polar or non-polar organic vapor and measuring the changes in crystal spacing (59).

Bradley (60) found a number of compounds with polyfunctional saturated aliphatic chains to bond with montmorillonite surface via a C-H-----O bond between methylene groups and oxygen surface ions. He pointed out that there is about one oxygen lacking in the X-ray diffraction diagram and that one oxygen is not significantly active in adsorbing atmospheric moisture.

Although MacEwan (61) suggested that the mechanism of formation of organic complexes by montmorillonite might be connected with surface adsorption, MacEwan and Talib-Uddin (62), in the case of alpha-zinc hydroxide, showed that the sodium salt of 1-hydroxy-2,4-dinitro-7-naphthalenesulfonic acid adsorbs by placing itself in the interlaminar positions. Cornet (2) has noted that the sorption of ammonia by unground hydrogen montmorillonite occurred on

interplanar surfaces as well as exterior planar surfaces. Ammonia, of course, is isoelectronic with water and has about the same molecular weight and hence it is not surprising that it behaves in a fashion similar to water.

In the case of protonized substituted amines (and other protonized compounds) the adsorption on neutralized montmorillonite is presumably of an ion-exchange nature. In the case of uncharged species this, however, cannot be the process. Wai and Banker (33) have shown that for many organic compounds adsorption on sodium montmorillonite is one of ion exchange.

From the description given, it is apparent that montmorillonite adsorbates could be brought about by either a surface adsorption or by an adsorption of the type described for alpha-zinc hydroxide or ammonia, where the "adsorbing" molecule actually penetrates into the crystal.

The taste masking of bitter drugs by adsorption must involve bonding forces of some strength. It is the purpose, here, to elucidate what forces participate in this bonding in an attempt to throw light on the apparent paradox of taste-masking vis-a-vis physiological availability. In cases where ion exchange plays a role, the bonding forces will (presumably) differ from forces involved in situations where ion exchange can be excluded as a possibility. It is prudent to approach the simplest case first, and the intent here has been limited to the study of compounds that will

not adsorb by ion exchange. Once the mechanism has been elucidated in such a case, further studies may be conducted to describe the bonding in more complicated situations.

II. EXPERIMENTAL

A. Experimental Design

Adsorption isotherm experiments from solution are traditionally carried out by exposing the adsorbent in a weighed amount to a solution of the adsorbing molecule in an appropriate solvent. By determining the concentration of solute prior to and after equilibration, the amount of solute adsorbed can be determined by difference. The problems in this type experimentation are several-fold. Both solute, solvent and adsorbent must be anhydrous (unless adsorption from water is being studied), the temperature must be carefully controlled, and the analytical procedure must be of a fairly high order of precision. The latter is necessitated by the fact that amounts adsorbed are differences between fairly large numbers. Determination of optimum amounts of adsorbent and concentration of solution is, therefore, necessary to carry out adsorption experimentation successfully.

It is of importance to know the surface areas involved in the adsorption process. To this end the surface may be determined by conventional means (B.E.T.) but it is not a priori to be assumed that surfaces available to nitrogen in the gas phase are the same as those available to a solute in liquid-solid contact.

B.E.T.-measurements, nevertheless, must be made, and they do, whether their quantitative results do or do not reflect available surface in liquid-solid experimentation, supply information of the active sites present on the surface.

It is obvious that the adsorption isotherms will be a function not only of temperature, but, for the same solute and adsorbent, also a function of solvent. For this purpose macroscopic properties of the solvent should be available to gauge which property affects the adsorption; such properties as polarity, basicity, density or viscosity might be visualized as being of importance; it shall be shown that the dielectric constant is the important parameter, and for this purpose, determination of dielectric constants are a necessary step in the experimental make-up.

Since capability of working under anhydrous conditions should be available, and since methods for dehydrating substances at room temperature are a necessity, high vacuum facilities are essential as part of the available equipment.

A detailed description of the equipment and the experimental procedures is part of the following text.

B. Vacuum Rack

For the purpose of B.E.T. surface measurements and for dehydrations at room temperature at high vacuum, a vacuum rack was built. The experimental design of the vacuum rack

is shown in Figure 3 and a schematic drawing of it is shown in Figure 4. The set-up makes possible pressures as low as 10^{-4} Torr and as high as 10^{2} Torr (63). This permits determination of gas adsorption over a wide range of pressures as required for differentiation between sites of different adsorption energy levels.

The vacuum rack is built entirely of Pyrex glass (except graded seals on electrodes as shall be mentioned later). All stopcocks are high precision bore stopcocks from Krebs and Eck Corporation in Long Island, N.Y. Two types are used, and will be described at the onset: (a) capillary stopcocks, which are hollow, ground, straight bore stopcocks, and (b) vacuum stopcocks. These latter are of the double-angular design; here the stopcock is seated in the housing, the bottom of which is spherical and attached directly to the vacuum end of the system. In this manner, the atmospheric pressure on the outside of the stopcock aids in the tight seating of the closure.

The vacuum rack consists of a main manifold of 35 mm I.D. Pyrex glass tubing, closed off and rounded at one end and, at the other end, connected to a 45/70 vacuum stopcock. This in turn is connected to the main trap, which is an internal seal with a 35/45 ground joint. The removable (female) part is 40 mm I.D. Pyrex stock, with the ground joint in one end and round-closed at the other. A

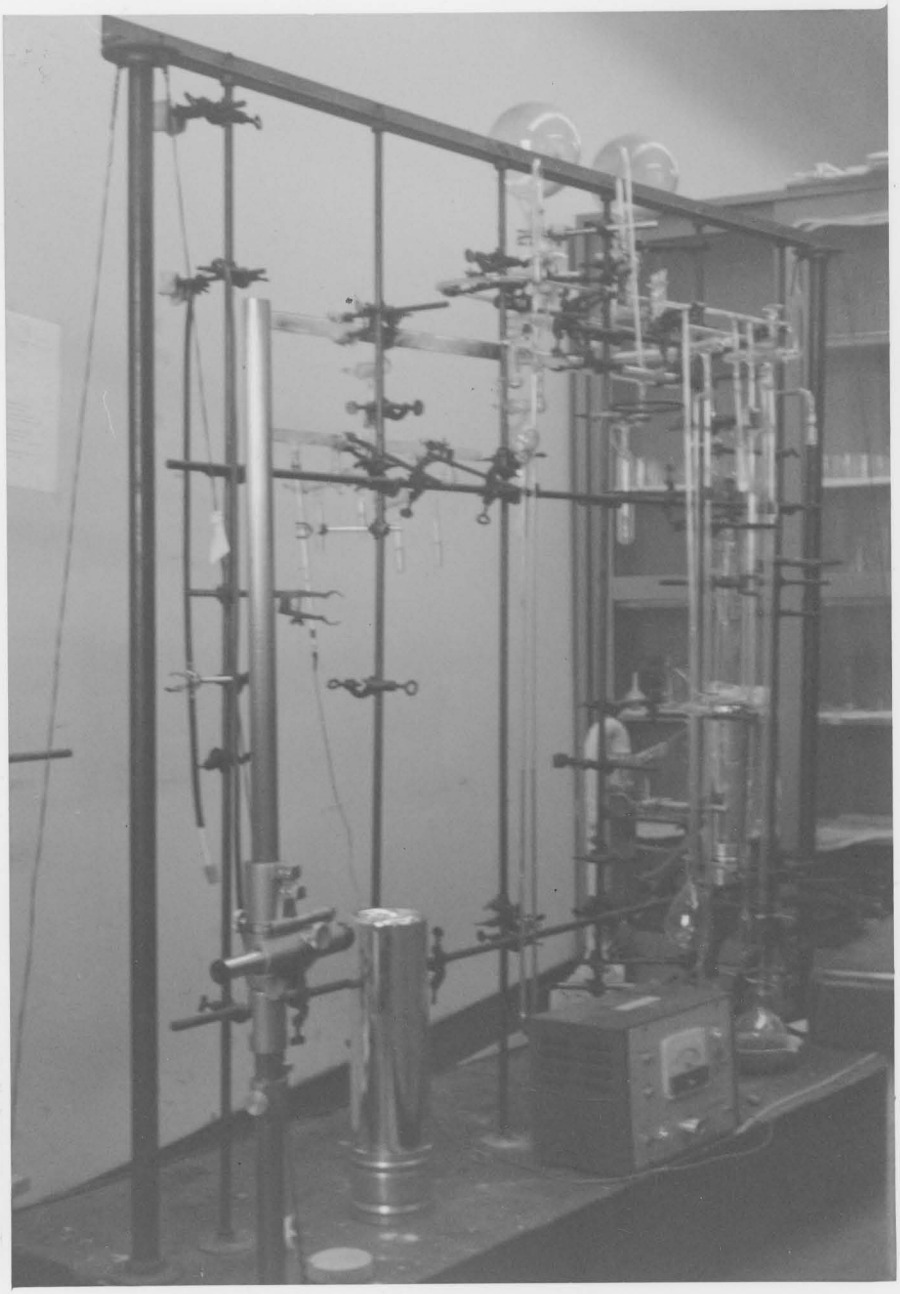

Figure 3. Vacuum rack.

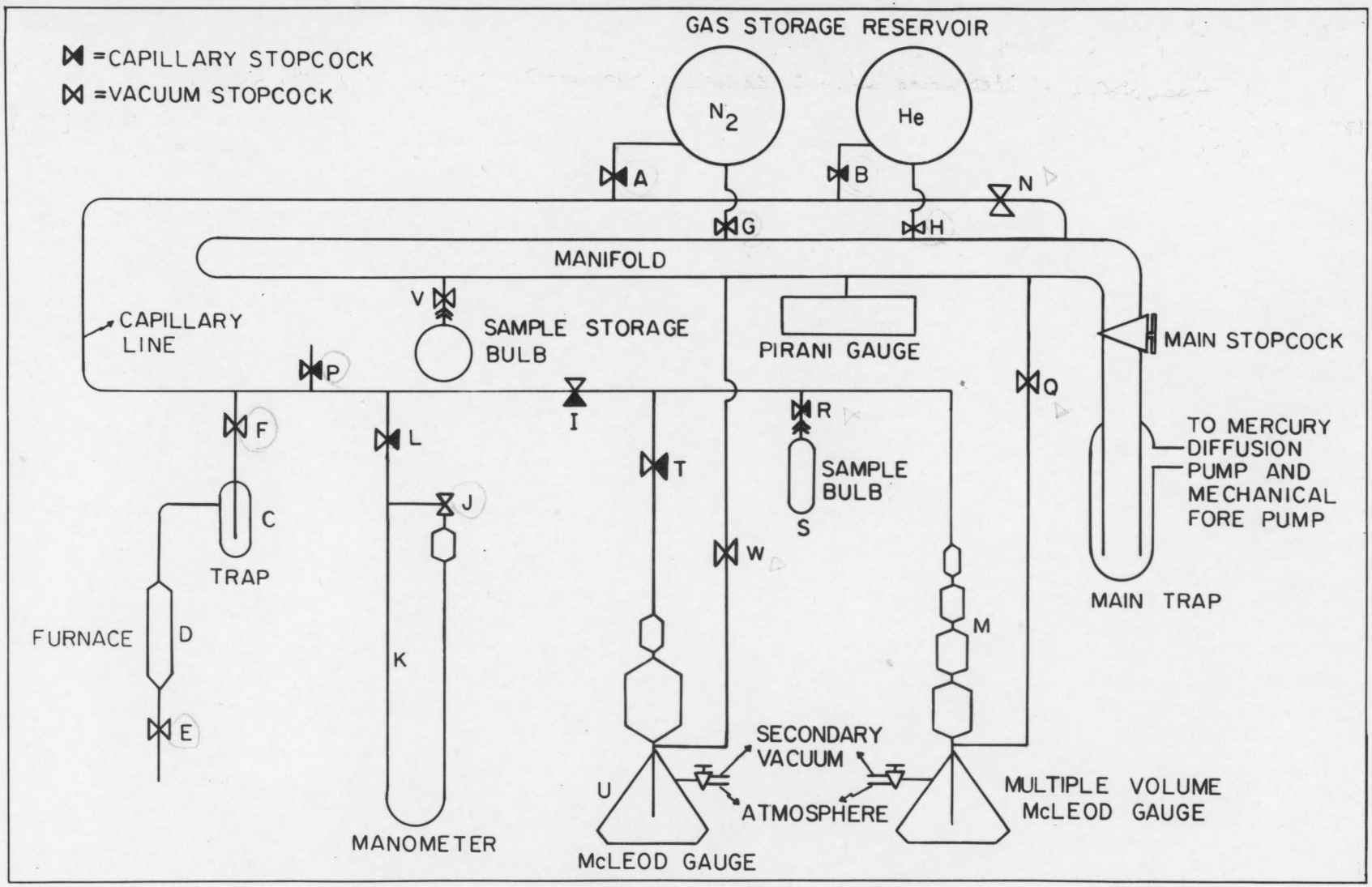

Figure 4. Schematic drawing of vacuum rack.

sidearm connects it to a mercury diffusion pump, which in turn is connected to a mechanical fore pump.

The diffusion pump is a conventional type water-cooled apparatus. The distillation bulb has a 150 cc capacity and is connected to the condenser by an asbestos-wrapped 18 mm bore distilling arm. A Glas-Col heating mantle is used to heat the mercury, and the power is supplied to the heating mantle from an autotransformer.

A capillary line is connected to the main manifold via a capillary stopcock, N.

Two-liter round bottomed flasks, tapered down at the neck, are fused onto tubing and via vacuum (G, H) and capillary (A, B) stopcocks connected to the manifold and capillary lines, respectively. These bulbs are used for storage of nitrogen and helium. A furnace (D) consisting of 30 mm I.D. tubing is filled with copper filings, wrapped with Nichrome wire and insulated with asbestos and then connected via a trap, C, to the capillary line via a spring-loaded pressure stopcock, F. The outlet end is connected to a spring-loaded stopcock E to 5 mm straight Pyrex tubing. Several capillary stopcocks (P) are connected to the capillary line; they are externally equipped with 10/20 joint which allows (a) venting, and (b) introduction of gases or vapors into the vacuum rack. A mercury manometer (K) is connected to the capillary line via a capillary stopcock, L; by opening the stopcock J, the

manometer can be completely degassed. Closing J, then accomplishes a permanent vacuum on the right side of the manometer.

The far end of the capillary line can be isolated by means of capillary stopcock, I. At this end a McLeod gauge, U, is connected to the capillary line via a stopcock, T, attached directly to the capillary measuring tubing of the gauge. The smaller (ca. 4 cc) and larger (ca. 300 cc) reservoirs of the gauge allow a ca. 10,000:1 compression ratio, since the smallest subdivision in the measuring tubing is ca. 0.04 cc. The operation and calibration of this is described in detail below.

The bottom part of the McLeod gauge is filled with mercury. A side arm connects the headspace of the mercury reservoir to either a secondary (mechanical) vacuum pump or to the atmosphere. If the sidearm is connected to the atmosphere (with T closed), the mercury will rise; once it passes the connecting point between the large reservoir and the sidearm leading to W, the gas in the system is divided into two portions. By raising the mercury all the way to the top mark in the measuring capillary, the gas is compressed about 10,000-fold; by applying vacuum to the sidearm via W, the measured pressure is about 10,000 times the pressure of the uncompressed gas. Mercury levels are measured with a precision cathetometer (Gaertner Scientific Corporation, Chicago), so that pressures down

to 1 mm (actually 0.05 mm Hg) can be measured accurately; this, then, means that pressures of 10^{-4} Torr (0.1 micron) can be monitored. In terms of gas amounts this amounts to n = (1/760) 0.04/(82 x 300) = i.e., of the order 10^{-8} moles being the lower level of detection. The main sidearm of the McLeod gauge is connected to the main manifold, via the stopcock W.

A joint of the type P is attached via a stopcock R to the capillary line. This allows attachment of a sample bulb, which can contain samples, the surface of which are to be measured. Both sample bulb and the tubing beyond stopcock R are equipped with ground joint (10/20), the sample bulb having the female joint.

The end of the capillary line is connected to a variable volume McLeod gauge, which operates in the same fashion as the high compression gauge. The operation and calibration of this gauge will be described at a later point. The sidearm of this gauge is connected, via a stopcock Q, to the main manifold.

The electrode of a Pirani gauge is attached to the main manifold. These electrodes are metal leads that are attached to a piece of Pyrex tubing via a graded seal, i.e., the initial seal to the metal leads is soft glass (which seals with metal) and consecutive layers of harder glass are fused onto this, eventually sealing it to the Pyrex tube. These electrodes are available commercially

(Autovac Corporation). The leads are connected to the Pirani gauge, which, in essence, is a Wheatstones bridge. The conductivity of a gas is a function of its pressure, and the Pirani gauge measures the conductivity and translates it into microns of pressure. The standard calibration applies to dry air, and if the gauge is to be used for precision measurements of other gases, it must be calibrated against them, by checking needle position against pressures measured on the McLeod gauge.

The purpose of the rack is, of course, to provide a means of attaining high vacuum at any spot. The Pirani gauge is here used as a check to ascertain that low pressures (below one micron) exist in the system at all times. To attain such low pressures necessitates certain precautions. First of all, as has been mentioned, precision bore stopcocks were used. Special previously degassed stopcock grease (Apiezon N) was used. All joints were glass blown and fresh surfaces created by blowing not by filing. (File marks introduce small pieces of metal into the Pyrex, and since these do not seal intimately they eventually degenerate into a leak.) The rack was checked for leaks whenever the Pirani gauge so indicated. This was done by means of a Tesla coil. Manipulation of stopcocks (i.e., isolation of certain areas) will, with skill, pinpoint the position of the pin hole rapidly. Pinholes, when they occurred, were repaired by glass blowing. All

glass stock was cleaned with nitric acid, benzene, nitric acid and water (in that order) prior to fusing onto the system.

C. General Operation of the Vacuum Rack

The first step in operating the vacuum rack is to open the main stopcock. If stopcock N and G are closed, this will evacuate the main manifold; but with the appropriate stopcocks open, evacuation of any part or the entire system is possible. Moisture has a tendency to cling to glass, and degassing operations are very lengthy (days) if a means of removing moisture is not provided. For this purpose the glass stock is cleaned meticulously prior to fusing it into the system. Nevertheless, moisture will appear in the system every time its interior is exposed to the atmosphere (e.g., when vented via stopcock P), and for this purpose, the main trap is always cooled with liquid nitrogen (in a Dewar jar), when the rack is operating.

Pressures in the system of over 10 Torr can be measured on the mercury manometer, K, and lower pressures can be monitored on the high compression McLeod gauge, U.

Samples can be degassed and dehydrated in sample bulbs at stopcock V, with all stopcocks other than V and the main stopcock closed.

By suitable manipulation of stopcocks, nitrogen or helium can be bled into any part of the system.

Pressures in the manifold or capillary line can be measured by opening stopcock W (or T), then closing T, raising the mercury from the reservoir evacuating the sidearm and measuring the pressure differential at the suitable calibration mark in the measuring capillary (below T). For accurate measurement it is, therefore, necessary to have precision calibration of the McLeod gauge.

D. Calibration of McLeod Gauges

The high compression McLeod gauge was calibrated prior to assembly. The capillary tube of a capillary stopcock was filled with mercury to various levels, each of which was marked by an etching with a diamond pencil. By weighing before and after addition of mercury, recording the temperature, and using the density of mercury at that particular temperature, the volumes corresponding to each mark can be determined. The large compression reservoirs were calibrated in a similar fashion but with water. After calibration the four parts (the mercury reservoir, the two compression reservoirs, and the capillary stopcock with tube) were fused together by glass blowing, and connected to the main manifold via

the sidearm and stopcock W and to the capillary line via the non-calibrated part of tube on stopcock T.

A similar procedure was used on the other McLeod gauge, the multiple volume gauge, except here all calibrations were made with water, due to the higher volumes involved. A schematic, showing all volumes, is presented in Figure 5.

E. Gas Charging of Storage Bulbs

Helium and nitrogen are used in B.E.T. surface measurements. High purity tank helium and nitrogen are used (Matheson, Carlstadt, N.J. and Chemetron, Chicago, Illinois, respectively). In introducing the gases from the cylinders into the system, it is necessary to connect the outlet of the cylinder to stopcock E, by means of rubber tubing. This by necessity introduces (a) air, i.e., oxygen and (b) moisture. In order to remove these impurities prior to introduction of the gas into the storage bulb, they are led over copper at 400°C (furnace) and then through a (liquid nitrogen) cooled trap. The first operation removes oxygen, the latter moisture.

The pressure for filling gas into a storage bulb is, then, as follows: all stopcocks are opened, except P, V, I, W, Q, and E, and the system is thoroughly evacuated. Stopcocks A, B, G and H are then closed. E is then connected via rubber tubing. The needle valve of the gas

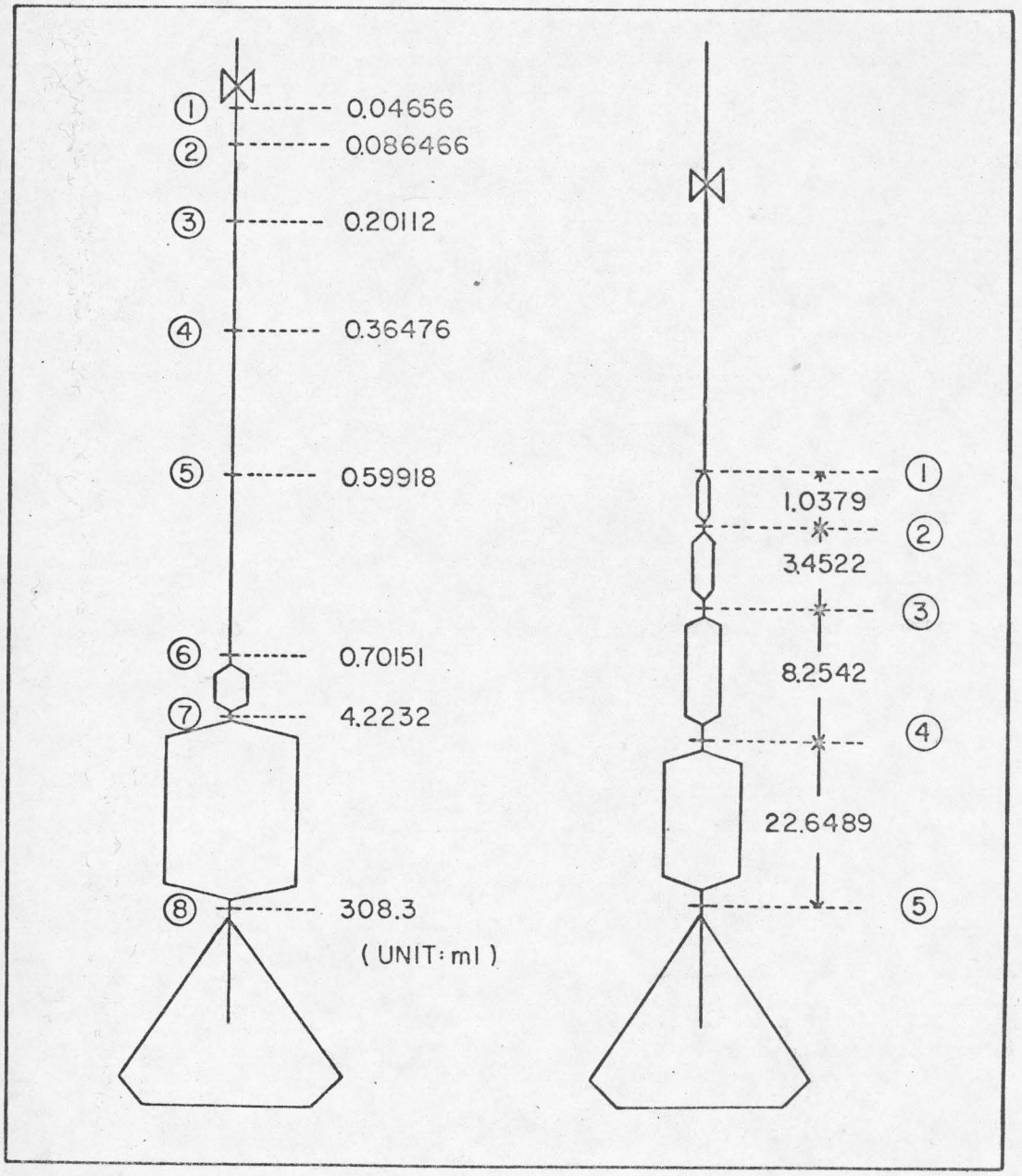

Figure 5. Schematic diagram of the adsorption gas glass bulbs indicating the volume of individual bulb and tubing.

cylinder is opened slightly and about 500 Torr of gas is introduced (as measured on the mercury manometer). The system is evacuated, again flushed with gas. The system is again evacuated. The furnace leads are connected to a Variac, at a predetermined setting which will effect the correct temperature in the furnace. The trap C is cooled by means of liquid nitrogen (in a Dewar flask), and A is now opened, and by opening the needle valve on the cylinder gas is allowed to flow in slowly until a pressure of about 650 Torr is measured on the mercury manometer. A is then closed, E and F are closed and the entire system once more evacuated. In this manner one storage bulb is filled with nitrogen, and the other with helium.

F. Volume Calibration in the Rack

Once the volume of the segments of the McLeod gauge are known, any volume in the remaining part of the vacuum rack can be calculated. The general procedure for obtaining an unknown volume (y) from a known volume (x) to which it can be connected by the opening of a stopcock is to evacuate x and y, and then charge helium into x to a pressure of P_x (cm Hg). Opening the stopcock between x and y, and re-registering the pressure P (cm Hg) allows calculation of y from the gas law:

$$P_x \cdot x = P(x + y) \qquad \text{(Eq. 1)}$$

The known volumes are the volumes in the high compression McLeod gauge, U, (referred to in the following simply as U) and the bulbs of the multiple volume McLeod gauge M (referred to in the following simply as M). The sum of the bulb volumes of M will be denoted V' below.

For operation of the rack, it is important to know the volume of certain sections of the rack. For B.E.T. measurements, to be described shortly, it is important to know the volume of the capillary line confined by stopcocks I, T, R and the upper mark of gauge M (V_c). It is also important to have an expansion (discard) volume of known capacity, and the main manifold volume was used for this purpose (V_m). Finally, in B.E.T. measurement, the volume of the space in the sample bulb which is not occupied by the sample is needed. Helium does not adsorb on surfaces at 25°C and volume determinations are therefore carried out at 25°C using helium to perform the expansion experiments.

For the convenience of further discussion the notations of the various volumes are listed below:

Gauge U, volume to mark 8: 308.3 cc

Gauge U, volume to mark 7: 4.2232 cc

Capillary confined by I, T, R and 1-mark of M: V_c

Sample Bulb S containing a weighed amount of montmorillonite: V_s (free space)

Manifold plus Sidearm to Gauge M: V_m

Volume of Bulbs in Gauge M: V'

The method leading to Eq. 1 was employed for determining the volumes V_c, V_s, and V_m as described below.

During all operations in the following the main trap is cooled with liquid nitrogen. Stopcocks A, B, G, H, F, J, E and P are in general considered closed in the following, unless otherwise stated. The entire system was evacuated by opening the main stopcock and all stopcocks (other than the ones specified and the three-way stopcocks at the two McLeod gauges) opened. The main stopcock was closed and the effectiveness of degassing and tightness of the system insured by leaving the system undisturbed for 5 minutes and making certain that the pressure on the Pirani gauge (or as measured on the high compression McLeod gauge) had not risen above 0.1 micron. Stopcocks N, W, R and Q were then closed. The mercury levels of the McLeod gauges were brought up above the 8 and 5 marks, and H was opened briefly. This introduced helium into the capillary system. T was then closed, and the system external to the gauge U, evacuated by opening stopcocks W and Q and lowering the mercury level in M below the 5-mark.

The mercury level in U was then brought up to the 7-mark, and the mercury level in the sidearm and at the 7-level measured with the cathetometer. The difference (P_o) should be about 30 cm, i.e., the number of moles of helium should be about $n = \frac{30}{76} \times \frac{4.2232}{82 \times 298}$ (if the temperature is 298), i.e., about 7×10^{-5} moles. If the

amount of helium was insufficient (i.e., if the recorded pressure difference was less than 30 cm) then more helium was introduced in a manner similar to the one described. If the pressure was too high, part of the helium was discarded by closing W, lowering the mercury level in U to below the 8-mark, and then raising it again. This would discard about 1/4 of the helium in the U-gauge. W was then opened and the amount of helium in the sidearm discarded.

The mercury level in gauge M was now raised to a point between marks 4 and 5, and stopcocks R, I and Q closed. The mercury in gauge U was next lowered to the 8-mark and stopcock T was opened. This would depress the level of the mercury in gauge M a little, and it is for this reason that the level was kept slightly high at the time T is opened. The mercury levels in U and M were then adjusted to positions 8 and 5, respectively, and T again closed. The system external to gauge U was evacuated, the mercury level in U raised to the 7-mark and the new pressure difference (P_1) recorded on the cathetometer. The application of Eq. 1 to this situation now yields:

$$[V_1 + 308.3] \cdot P_1 \frac{4.2232}{308.3} = 308.3\ P_o \cdot \frac{4.2232}{308.3}$$

or simply

$$[V_1 + 308.3]P_1 = 308.3\ P_o \qquad \text{(Eq.2)}$$

where V_1 is the volume consisting of the capillary volume V_s plus the (known) volume of the bulbs (V') in gauge M, i.e., $V_1 = V_s + V'$. Stopcocks T and R were then opened, mercury levels adjusted in gauges U and M to 8- and 5-positions, respectively, T closed, and the pressure at the 7-mark (P_2) measured again. This, of course, would be smaller, since the expansion volume, in this case, included the volume of the sample bulb S (V_s). The expansion volume (V_2) can then be found by

$$[V_2 + 308.3]\, P_2 = 308.3\, P_o \qquad \text{(Eq. 3)}$$

where $V_2 = V_c + V' + V_s$. There was as mentioned a need to have a large discard volume of known magnitude for some operations, and the volume (V_m) of the manifold was determined for this purpose: The main stopcock was closed, stopcocks Q and T were opened, and the mercury level in gauge M lowered below the 5-mark. This expands the gas in gauges U and M and the capillary volume into these volumes plus the volume of the manifold. In other words, if the system is now equilibrated the expansion volume will be $V_3 = V_c + V_s + V' + V_m$. After equilibration, stopcock T was closed and the mercury level in U brought up to mark 7, and the pressure difference, P_3, measured with the cathetometer. P_3 and V_3 are now related by the equation

$$[V_3 + 308.3]\, P_3 = 308.3\, P_o \qquad \text{(Eq. 4)}$$

G. B.E.T. Surface Measurements

The system was evacuated by opening all the stopcocks (except A, B, G, H, P and F). The main trap was cooled with liquid nitrogen and it was ascertained that the pressure was less than 0.1 micron. The mercury in gauge U was then raised halfway up into the large reservoir, thereby isolating the gauge space from the remaining system. The stopcocks N, I, W and Q were closed and stopcock A was opened thereby introducing nitrogen into the capillary line. Stopcock I was then opened carefully to allow nitrogen to flow into the gas analysis section. Care was taken not to let the mercury level fall below the dividing T's of the two McLeod gauges. The stopcocks A and I were then closed and the mercury level in gauge M was raised until the mercury level in gauge U was at the 8-mark. The pressure P_A was recorded with the cathetometer and the number of moles (n_a) of nitrogen in gauge U was calculated. Stopcock T was then closed, stopcocks I and N opened and the nitrogen remaining in the capillary line of the system was evacuated.

The sample bulb S was then cooled with liquid nitrogen in a Dewar flask; cooling was maintained for at least one-half hour to permit the sample to reach thermal

equilibrium with the liquid nitrogen. This is a slow process due to the vacuum in the sample bulb. The mercury was now raised in gauge M to a position about halfway up through the bulbs. Stopcock T was then opened and the mercury level raised in gauge U until the level in gauge M is at position 5. If the level in M were raised further, the mercury level in gauge M would fall below the T to the sidearm and the gas would be lost. This is the reason for originally raising the level to midway up the bulbs in gauge M. The mercury level in gauge M is again raised halfway up the length of the bulbs, and the process repeated until the level of the mercury in gauge U is at mark #1. At this point virtually all the gas in gauge U has been transferred to the space occupied by the sample bulb and gauge M. The pressure (P_B) is recorded and the number of moles (n_b) of nitrogen remaining in gauge U is calculated from the known volume at mark #1 (0.04656 cc). Stopcock T is then closed, and the number of moles of nitrogen in the sample section is now known to be

$$n = n_a - n_b.$$

The mercury level in gauge M was then lowered to mark #5, and the system is left standing for 24 hours. This is the length of time required for initial equilibration, the limiting factor being temperature equilibration in the sample bulb. Care is taken to

maintain the level of liquid nitrogen at a preset mark of the capillary tube above the neck of the sample tube.

After equilibration, the difference between the mercury levels at mark #5 of gauge M and the mercury level in its sidearm was determined by means of the cathetometer.

The mercury was then raised to mark #4, equilibration (at this point requiring about one to two hours) achieved, and the pressure differential recorded. This was then repeated for the remaining marks on gauge M, i.e., eventually measuring the pressure at mark #1.

The mercury was then lowered to mark #2, the pressure recorded, then to mark #3, and so on. The reason for recording the pressures in descending fashion as well as in ascending order, is to check porosity characteristics of the powder. The mercury level in gauge M was then lowered below the sidearm level, Q and the main stopcock opened, and the Dewar jar removed from the sample bulb. The system was evacuated.

In some experiments the initial amount of nitrogen was not recorded (especially where high pressures of nitrogen are involved). In this case, the amount of nitrogen was determined after the pressure recordings by lowering the level of mercury in gauge M below that of the sidearm, keeping the main stopcock closed, and removing the liquid nitrogen from the sample bulb. The level of mercury in gauge U was then raised to a level halfway up

the large reservoir (i.e., between the 7- and 8-marks) and the sample was allowed to warm up. In this manner the nitrogen was allowed to escape into the large expansion volume of the manifold, and hence pressures above one atmosphere would not be created in the system. The level of the mercury in gauge U was continually watched, and in essence this gauge was used as a gross manometer in the operation to insure that the pressure remained below atmosphere. When the sample had reached room temperature (when the pressure was steady), the mercury level in gauge U was lowered to level 8, stopcock T was closed and the mercury raised to the 7-mark. The pressure was recorded (P'). The number of molecules in the system (n) was then calculated from the relation corresponding to these measurements:

$$\frac{P'}{76}\ \frac{4.2232}{308.3}\ V_3 = n \cdot 82 \cdot 298 \qquad \text{(Eq.5)}$$

In whichever way the number of moles of nitrogen introduced into the system is calculated, the general calculation for number of moles adsorbed is carried out as follows:

Let n be the number of moles introduced into the system (i.e., $n = n_A - n_B$ or as given by Eq. 5). After cooling the sample bulb, the number of molecules (n_g) present in the gas phase is given by:

$$n_g = \frac{P_a}{82.1 \cdot 76} \left[\frac{V_b}{T} + \frac{V_s}{77}\right] \qquad \text{(Eq. 6)}$$

V_b is here the volume of the bulbs not occupied by mercury in gauge M plus the capillary volume (V_c).

The difference $n - n_g$ then reflects the number of moles of gas adsorbed at the pressure P_a registered.

It will be noted that in each experiment four sets of n_g-values and corresponding P_a-values are obtained. The experiments were repeated with different initial amounts of nitrogen, each experiment providing four more points. All the values were then compiled and graphed to give the entire isotherm.

H. Chemicals

The montmorillonite used was micronized, neutralized montmorillonite as received from the supplier (R. T. Vanderbilt Co., Inc., 230 Park Avenue, New York, N.Y. 10017). Except where noted the entire study refers to one single lot (Type S-6814, Lot FX 329). In some of the initial studies (relative to benzoic acid isotherms), different lots were tested giving results identical to those found with the stated lot. Samples were also prepared by acid washing the montmorillonite with 0.1 N HCl, but several difficulties arose; grinding to a uniform particle size is difficult, and in the cases where this was attempted results did not differ from samples

prepared with the lot as received from the supplier. Acid treatment entails the danger of chemical change of the clay. One sample treated with 0.2 N HCl changed, presumably to kaolinite or ilite. This is in line with the findings of Schofield (34), Caillere, et al. (35,36) and Weaver (64) who found that the pure H-form is difficult to obtain with acid because Al^{+++} ions are liberated from the interlaminar space and then remain as cations on the surface.

Drying of the sample is obviously of importance; this cannot be accomplished by heat without possibility of chemical changes, and samples were therefore placed in a bulb with a 10/30 ground joint and attached to point P of the rack, and degassed for two weeks at room temperature. The equilibrium moisture pressure of these samples was less than 1 micron Hg. The samples were stored in vacuum desiccators after drying.

Benzoic acid (Merck) was recrystallized from boiling water and the crystals were colorless, needles of melting point 121.6-121.8°C (65).

Solvents: Methyl alcohol (Mallinckrodt), 2-Propanol (J. T. Baker), n-Amyl alcohol (Baker and Adamson), n-Propanol (Mallinckrodt), Ethyl alcohol (Commercial Solvents Corp.), Isobutyl alcohol (Mallinckrodt), Isoamyl alcohol (Baker and Adamson), tert-Butanol (Fisher Scientific Company), Acetonitrile (Fisher Scientific

Company, Certified Reagent), and Dichloroethane (Aldrich Chemical Company) were all reagent grade and were used without further purification.

Benzodiazepine derivatives tested were kindly supplied by Hoffmann-La Roche, Inc., Nutley, N.J. and were regarded as pure and were used without further purification. These compounds have all been subjected to stringent quality control and have been shown by TLC, polarography and other highly sensitive methods to be of 99.8% purity or better. The compounds tested are listed in Table I. Oxazepam (7-chloro-1,3-dihydro-3-hydroxy-5-phenyl-2H-1,4-benzodiazepine-2-one) was kindly supplied by Wyeth Laboratories, Inc., Radnor, Pa., and was used without further purification.

Moisture determinations were indicated at various stages of this study and were performed by Karl Fischer titration. The Karl Fischer reagent is a solution of iodine, sulfur dioxide and pyridine in methanol; reagent purchased from Fisher Scientific Co. (Catalog No. So-k-3) was used. The reagent was restandardized daily by titrating known quantities of water with it before use.

TABLE I

Structure Relationship of Benzodiazepine Derivatives

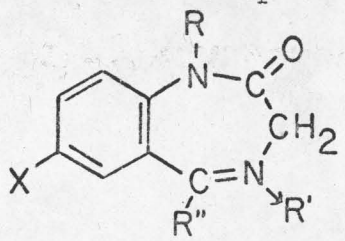

No.	X	R	R'	R"	Molecular Weight	λ_{max} (mμ)	Extinction Coefficient	Note*
1	Cl	CH_3	-	C_6H_5	285	230	33097	a
2	Cl	H	O	C_6H_5	287	236	29000	b
3	Br	H	-	C_5H_4N	316	232	32000	c
4	NO_2	H	-	C_6H_5	281	198	28000	d
5	NO_2	CH_3	-	O-C_6H_4F	312	199	21500	e
6	NO_2	H	-	O-C_6H_4Cl	316	201	30500	f
7	Cl	H	-	C_6H_5	287	230	32500	g

Notes*

a) Diazepam

b) 7-Chloro-1,3-dihydro-5-phenyl-2H-1,4-benzodiazepine-2-one-4-oxide.

c) 7-Bromo-1,3-dihydro-5-(2-pyridinyl)-2H-1,4-benzodiazepine-2-one.

(Cont.)

TABLE I - Cont.

Notes*

d) 7-Nitro-1,3-dihydro-5-phenyl-2H-1,4-benzodiazepine-2-one.

e) 7-Nitro-1,3-dihydro-1-methyl-5-(2-fluorophenyl)-2H-1,4-benzodiazepine-2-one.

f) 7-Nitro-1,3-dihydro-5-(2-chlorophenyl)-2H-1,4-benzodiazepine-2-one.

g) Oxazepam (hydroxyl group substitutes one hydrogen at position 3).

I. Adsorption Measurements

In an adsorption isotherm, the quantities measured are the amount of solute in solution before and after attainment of equilibrium; the difference yields the amount of solute on the adsorbent. In other words, the adsorbent is added to a solution of the solute, which has been previously assayed, and then assaying the solution after equilibrium is established. By multiplying the assays ($C_{initial}$ and C_{final}) by the volume of solution, the total amounts in solution before and after are obtained. The difference is C_{solid}, the amount adsorbed by the solid. This latter figure is, in essence, the difference between two large figures, and good assay precision is therefore a mandate for obtaining good adsorption isotherms. Also a fair amount of initial investigation is necessary to establish the optimum concentrations of solute for a particular isotherm. The isotherms, if C_{solid} is plotted versus $C_{solution}$, will be downwards concave and asymptotic; it is important to obtain points in the curved part of the plot (i.e., not just saturation, or plateau values), and for this reason as well, it is essential to operate in optimum concentration ranges. The various points of the isotherm can be obtained in two fashions. Either various amounts of adsorbent can be added to a stock solution of solute in solution, and assays performed before and after as

described, or, a standard amount of adsorbent can be added to various concentrations of solute. In this study the former procedure has been used most often, but the latter has also been applied. The analytical methods for benzoic acid isotherms and benzodiazepine derivative isotherms differ and will be described separately.

Benzoic acid isotherms were performed as follows: approximately 4 grams of montmorillonite which had been stored in a vacuum desiccator were rapidly transferred to a tared Erlenmeyer flask with ground joint top and stopper. 100 cc of benzoic acid stock solution in anhydrous solvent were then added and the flask weighed again and sealed with parafilm. The flask was shaken mechanically at 25°C for 48 hours on a Metabolyte Water Bath Shaker (New Brunswick Scientific Co., Inc.). The sample was then centrifuged at 1500 rpm and a large aliquot of the supernatant titrated with 0.02 N NaOH. The stock solution was titrated and the amount adsorbed was calculated by difference. Blanks, containing no benzoic acid, were treated similarly and showed no significant titer. The experiments were then repeated using different concentrations of benzoic acid. Experiments were performed in the same fashion using the following solvents: methanol, ethanol, tertiary-butanol, isopropanol and water-isopropanol mixture (50% w/w).

The benzodiazepine isotherms were determined by making a stock solution of the solute and adding to it various amounts of montmorillonite and proceeding in the fashion described above. Stock solutions were assayed spectrophotometrically before and after by using a Cary 14 (Applied Physics Corporation) spectrophotometer. Matched cells with 1 cm optical path were used. Approximately 1 to 10 grams of montmorillonite were weighed accurately and rapidly transferred to a tared Erlenmeyer flask with ground joint top and stopper. 50 cc of stock solution in anhydrous solvent were then added and the flasks were sealed with parafilm. The flasks were shaken mechanically overnight. The samples were then centrifuged and an aliquot of the supernatant was diluted with absolute methanol and assayed spectrophotometrically at the wavelength shown in Table I. The stock solution was assayed in the same fashion and the amount of each solute was calculated by difference. The adsorptivity of each solute was determined by Beer's law plots. The absorptivity values of the benzodiazepine derivatives tested are shown in Table I.

Moisture adsorption isotherms were determined by exposing 5 gram samples of montmorillonite to 100 cc of water-isopropanol mixture (12.5%, 25%, 37.5%, 50%, 62.5%, 75% and 87.5% of isopropanol, v/v) in sealed flasks and

then shaking mechanically overnight. The suspensions were then transferred to sedimentation tubes of 4.2 cm inside diameter, of the type described elsewhere (66,67), for three weeks. The water content of the system was determined before and after equilibrium by means of Karl Fischer titration (68).

J. Dipole Moment Determinations

To determine the dielectric dipole moment of a solute molecule, the measurement of dielectric constant, density and refractive index are necessary.

The dielectric constants of the various solvents were determined by using a Sargent Chemical Oscillometer, model V# (Sargent-Welch Scientific Company, 7300 North Linder Avenue, Skokie, Illinois), according to the manual (69).

In order to obtain reproducible readings, the instrument was pre-warmed for two hours. The 10 ml sample cell was rinsed carefully with water, alcohol and anhydrous ether and then dried thoroughly with air to insure complete dryness. If the surfaces are not dry (for instance if they are contaminated with perspiration moisture from handling) the value of the cell filled with air may vary several magnitudes. This is important since the zero adjustment of the instrument is performed using

an empty cell. The empty cell was installed at its selected position in the cell holder and the zero adjustment was performed by means of the center adjust knob and the zero set. With the range switches set at full capacitance (toward the operator) and the measuring dial counterclockwise to read zero, the center adjust knob was rotated until the meter needle pointed to or was close to center zero scale position. The final zero adjustment was then made with the zero set so the needle would point at center position with the high sensitivity switch depressed. Without removing the cell, the sample under investigation was carefully poured into the cell until its level was approximately 1 cm over the electrode. The range switches were thrown (away from the operator) and the measuring dial rotated until enough capacitance units have been removed to restore the meter needle to center position while the high sensitivity switch is depressed. The scale reading was then obtained by adding the values for each switch and that indicated by the dial. The cell was then emptied, cleaned and dried, and the procedure was repeated in the same manner for the next sample. When after measurement of a sample the zero point is to be re-established some alteration of the position of the zero adjust control may be necessary. Such alterations in the apparent capacitance is due to slight instrument drift, residual moisture or sample

contamination in or on the cell or change of position of the sample cell with respect to the cell holder. Particularly, the orientation of the cell in the cell holder is important in reproducing the same conditions for repeated readings. If it is found that the cell position is critical, the cell and cell holder should be marked to indicate the orientation of the cell.

The dielectric constants of the diazepine derivatives were determined by the Heterodyne-Beat method. The principle on which this is based is schematically represented in the following page.

A radiofrequency signal of constant frequency f_o is generated by a fixed-frequency oscillator, and a second signal of frequency f is generated by a variable-frequency oscillator; they are fed into a mixer, whose function is to produce in its output voltage a component of frequency $[f - f_o]$. This difference frequency, or beat frequency, will be in the audio range when f and f_o are nearly equal which can be accomplished by introducing a 1000 cycle per second wave frequency into the beat indicator. The beat frequency can then be detected by oscilloscope by its particular pattern.

The heterodyne-beat apparatus was kindly provided by the Division of Physical Chemistry, Department of Chemistry, the University of Wisconsin. A method of generating a calibration chart to compensate for condenser nonlinearity

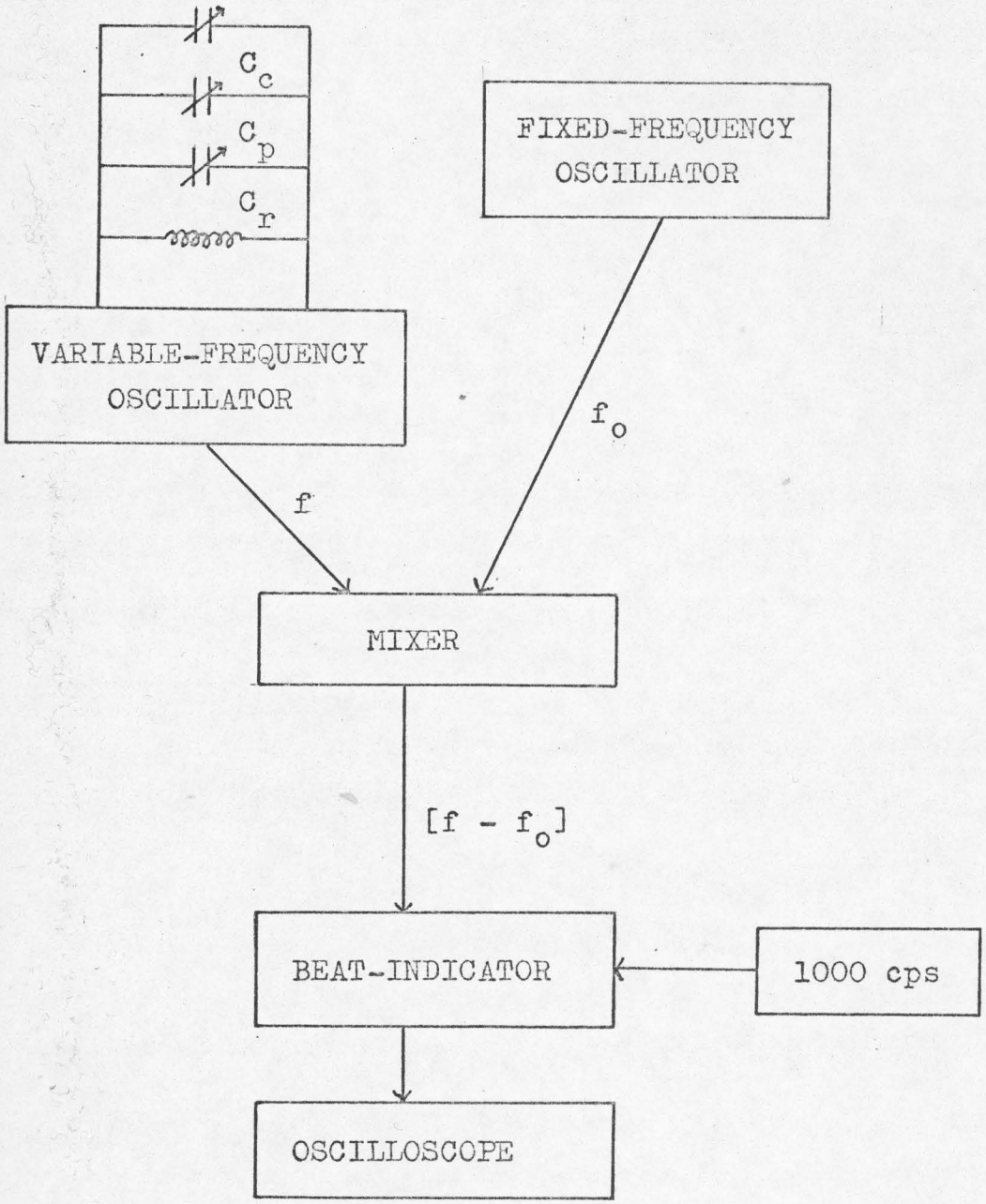

Schematic Diagram of the Heterodyne-Beat Method

C_c: dielectric constant cell

C_p: precision capacitor

C_r: rough tuning capacitor

has been described (70) and prepared in the course of this measurement. A two terminal cell was chosen for determining the permitivity of liquids and its construction according to Bender (71). Solutions of diazepam and the remaining benzodiazepine derivatives were prepared by dissolving approximately 1 gram of solid in 100 ml purified 2,4-dioxane and then poured into the cell case (cell volume 100 ml). The two positions of the cell are located by moving the insulated handle to the stops. The stops may be moved relative to one another to provide a range of capacitance differences between the two positions. The theory and application of the two terminal cell have been described elsewhere (72).

2. Density Measurement

The density measurement used was a buoyancy method in which a Christian Beckers Balance was precalibrated with water at 25°C. The scale reading equals the ratio of the density of the liquid to the density of water at 25°C. The sinker is suspended with a very fine platinum wire so that the surface tension effect on this wire is negligible. The wire was always immersed to the same depth and the sinker was rinsed with alcohol and dried for each measurement.

3. Refractive Index Measurement

The refractive indices of the benzodiazepine derivatives were determined by means of Abbe refractometer (W. H. Kessel & Co. Scientific Instruments, Chicago, Illinois) at 25°C with a constant temperature water bath; a circulating pump was connected with rubber tubing to the inlets and outlets provided for temperature control on the refractometer.

The Abbe refractometer makes use of the principle of the grazing angle; the telescope is stationary and the prism is moved. The prism must be moved through a certain angle so the critical boundary in the field of view corresponds to the critical angle of refraction. The field in the telescope will show a light region and a dark region and the sharp line of demarcation corresponds to the grazing angle. The scale of the Abbe refractometer is calibrated directly in refractive index, so no calculations are necessary.

K. Infrared Absorption Spectrometry

In some types of adsorbates it is possible to obtain information regarding the bonding involved via infrared absorption spectrometry. An example of this is the work by Herl and Hair (73) who demonstrated that interaction in silica adsorbates was confined to hydroxyl groups (by the

shift of the OH stretching frequency). It was hoped that IR spectra would throw light on montmorillonite adsorption in the same way and KBr pellets were therefore prepared of (a) montmorillonite, (b) diazepam, (c) diazepam adsorbed on montmorillonite, and (d) oxazepam adsorbed on montmorillonite. The spectra were obtained on Beckman model IR5 infrared spectrophotometer. Adsorbates were prepared by drying the solids from an adsorption experiment (1 gram of montmorillonite in a solution which was 2.1×10^{-3} molar in solute).

L. Reflectance Spectra

Reflectance spectra of (a) montmorillonite, (b) diazepam adsorbed on montmorillonite, and (c) diazepam were performed on a Beckman model DB spectrophotometer with integrating (barium oxide) sphere. These spectra were performed by Mr. James B. Johnson at Hoffmann-La Roche, N.J.

III. RESULTS

A. Benzoic Acid Isotherms

The amount of benzoic acid adsorbed from isopropanolic solution by montmorillonite was calculated by difference before and after equilibration and the data shown in Table II. Reciprocal plotting of the data yields straight lines as exemplified in Figure 6; as seen in Figure 7, straight lines are also obtained with other solvents. The dehydrated clay still contains 5-6% water in the interlaminar spacing as shall be discussed shortly.

Since anhydrous solvents (e.g., methanol) have been reported to (and were found to) extract and replace the structural water from montmorillonite, the solvent after equilibrium will contain small amounts of water. Experiments were therefore performed as follows: one to six grams of montmorillonite in a tared container were used per 100 cc of solvent, so the moisture content of the solvent would be 60-360 mg per 100 cc. To ascertain that this small amount did not affect the results, two runs were made with montmorillonite pre-extracted with solvent, results from these fall in line with the remaining results (Figure 6); hence, the effect of the small amount of water is within experimental error. Two runs were made

TABLE II

Benzoic Acid Isotherm on Veegum from Isopropanol

C_v (10^5 moles gm^{-1})	C_s (10^2 molar)	C_v^{-1} (10^{-4} gm $moles^{-1}$)	C_s^{-1} ($molar^{-1}$)	C_v^{-1} (10^{20} gm $molecule^{-1}$)
5.2246	4.339	1.9140	23.05	3.19
4.1893	3.533	2.3872	28.31	3.98
3.5223	2.486	2.8393	40.23	4.73
3.4892	1.971	3.4892	50.74	5.82
2.5233	1.635	3.9631	61.16	6.61

Figure 6. Benzoic acid isotherm from anhydrous isopropanol.

Key:

○ = the procedure described in the text

◒ = pre-extracted montmorillonite (see text)

◑ = a lot of Veegum different from the lot used in the main portion of the study

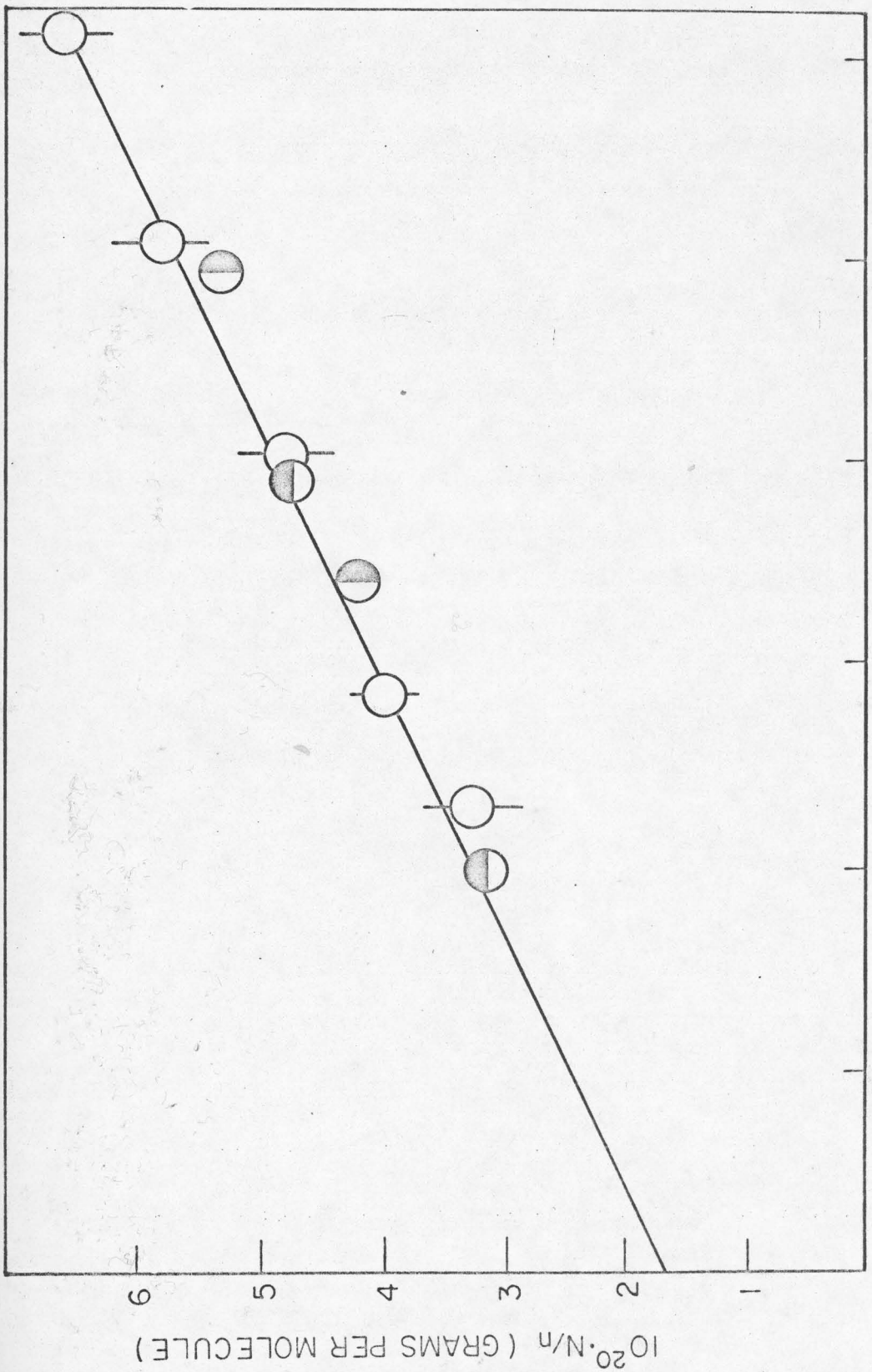
$10^{20} \cdot N/n$ (GRAMS PER MOLECULE)
1
2
3
4
5
6
10
20
30
40
50
60
C_b^{-1} (MOLAR^{-1})

Figure 7. Benzoic acid isotherm on montmorillonite from various solvents.

Key:

Solvent ◐ = tert-butanol

◒ = ethanol

○ = 50% isopropanol

◑ = methanol

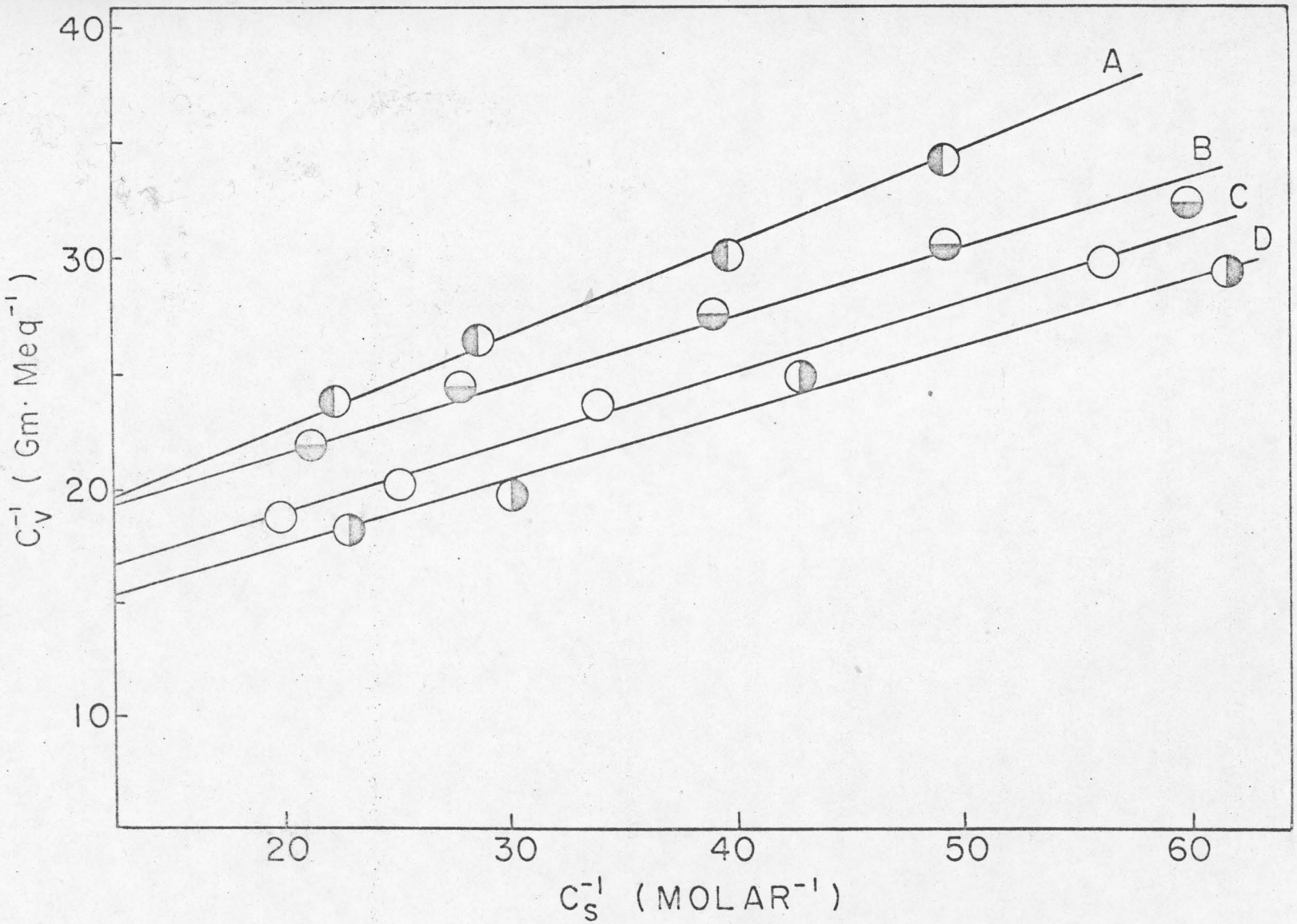
40
30
20
10
20
30
40
50
60
A
B
C
D
C_v^{-1} (Gm· Meq^{-1})
C_s^{-1} ($MOLAR^{-1}$)

with a different lot of montmorillonite, also giving consistent results (see Figure 6).

B. Moisture Isotherm

It should be pointed out that in spite of the low equilibrium moisture pressure of the montmorillonite obtained with the high vacuum capability of the vacuum rack, it still contains about 5.6% structural water as determined by the Karl Fischer titration.

Montmorillonite swells in contact with solvent (51) although not nearly to the degree experienced with water. Wai and Banker (33) have described a method for determining swelling volume and a similar method was used here. Figure 8 demonstrates that the swelling volume does not change too markedly up to about 50% water content. Samples of supernatant of the systems were tested before and after equilibrium for water content by Karl Fischer titration. The calculated results are shown in Table III. A plot of moisture content of the montmorillonite as a function of water content of solvent is shown in Figure 9.

C. Diazepam Isotherms on Montmorillonite in Various Solvents

Diazepam isotherms were determined in hydroisopropanolic vehicles in a similar fashion as described previously. For reasons to be discussed later (future

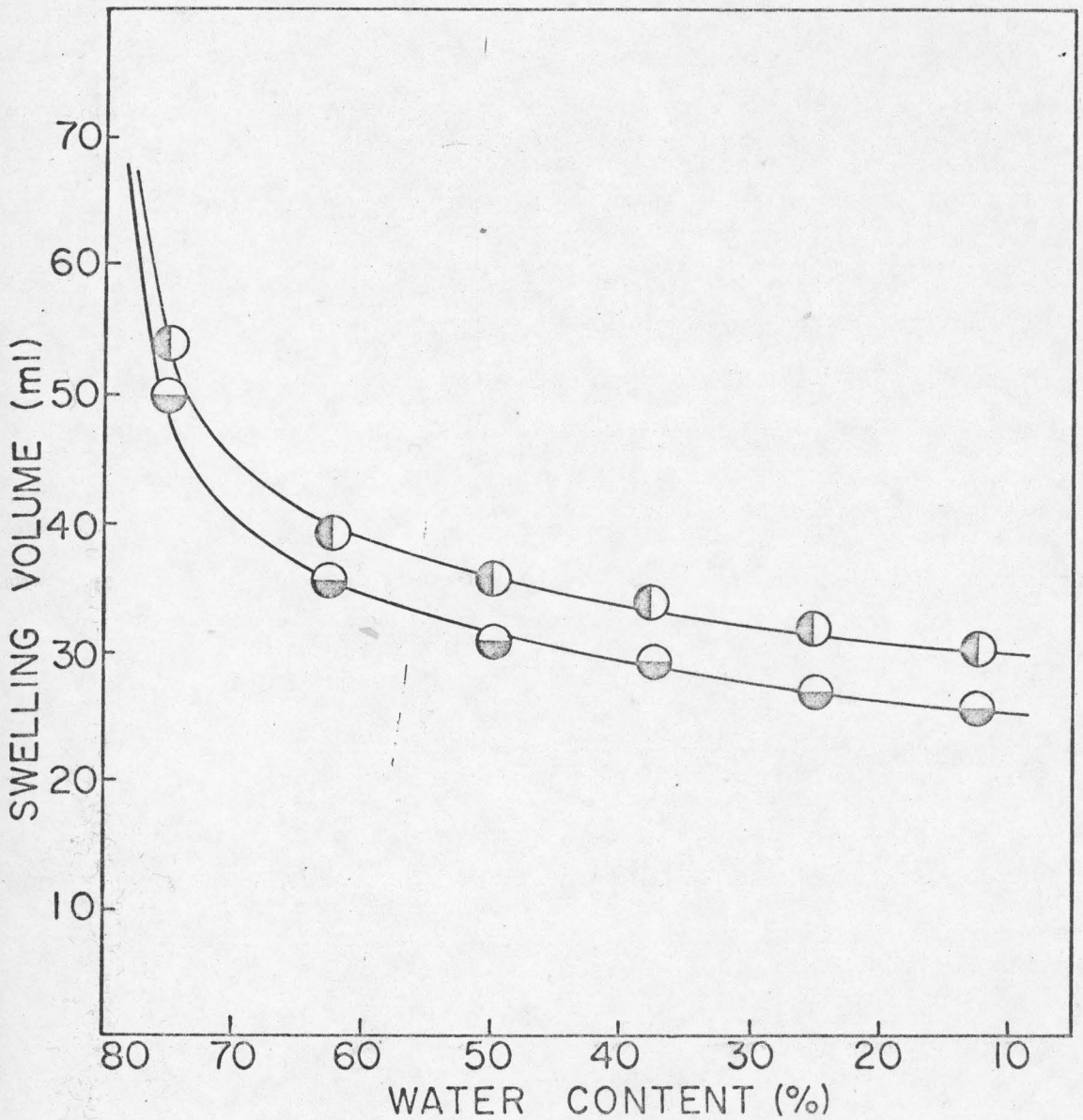

Figure 8. The swelling volumes of montmorillonites in isopropanol containing various concentrations of water.

Key: ◐ and ⊖ show different runs.

TABLE III

Karl Fischer Titration Data

% of H_2O (v/v) in solvent	12.5	25.0	37.5	50.0	75.0
% of H_2O (w/w) before reaction	18.42	33.03	45.61	56.60	76.86
% of H_2O (w/w) after reaction	17.55	31.10	43.53	54.22	74.39
$C_{(H_2O)}$ (molar)	8.5	16.3	23.4	30.3	43.0
Density (gm/ml) (26°C±0.5°C)	0.8117	0.8421	0.8720	0.9021	0.9575
Amount of H_2O in solvent before reaction (gm)	14.95	27.81	39.77	51.06	73.59
Amount of H_2O in solvent after equilibrium (gm)	14.25	26.19	37.96	48.91	71.23
Amount of H_2O gone into M.M. (gm)	0.70	1.62	1.81	2.15	2.36

(Cont.)

TABLE III - Cont.

H_2O content in original 5 gm of M.M. (gm)	0.3450	0.3450	0.3450	0.3450	0.3450
Total H_2O content in 5 gm M.M. after equilibrium (gm)	1.05	1.97	2.16	2.50	2.71
$\frac{\text{gm } H_2O}{\text{gm M.M.}}$	0.21	0.39	0.43	0.50	0.54
$\frac{\text{meq } H_2O}{\text{gm M.M.}}$	11.6	21.9	24.0	27.7	30.1

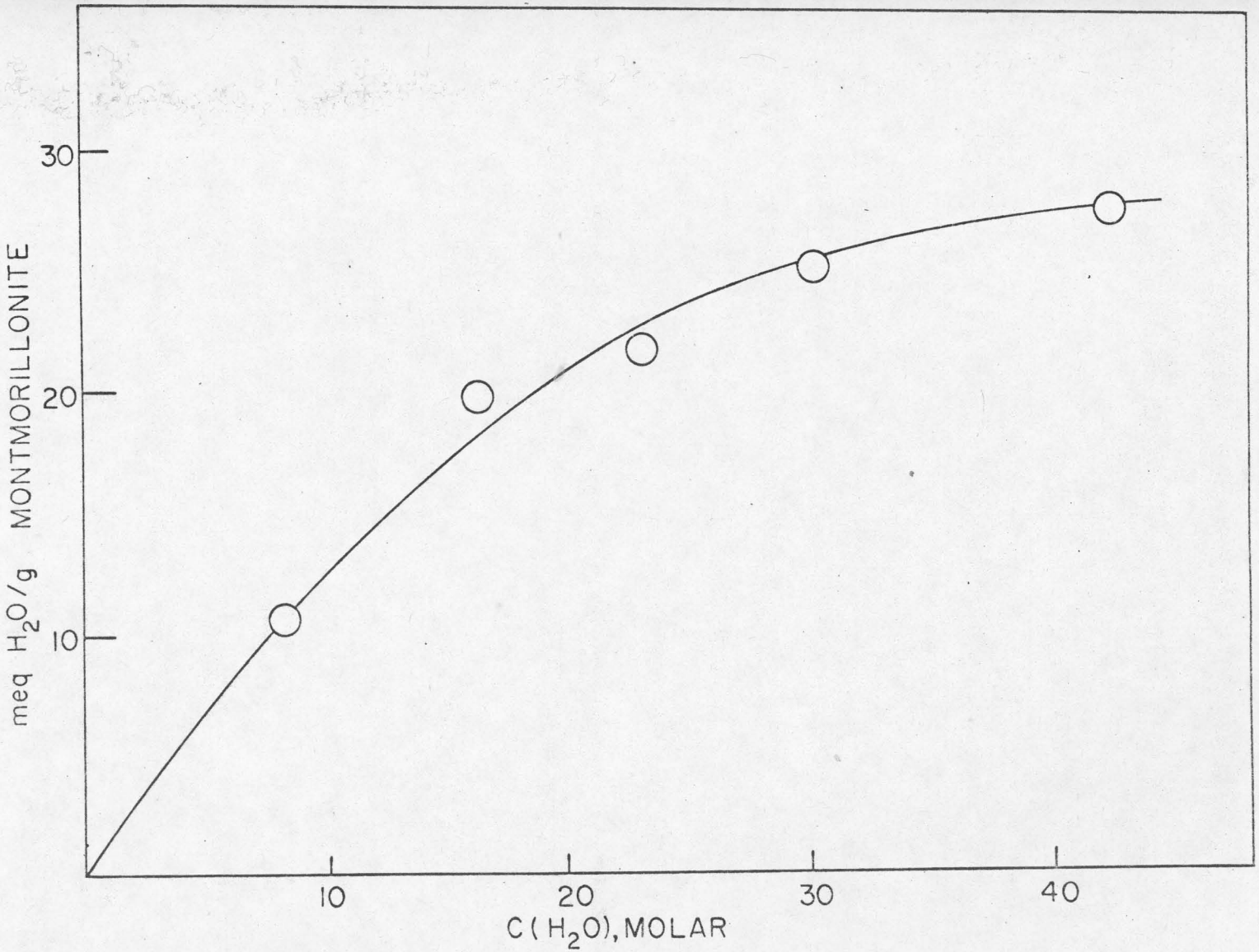

Figure 9. Moisture isotherm of montmorillonite from aqueous solutions of isopropanol.

work), the initial part of the Langmuir isotherm cannot be detected, but the plateau can be accurately established by conducting experiments at constant solute concentration and varying the amount of montmorillonite added. In this fashion the plateau value (meq. diazepam per gram montmorillonite) emerges as the slope of a (linear) plot of meq. diazepam as a function of the number of grams of montmorillonite added. Figure 10 shows such a plot.

It is noted from Figure 10 that the amount of diazepam adsorbed decreases with increasing water content and this is probably due to the effect of the increasing dielectric constant of the solvent. Isotherms from anhydrous solvents are shown in Figure 11 through Figure 21. The equations for the lines are unweighted best fits. In most instances the isotherms emerge directly. In the three cases with the highest dielectric constant, however, solvent will penetrate into the crystal in excess of the number of solvent layers there initially. This causes a reduction in the external volume; the result is that if this is not accounted for then the isotherm will not be linear. Figures 11, 12, and 13 show isotherms with and without adjustment. Only acetonitrile, methanol and ethanol (Figures 11, 12, and 13) fall into this category.

Figure 10. Diazepam adsorbed as a function of the amount of montmorillonite in a hydro-isopropanolic system.

Key:

Line A = 2.5% H_2O content

B = 7.5% H_2O content

C = 12.5% H_2O content

D = 20.0% H_2O content

E = 25.0% H_2O content

F = 31.5% H_2O content

G = 37.5% H_2O content

H = 50.0% H_2O content

I = 60.0% H_2O content

J = 75.0% H_2O content

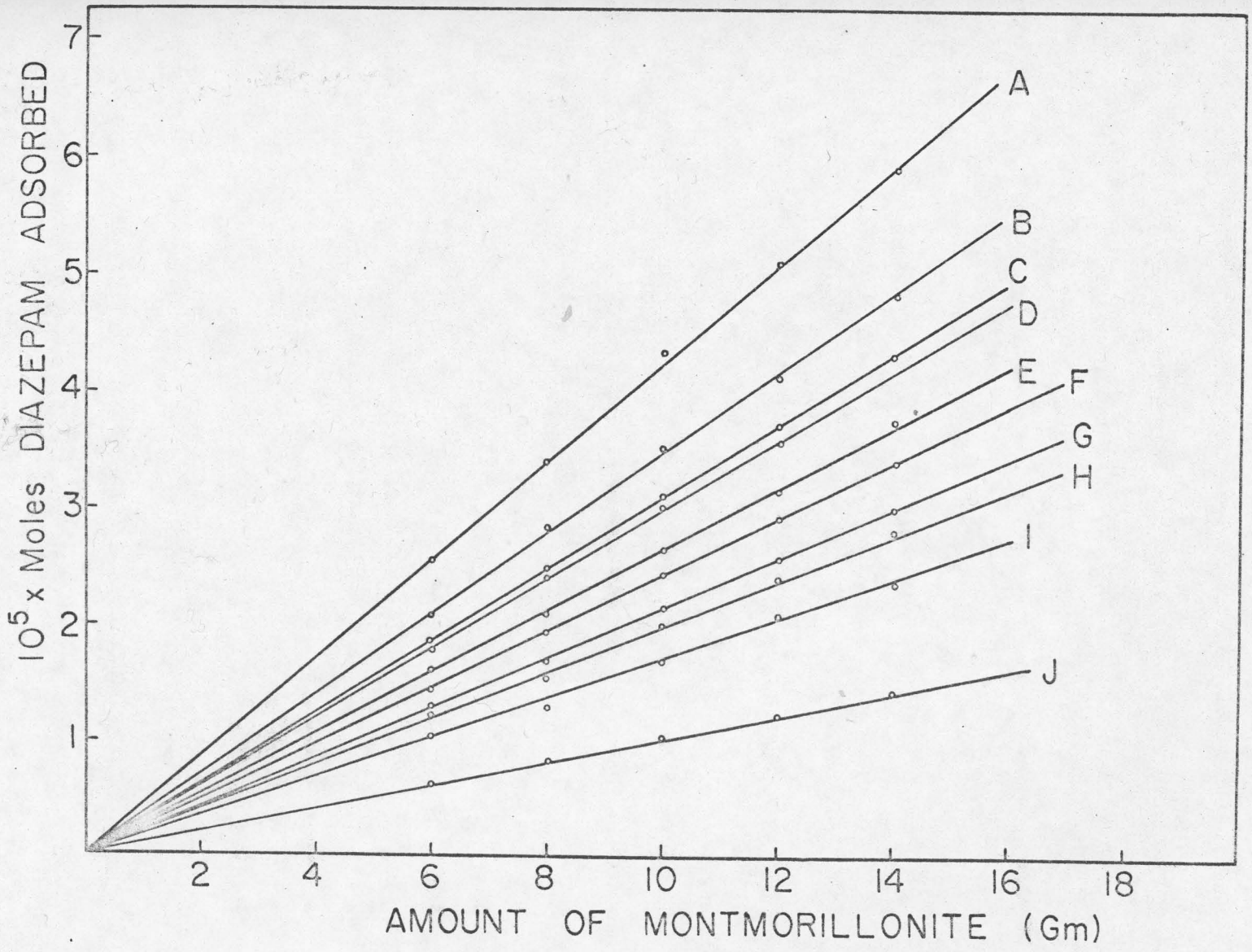
10^5 x Moles DIAZEPAM ADSORBED
1
2
3
4
5
6
7
2
4
6
8
10
12
14
16
18
AMOUNT OF MONTMORILLONITE (Gm)
A
B
C
D
E
F
G
H
I
J

Figure 11. Diazepam isotherms on montmorillonite from acetonitrile.

Key:

Curve A is the conventionally treated curve, where no allowance is made for solvent intercalation

Curve B, C and D are lines where allowance is made for 12, 12.5 and 13 layers of acetonitrile between silicate layers.

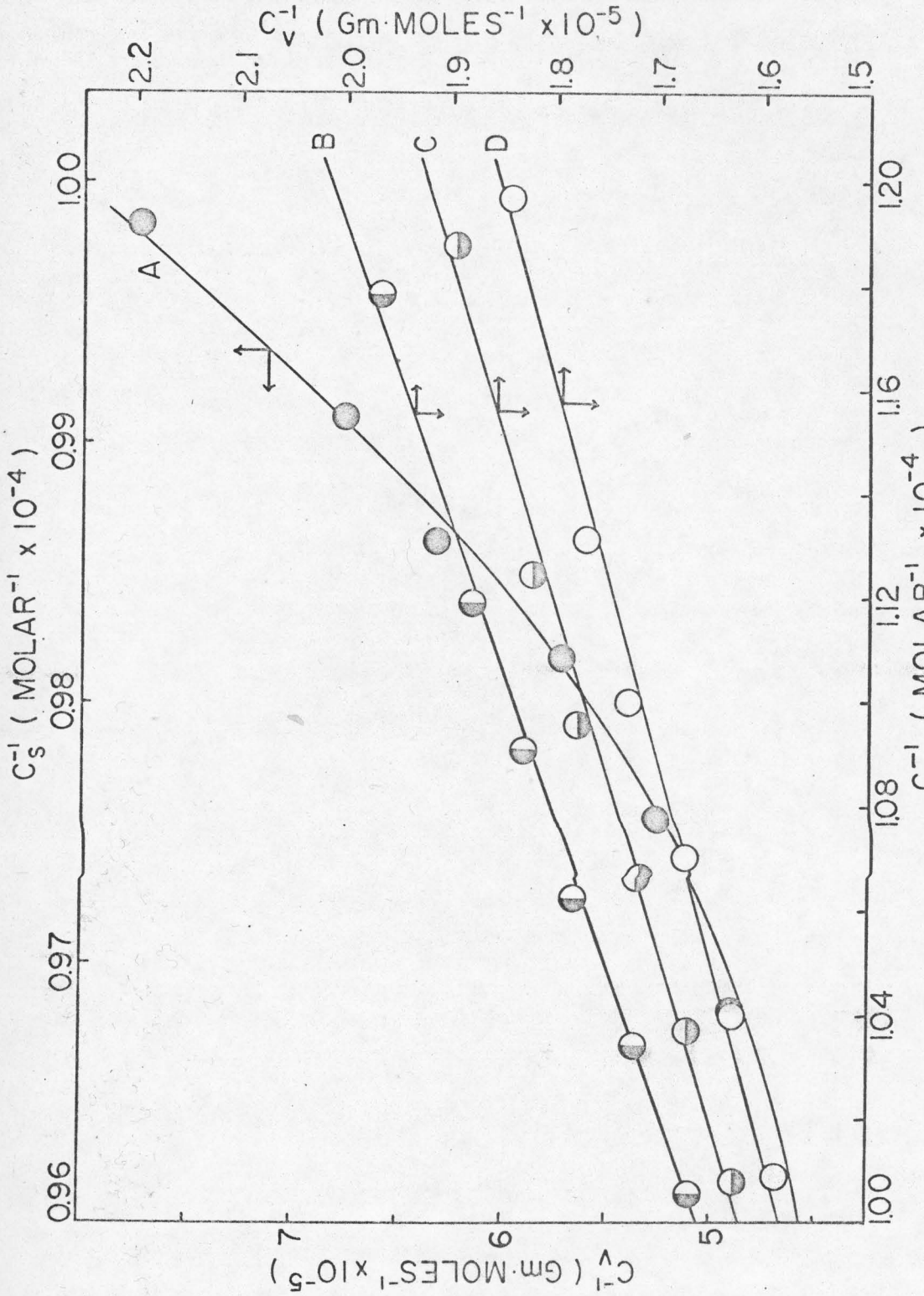
C_v^{-1} (Gm·MOLES^{-1} x10^{-5})
2.2
2.1
2.0
1.9
1.8
1.7
1.6
1.5
A
B
C
D
1.00
0.99
0.98
0.97
0.96
C_s^{-1} (MOLAR^{-1} x 10^{-4})
1.20
1.16
1.12
1.08
1.04
1.00
C_s^{-1} (MOLAR^{-1} x 10^{-4})
7
9
5
C_v^{-1} (Gm·MOLES^{-1} x10^{-5})

Figure 12. Diazepam isotherms on montmorillonite from methanol.

Key:

Curve A is conventionally treated, without allowance for solvent intercalation.

Lines B, C and D are lines where allowance is made for 6, 7 and 8 layers of methanol.

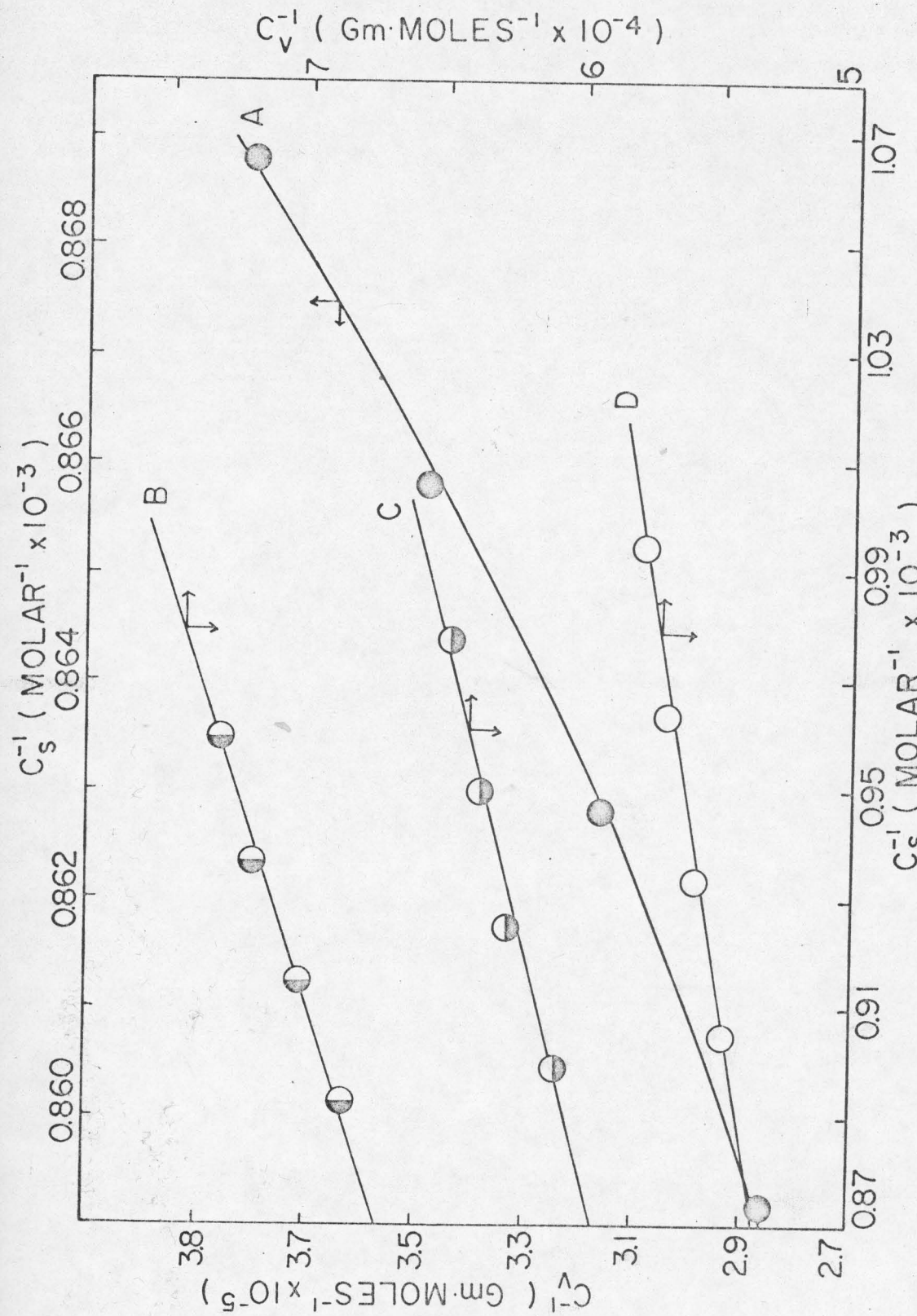
C_v^{-1} (Gm·MOLES^{-1} x 10^{-4})
7
6
5
A
B
C
D
0.868
0.866
0.864
0.862
0.860
C_s^{-1} (MOLAR^{-1} x 10^{-3})
1.07
1.03
0.99
0.95
0.91
0.87
C_s^{-1} (MOLAR^{-1} x 10^{-3})
3.8
3.7
3.5
3.3
3.1
2.9
2.7
C_v^{-1} (Gm·MOLES^{-1} x 10^{-5})

Figure 13. Diazepam isotherms on montmorillonite from ethanol.

Key:

Curve A is the conventionally treated curve, where no allowance is made for solvent intercalation.

Lines B, C and D are lines where allowance is made for 4, 5 and 6 layers of ethanol.

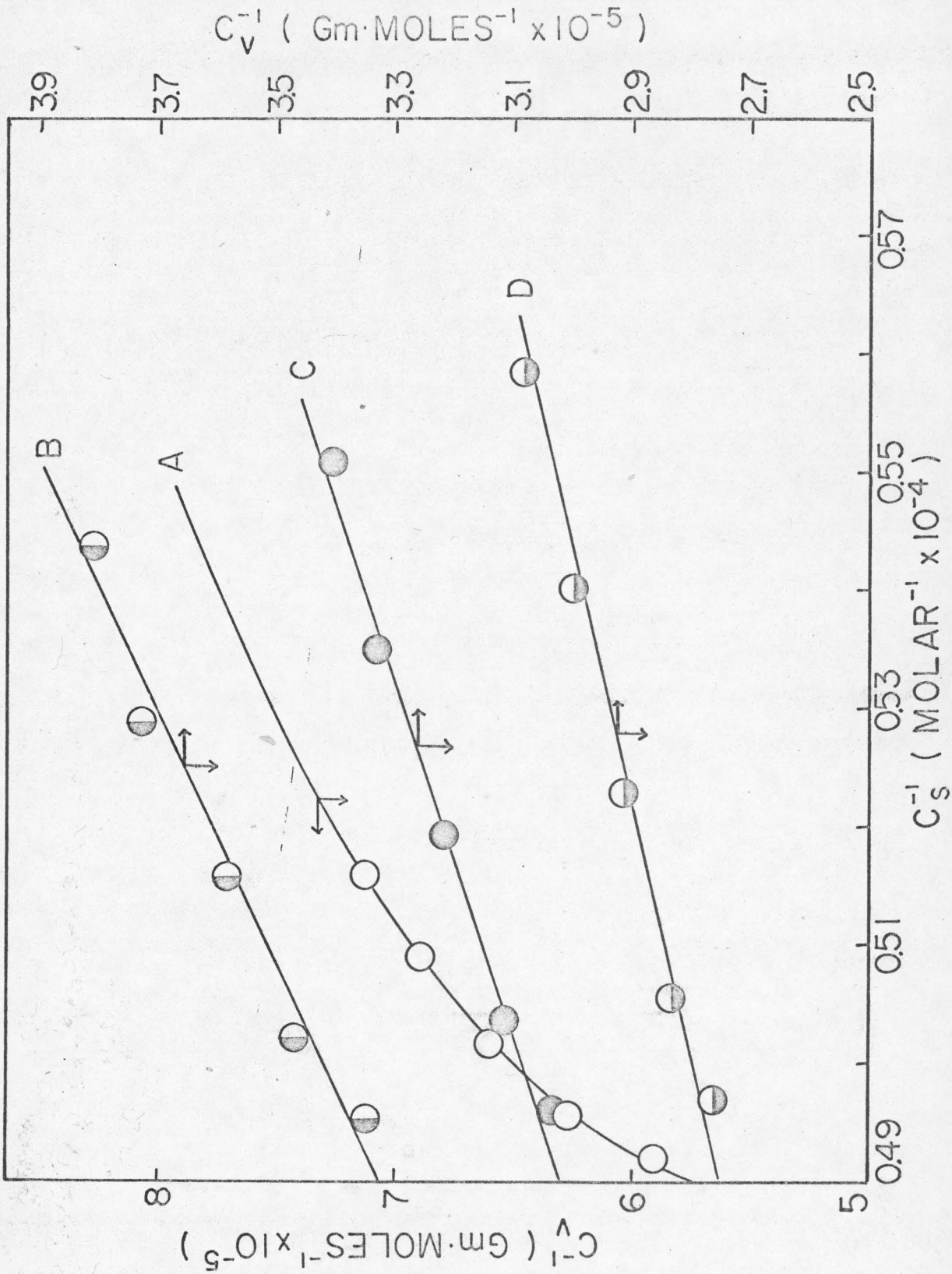
C_V^{-1} (Gm·MOLES^{-1} x10^{-5})
3.9
3.7
3.5
3.3
3.1
2.9
2.7
2.5
B
A
C
D
0.49
0.51
0.53
0.55
0.57
C_S^{-1} (MOLAR^{-1} x10^{-4})
C_V^{-1} (Gm·MOLES^{-1} x10^{-5})
8
7
6
5

D. Adsorption of Other Benzodiazepine Derivatives on Montmorillonite

Isotherms were also performed using one solvent (anhydrous isopropanol) and different solutes and repeating the experiments. The Langmuir type plots are shown in Figures 22 through 27.

E. The Estimated Values of the Cross Sectional Area of Solutes

The cross sectional area of benzoic acid was estimated by a tracing from a C.P.K. atomic model. The tracing was cut off and then weighed and the total area was estimated by comparing with unit weight of the original tracing paper.

The estimated value for the cross sectional area of benzoic acid was 10 Å.

In the same fashion, the cross sectional area of diazepam was estimated as 25 $Å^2$.

Figure 14. Diazepam isotherm on montmorillonite from n-propanol.

The equation of the line is $y = 5.4x + 1.0$ where $y = 10^{-4} \cdot C_v^{-1}$ and $x = 10^{-4} \cdot C_s^{-1}$.

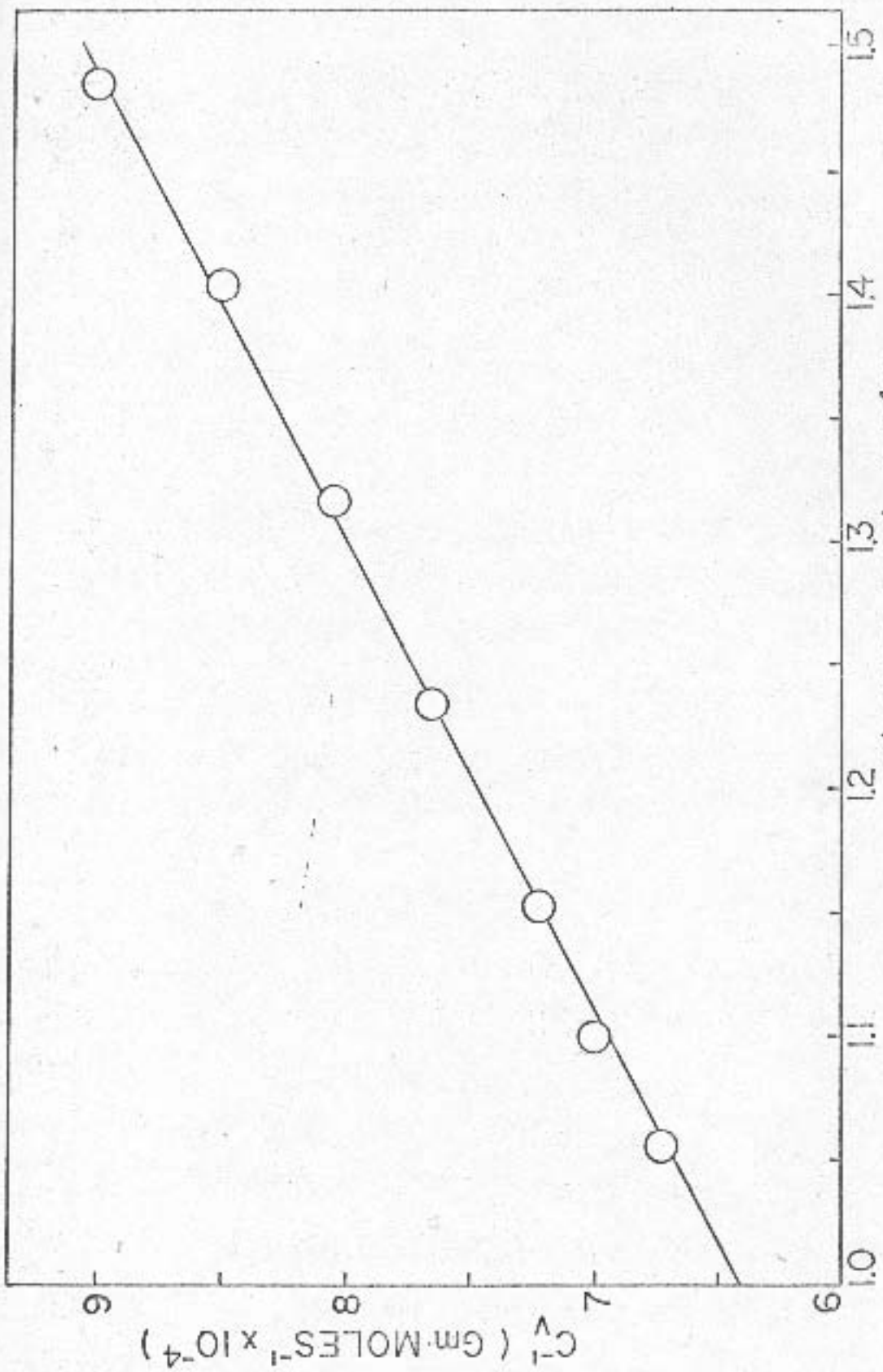
C_v^{-1} (Gm·MOLES^{-1} x 10^{-4})
6
7
8
9
1.0
1.1
1.2
1.3
1.4
1.5
C_s^{-1} (MOLAR^{-1} x 10^{-4})

Figure 15. Diazepam isotherm on montmorillonite from isoamyl alcohol.

The equation of the line is $y = 0.84x + 0.74$ where $y = 10^{-4} \cdot C_v^{-1}$ and $x = 10^{-4} \cdot C_s^{-1}$.

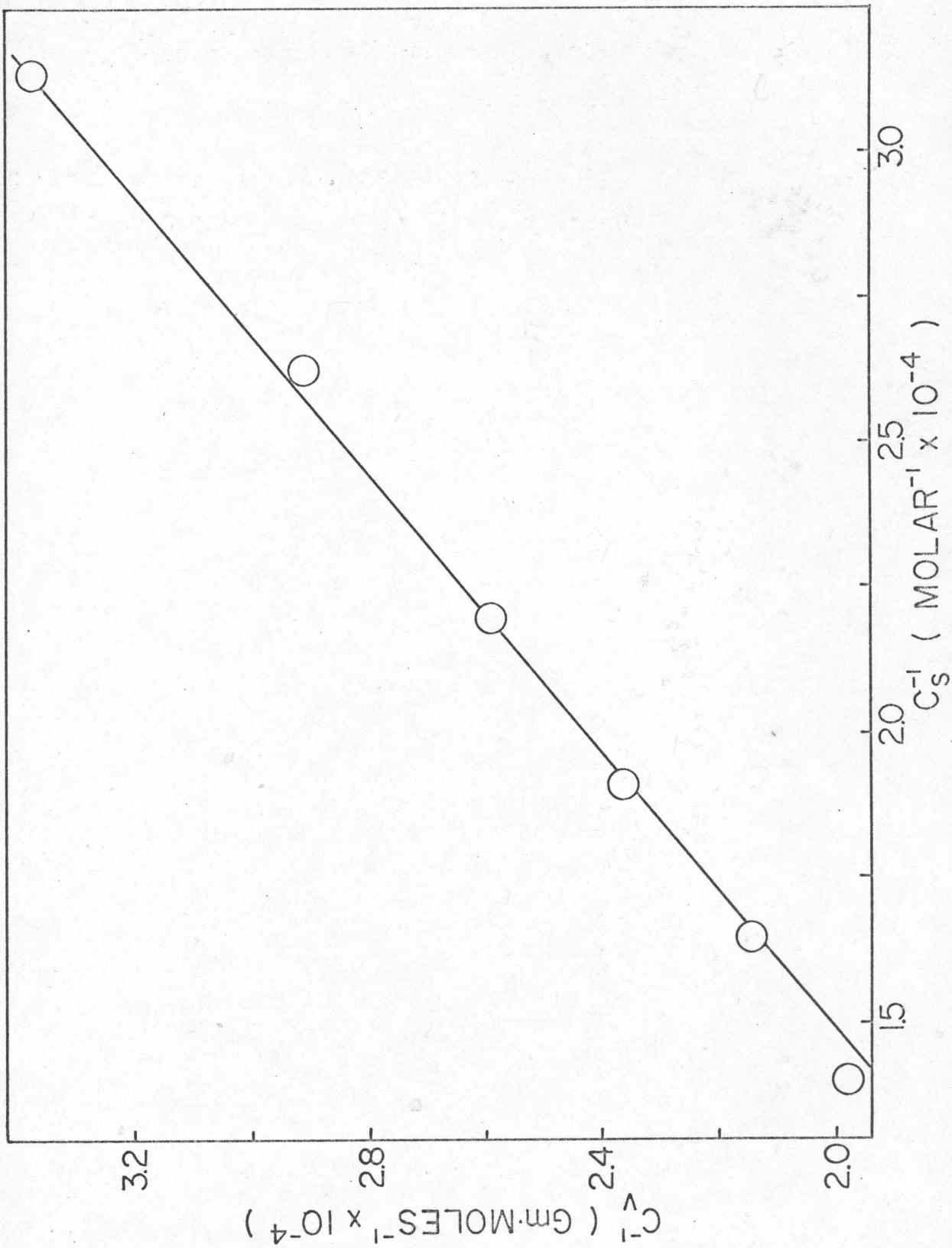
3.2
2.8
2.4
2.0
C_v^{-1} (Gm·MOLES^{-1} x 10^{-4})
1.5
2.0
2.5
3.0
C_s^{-1} (MOLAR^{-1} x 10^{-4})

Figure 16. Diazepam isotherm on montmorillonite from n-amyl alcohol.

The equation of the line is $y = 0.68x + 0.64$ where $y = 10^{-4} \cdot C_v^{-1}$ and $x = 10^{-4} \cdot C_s^{-1}$.

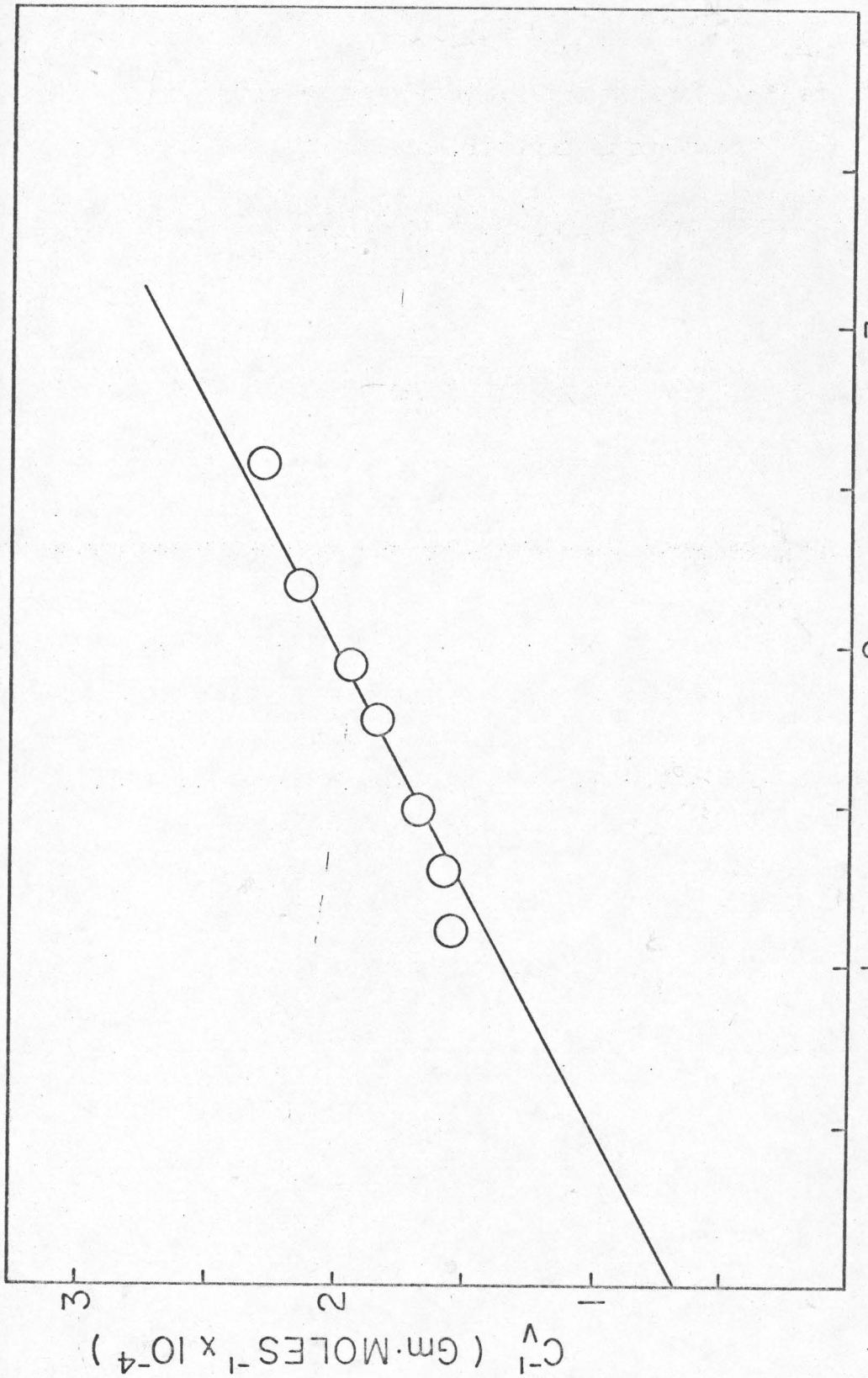
C_V^{-1} (Gm·MOLES^{-1} x 10^{-4})
3
2
1
1
2
3
C_S^{-1} (MOLAR^{-1} x 10^{-4})

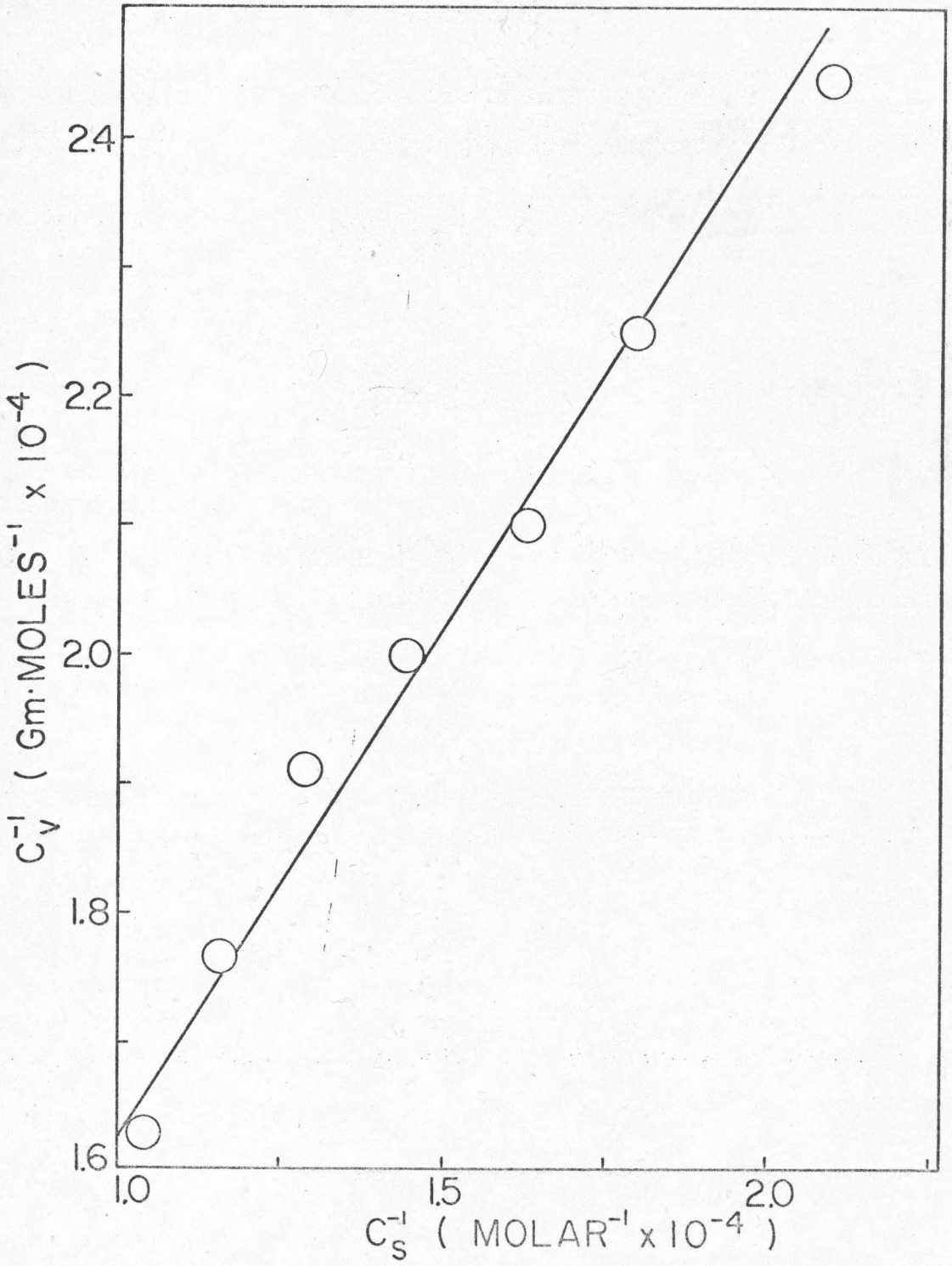

Figure 17. Diazepam isotherm on montmorillonite from isobutyl alcohol. The equation of the line is $y = 0.8x + 0.82$ where $y = 10^{-4} \cdot C_v^{-1}$ and $x = 10^{-4} \cdot C_s^{-1}$.

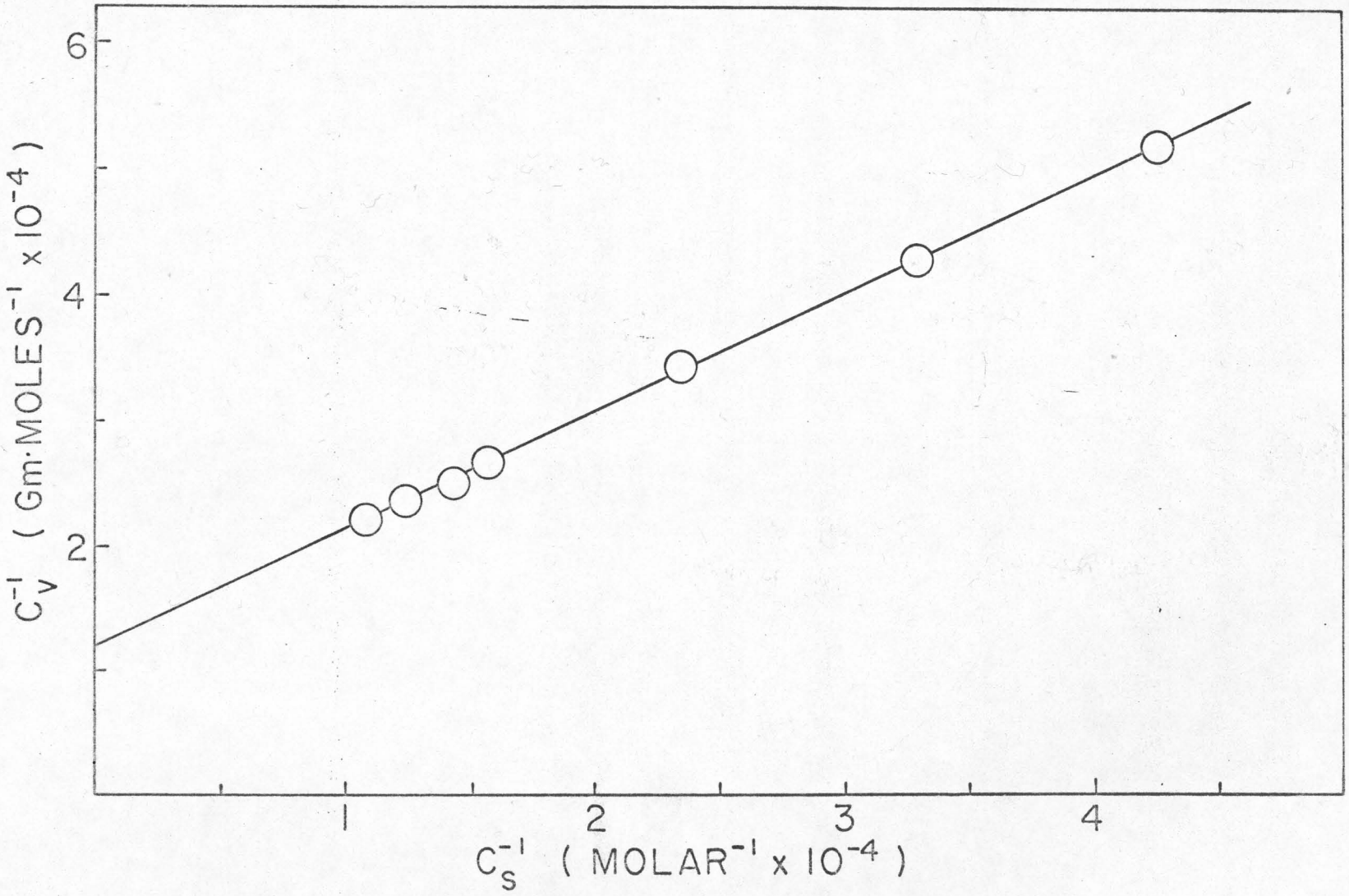

Figure 18. Diazepam isotherm on montmorillonite from isopropanol. The equation of the line is $y = 0.96x + 1.2$ where $y = 10^{-4} \cdot C_v^{-1}$ and $x = 10^{-4} \cdot C_s^{-1}$.

Figure 19. Diazepam isotherm on montmorillonite from tert-butanol.

The equation of the line is $y = 0.302x + 1.52$ where $y = 10^{-4} \cdot C_v^{-1}$ and $x = 10^{-4} \cdot C_s^{-1}$.

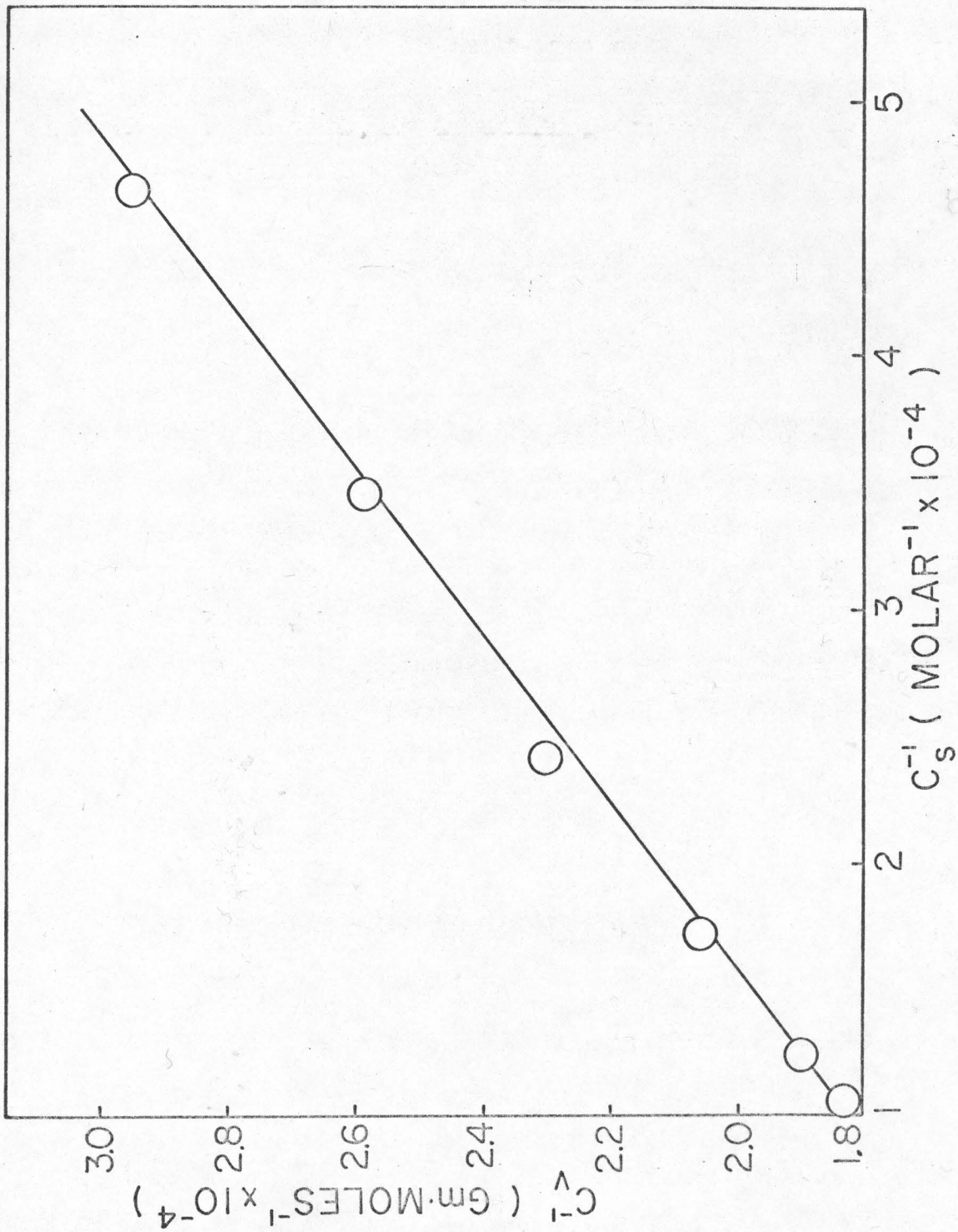
3.0
2.8
2.6
2.4
2.2
2.0
1.8
C_v^{-1} (Gm·MOLES^{-1} x 10^{-4})
1
2
3
4
5
C_s^{-1} (MOLAR^{-1} x 10^{-4})

Figure 20. Diazepam isotherm on montmorillonite from dichloroethane.

The equation of the line is $y = 0.135x + 0.61$ where $y = 10^{-4} \cdot C_v^{-1}$ and $x = 10^{-4} \cdot C_s^{-1}$.

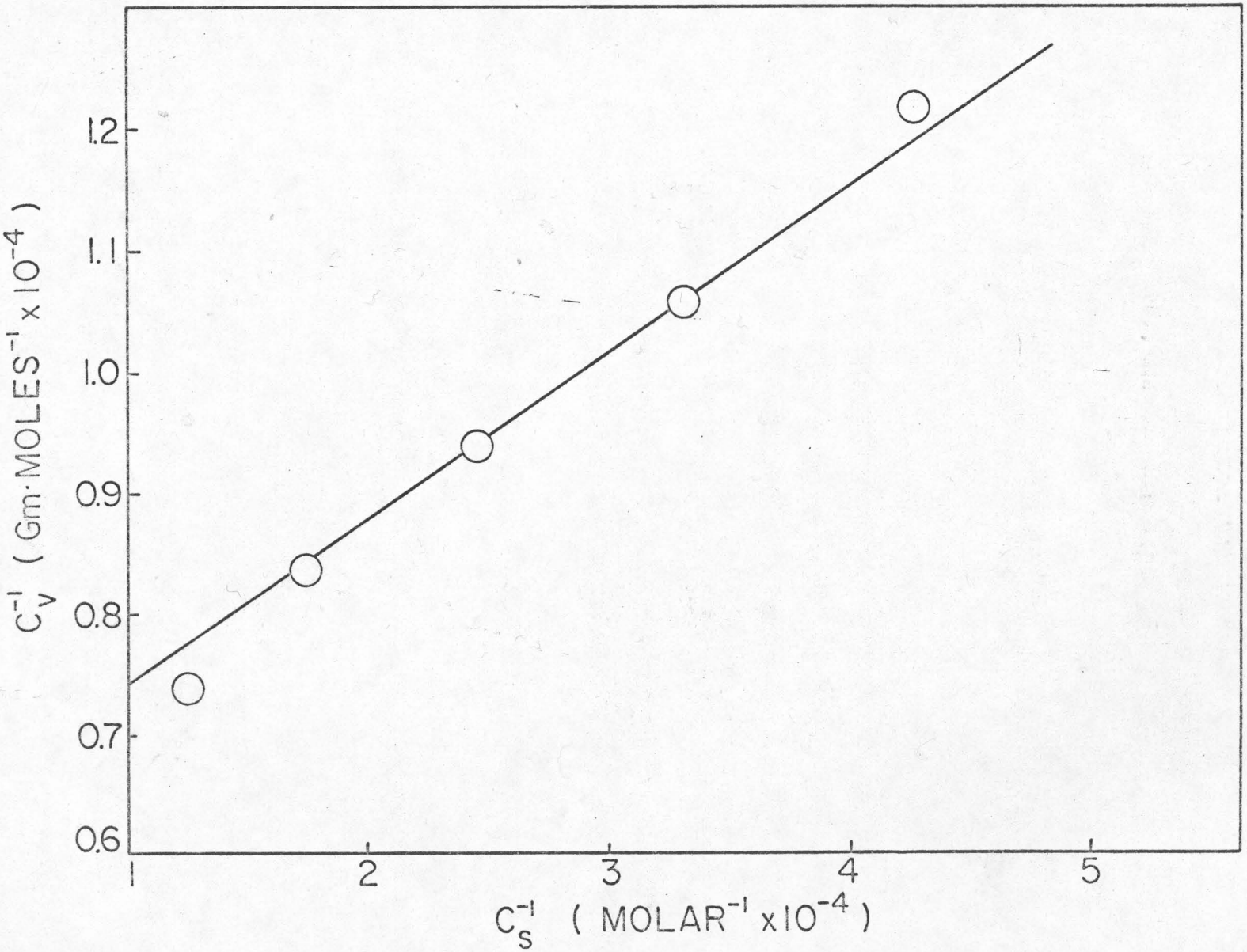
1.2
1.1
1.0
0.9
0.8
0.7
0.6
1
2
3
4
5
C_v^{-1} (Gm·MOLES^{-1} x 10^{-4})
C_s^{-1} (MOLAR^{-1} x 10^{-4})

Figure 21. Diazepam isotherm on montmorillonite from isopropanol at 6°C.

The equation of the line is $y = 4.1x + 0.1$ where $y = 10^{-4} \cdot C_v^{-1}$ and $x = 10^{-3} \cdot C_s^{-1}$.

○ and ⊖ show different runs.

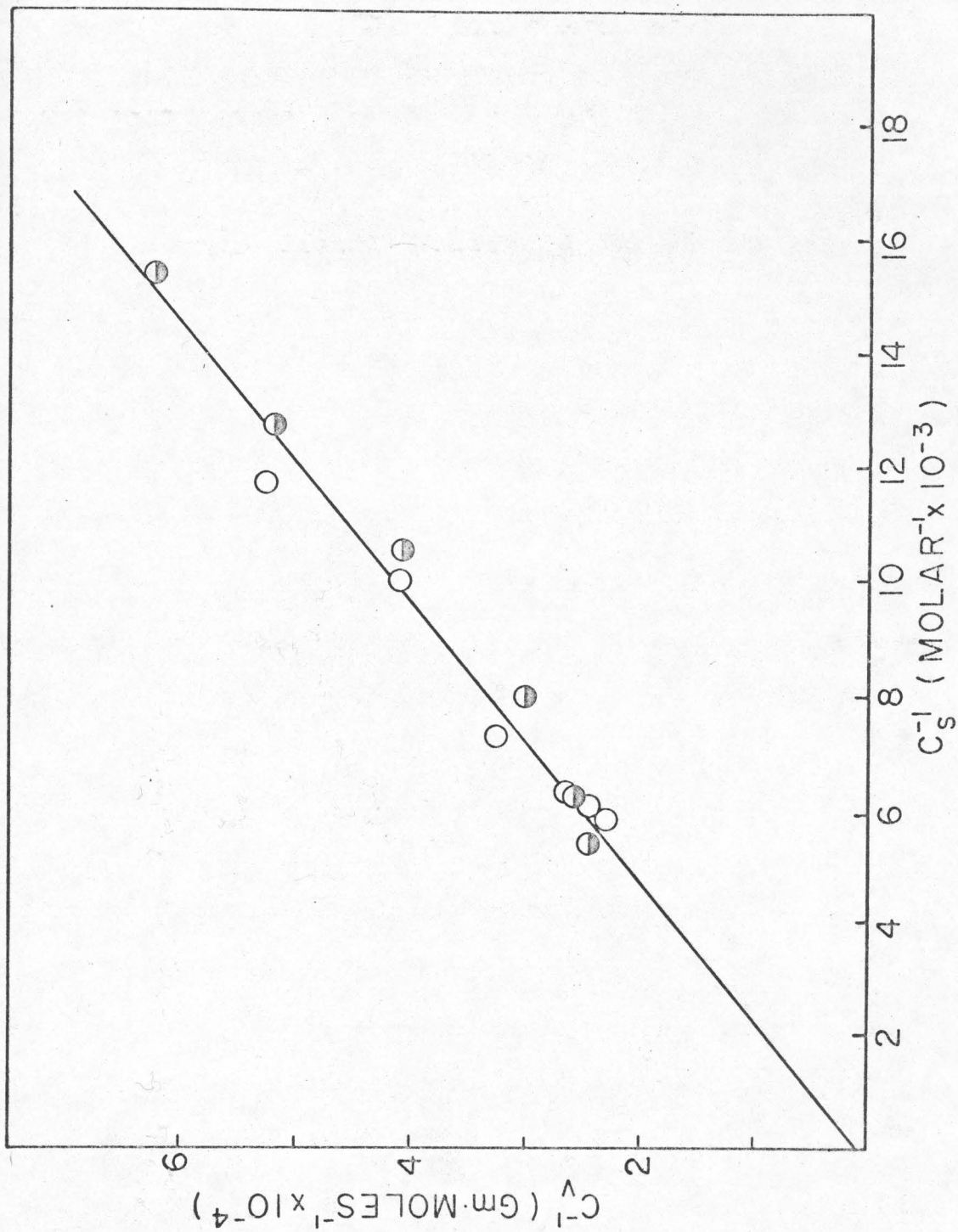
C_v^{-1} (Gm·MOLES^{-1} x 10^{-4})
2
4
6
C_s^{-1} (MOLAR^{-1} x 10^{-3})
2
4
6
8
10
12
14
16
18

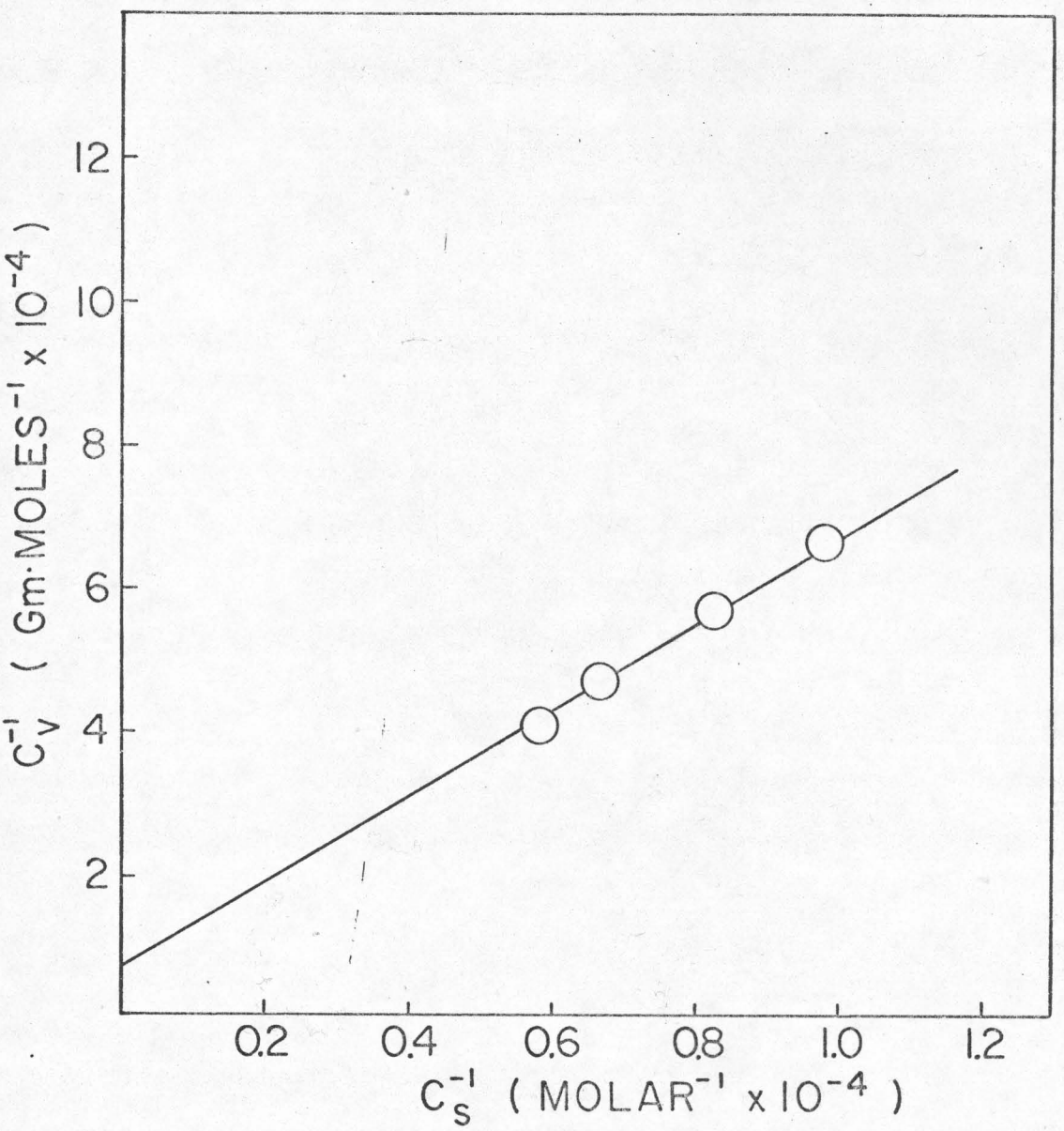

Figure 22. 7-Nitro-1,3-dihydro-1-methyl-5-(2-fluorophenyl)-2H-1,4-benzodiazepine-2-one isotherm on montmorillonite from isopropanol.

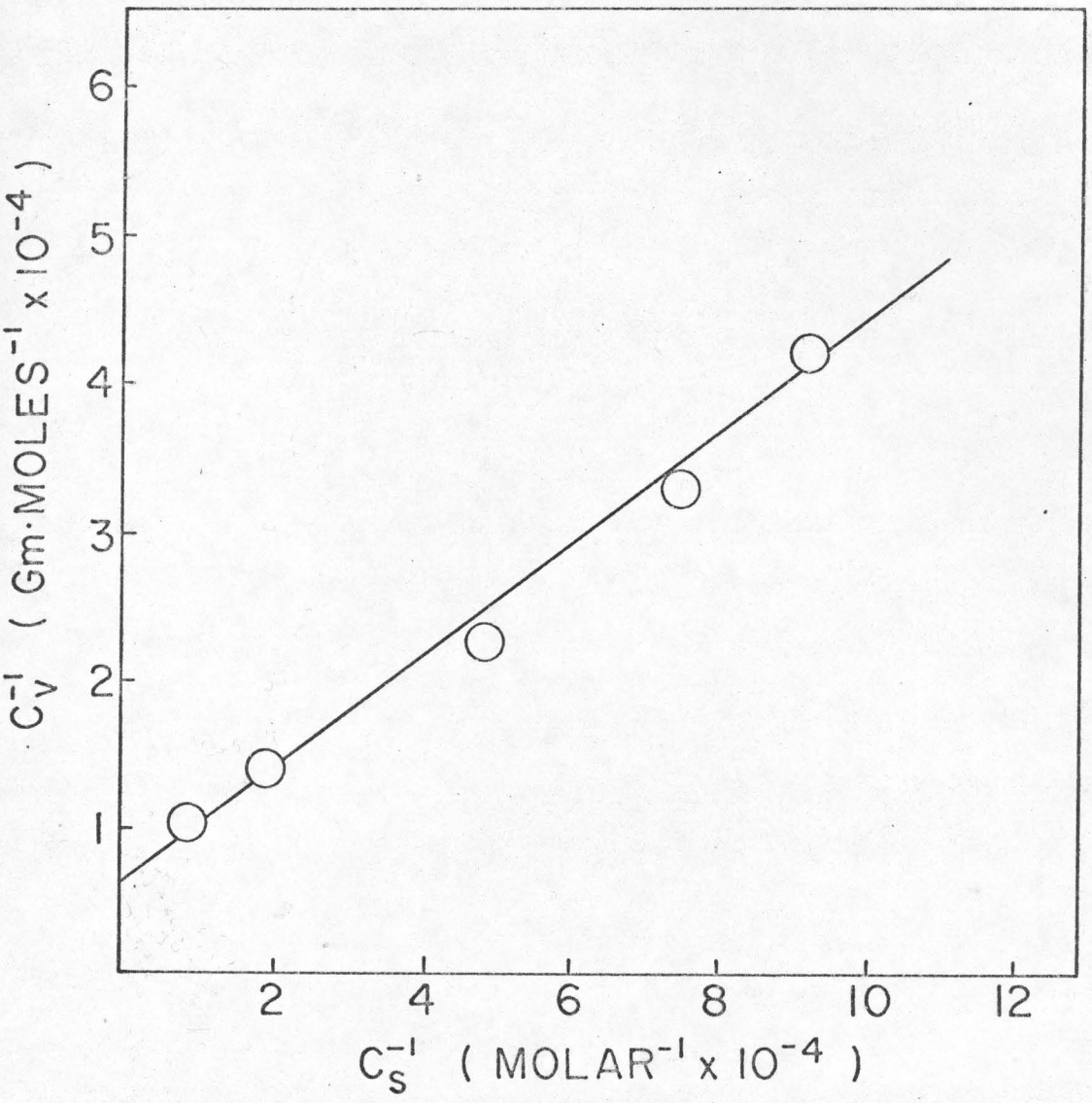

Figure 23. 7-Bromo-1,3-dihydro-5-(2-pyridinyl)-2H-1,4-benzodiazepine-2-one isotherm on montmorillonite from isopropanol.

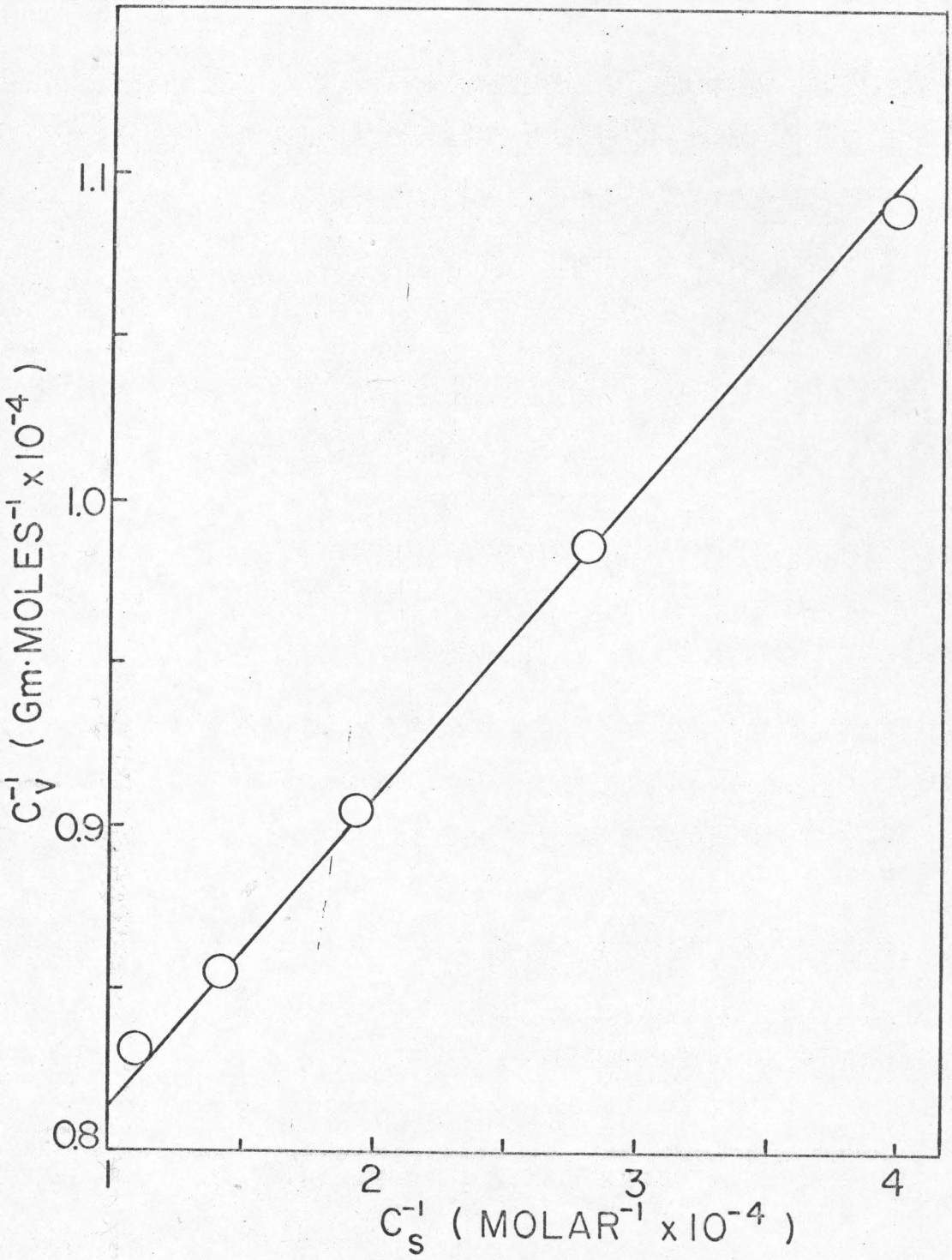

Figure 24. Oxazepam isotherm on montmorillonite from isopropanol. The equation of the line is $y = 9.6 \times 10^{-2}x + 7.14$ where $y = 10^{-4} \cdot C_v^{-1}$ and $x = 10^{-4} \cdot C_s^{-1}$.

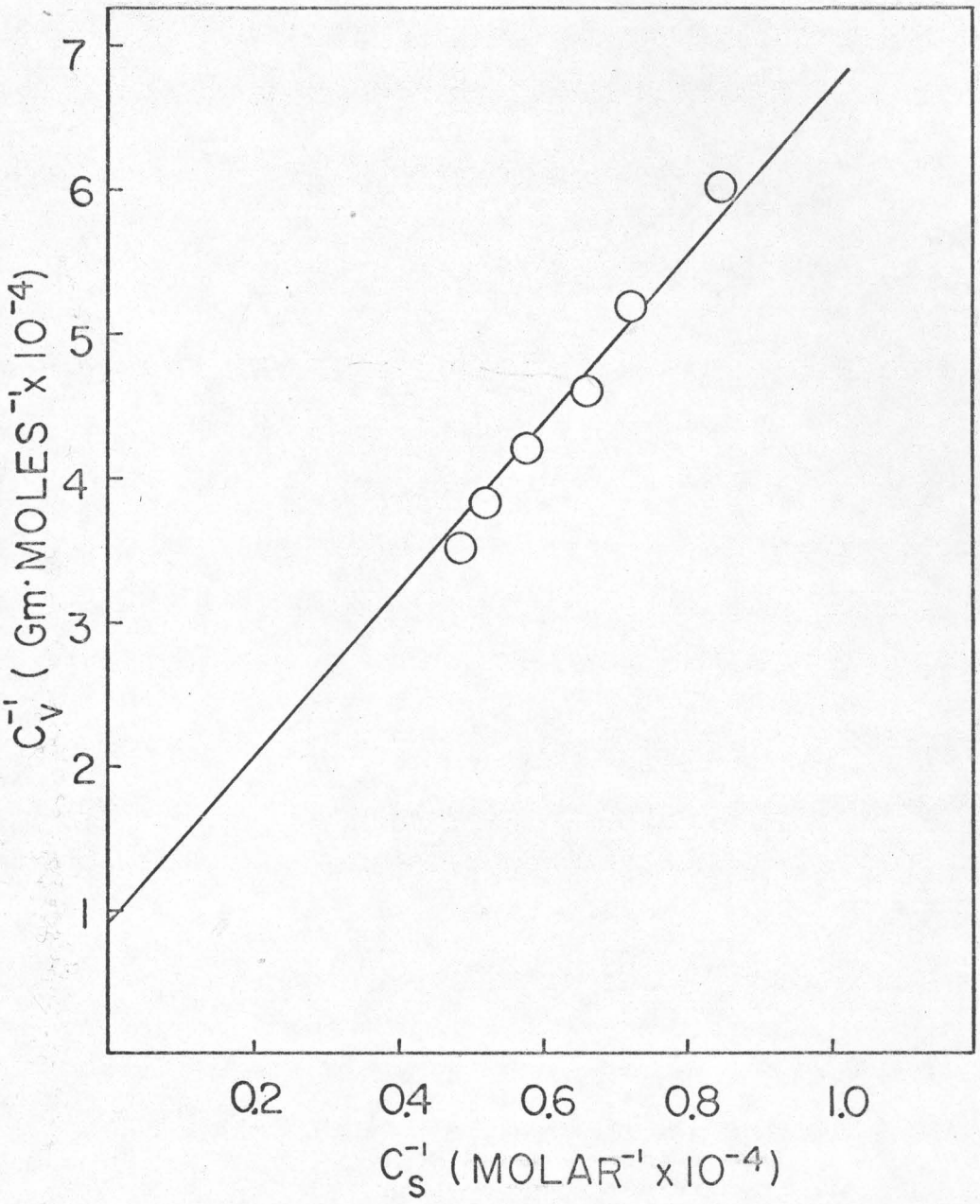

Figure 25. 7-Nitro-1,3-dihydro-5-phenyl-2H-1,4-benzodiazepine-2-one isotherm on montmorillonite from isopropanol.

Figure 26. 7-Nitro-1,3-dihydro-5-(2-chlorophenyl)-2H-1,4-benzodiazepine-2-one isotherm on montmorillonite from isopropanol.

The equation of the line is $y = 14.4x + 4.2$ where $y = 10^{-4} \cdot C_v^{-1}$ and $x = 10^{-4} \cdot C_s^{-1}$.

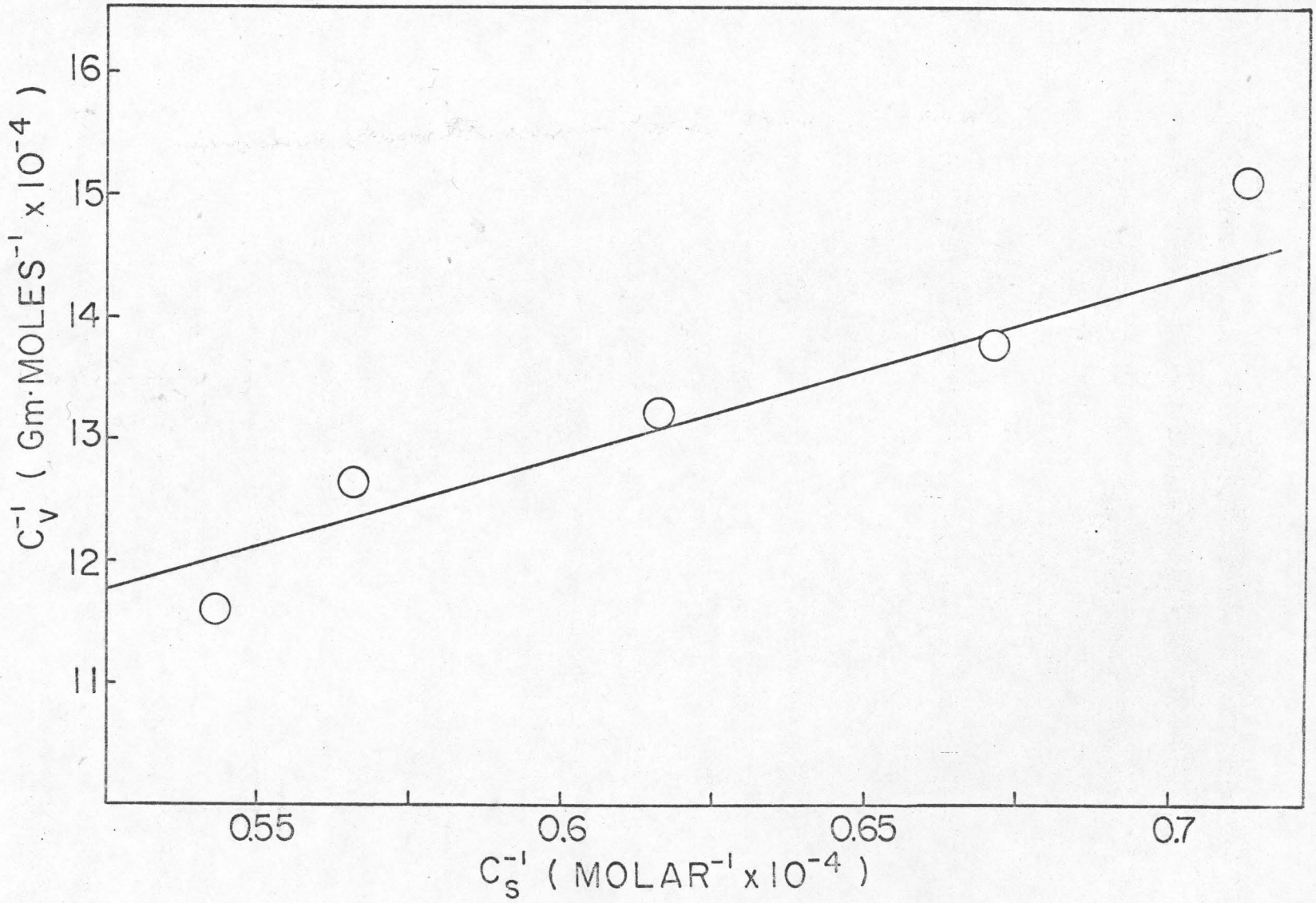
16
15
14
13
12
11
C_v^{-1} (Gm·MOLES^{-1} x 10^{-4})
0.55
0.6
0.65
0.7
C_s^{-1} (MOLAR^{-1} x 10^{-4})

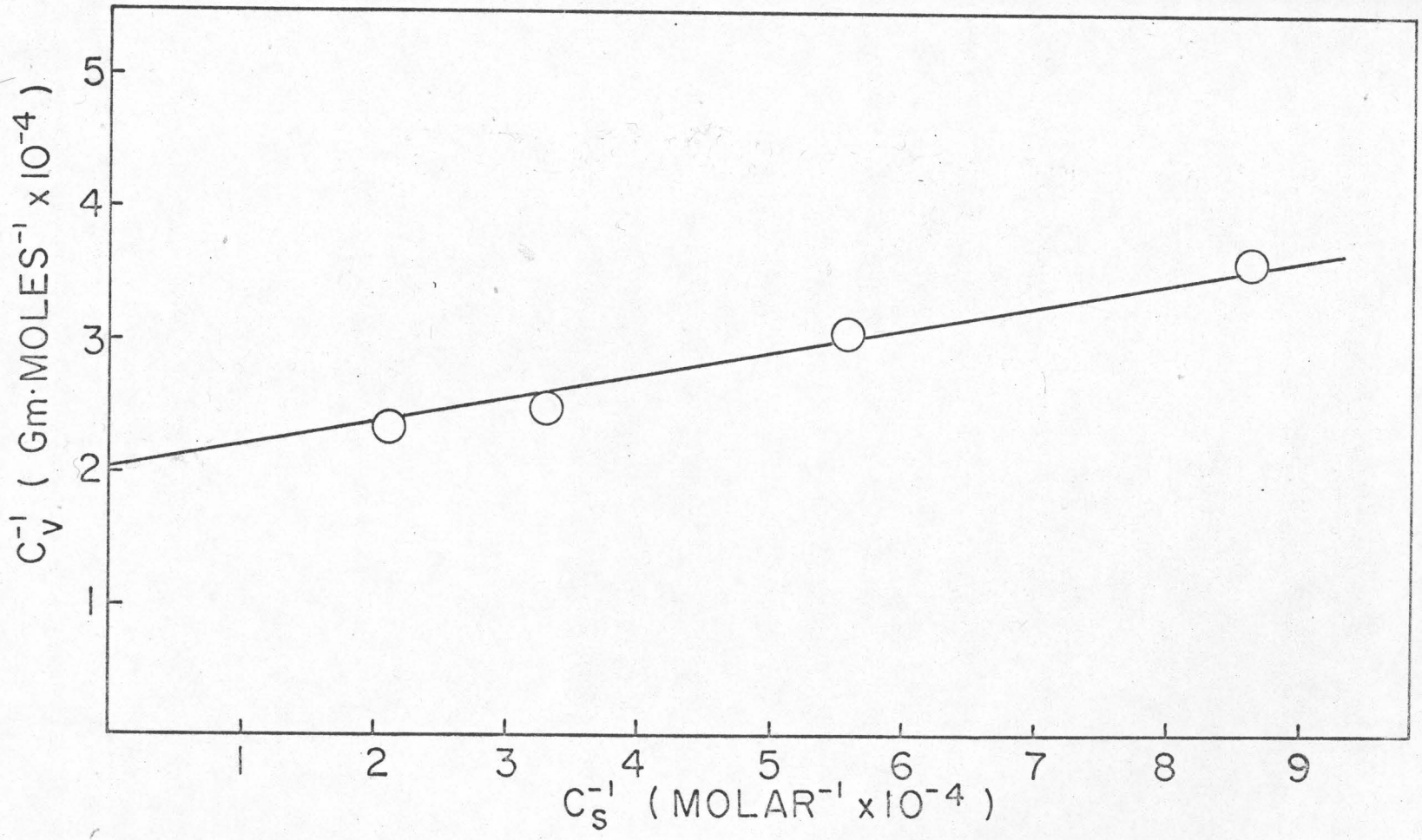

Figure 27. 7-Chloro-1,3-dihydro-5-phenyl-2H-1,4-benzodiazepine-2-one-4-oxide isotherm on montmorillonite from isopropanol.

The equation of the line is $y = 0.17x + 2.01$ where $y = 10^{-4} \cdot C_v^{-1}$ and $x = 10^{-4} \cdot C_s^{-1}$.

F. B.E.T. Nitrogen Isotherms

Surface area measurement on montmorillonite by B.E.T. nitrogen isotherm:

The volume of capillary, glass bulbs, sample bulb and discard portion were obtained by the methods indicated in Section II-F. They are summarized in Table IV.

TABLE IV

Determination of Volumes on Vacuum Rack (cc)

P_o	P_1	V_1	Average V_1
32.835	29.010	40.68	
31.320	27.605	41.49	41.70
27.180	23.860	42.90	

P_o	P_2	V_2	Average V_2
29.010	24.140	62.20	
31.320	25.990	63.23	63.00
27.180	22.530	63.63	

P_o	P_3	V_3	Average V_3
29.010	7.380	903.4	
31.320	7.965	904.0	903.7

Therefore, the discard volume $V_4 = V_3 - V_2$ is 840.8.

The total volume of glass bulbs can be computed by adding the individual volume of each glass bulb (refer to

Figure 5) and is equal to 35.39 cc.

the total volume V_1 (glass bulbs and capillary)	=	41.7 cc
the total volume V_2 (V_1 plus sample bulb)	=	63.0 cc
therefore,		
the volume of sample bulb	=	63.0 - 41.7
	=	21.3 cc.

The volumesincluding capillary to the different marks of the multiple volume McLeod gauge were calculated as follows:

the volume up to mark 5	=	41.7 cc
the volume up to mark 4	=	41.7 - 22.650
	=	19.05 cc
the volume up to mark 3	=	41.7 - (22.650 + 8.2542)
	=	10.8 cc
the volume up to mark 2	=	41.7 - (22.650 + 8.254 +3.452)
	=	7.345 cc
the volume up to mark 1	=	41.7 - 35.39 = 6.31 cc

The actual computations, now, take into account that during measurements part of the nitrogen is at room temperature and part at -196°C.

We denote by

n_1: the number of moles of nitrogen contained in the sample bulb which is immersed in liquid nitrogen

V_1: the volume of sample bulb which is equal to 21.3 cc, and

P_a: the partial pressure of the nitrogen at the temperature of the experiment.

According to the ideal gas equation,

$$n_1 = \frac{P_a \cdot 21.3}{(82.1)(77.15)(76)} \qquad \text{(Eq. 7)}$$

Again, denoting by

n_g: the total number of moles of nitrogen utilized for adsorption study

n_2: the number of moles of nitrogen beyond the sample bulb during adsorption, i.e., $n_g = n_1 + n_2$, and

V_b: the volume of the capillary up to a certain mark during adsorption study.

Then:

$$n_2 = n_g - n_1 = n_g - \frac{P_a \cdot 21.3}{(82.1)(77.15)(76)} \qquad \text{(Eq. 8)}$$

and

$$n_2 = \frac{P_a \cdot V_b}{82.1 \cdot (273.15 + t) \cdot 76} \qquad \text{(Eq. 9)}$$

where t is the temperature during the experiment. By substituting Eq. 8 into Eq. 9 we get

$$n_g - \frac{P_a \cdot 21.3}{(82.1)(77.15)(76)} = \frac{P_a \cdot V_b}{82.1 \cdot (273.15 + t) \cdot 76}$$

This can be rearranged to

$$n_g = \frac{P_a \cdot V_b}{82.1 \cdot (273.15 + t) \cdot 76} + \frac{P_a \cdot 21.3}{(82.1)(77.15)(76)} \qquad \text{(Eq. 10)}$$

Therefore,

$$n_g = \frac{P_a}{(82.1)(76)} \left[\frac{V_b}{(273.15 + t)} + \frac{21.3}{77.15}\right] \qquad \text{(Eq. 11)}$$

Denote by

n : the number of moles of registered nitrogen ready for adsorption study, and

Δn : the number of moles of nitrogen adsorbed onto montmorillonite,

then,

$$\Delta n = n - n_g \qquad \text{(Eq. 12)}$$

If we convert the moles of nitrogen adsorbed onto montmorillonite to the volume at STP (0°C, 1 atm), then,

$$V\,(STP) = \frac{\Delta n(82.1)(273.15)}{1} \qquad \text{(Eq. 13)}$$

Brunauer, et al. (74) arrived at the following equation for the treatment of multilayer adsorption:

$$\frac{P_a}{V(P_s - P_a)} = \frac{(C-1)\,P_a}{V_m C\,P_s} + \frac{1}{V_m C} \qquad \text{(Eq. 14)}$$

where

V: the total volume of adsorbate per sample of adsorbent

V_m: the volume of adsorbate adsorbed when the entire adsorbent surface is covered with a complete unimolecular layer

P_a: partial pressure of the adsorbate at the temperature of the experiment

P_s: the saturated pressure of the adsorbate at the temperature of the coolant

$\frac{P_a}{P_s}$: the relative pressure

C: a constant at a given temperature expressing the net adsorption energy.

The constant C is usually large when compared to unity and is given by the equation:

$$C = \exp.[(E_1 - E_2)/RT] \qquad \text{(Eq. 15)}$$

where

E_1: the heat of adsorption of the monolayer

E_2: the heat of condensation for subsequent layers

R: the gas constant

T: the absolute temperature.

According to the B.E.T. equation (Eq. 14), a plot of $P_a/V(P_s - P_a)$ versus P_a/P_s should give a straight line with a slope of $(C-1)/V_mC$ and an intercept of $1/V_mC$.

The adsorption and desorption data have been treated according to the B.E.T. equation and are tabulated in Table V and Table VI and the ensuring B.E.T. plots are shown in Figure 28 and Figure 29, respectively.

From the graph, it is seen that the intercept is equal to 2×10^{-4} and the slope is equal to 400×10^{-4}. Therefore,

$$\frac{C-1}{V_mC} = 400 \times 10^{-4} \qquad \text{(Eq. 16)}$$

$$\frac{1}{V_mC} = 2 \times 10^{-4} \qquad \text{(Eq. 17)}$$

By solving equation 16 and equation 17, we obtain

$$C = 201$$

$$V_m = 24.9 \text{ (unit in cc)}$$

The number of moles (n_o) at S.T.P., then, can be calculated as follows:

$$PV = n_oRT$$

so

$$n_o = \frac{PV}{RT} = \frac{(1)(24.9)}{(82)(273.15)} = 1.112 \times 10^{-3} \text{ moles}$$

TABLE V

Data Pertinent to the Determination of Adsorption Curve from B.E.T. Measurements
(Decimals are not significant figures except in last two columns)

n ($\times 10^{+3}$)	V_b	P_a	$\frac{V_b}{[(273.15+t)/21.3 + 77.15]}$	n_g ($\times 10^{+3}$)	Δn ($\times 10^{+3}$)	V (STP) per sample	$P_s - P_a$	$\frac{P_a}{V(P_s-P_a)}$ (10^{+4})	P_a/P_s
3.1392	41.70	25.130	0.41455	1.66961	1.46959	32.95645	50.870	150	0.331
3.1392	19.05	29.810	0.33934	1.62122	1.51798	34.04163	46.190	190	0.392
3.1392	10.80	31.170	0.31195	1.55833	1.58087	35.45198	44.830	196	0.410
2.3858	41.70	15.940	0.41525	1.06080	1.32500	29.71394	60.060	89	0.210
2.3858	19.05	19.105	0.33906	1.04000	1.34580	30.18039	56.895	111	0.251
2.3858	10.80	20.000	0.31213	1.00047	1.38530	31.06620	56.000	115	0.263
2.3858	7.34	20.405	0.30058	0.98200	1.40290	31.46089	55.595	117	0.269
2.3858	6.31	20.250	0.29714	0.96430	1.42150	31.87801	55.750	114	0.267
1.9994	41.70	10.785	0.41502	0.71730	1.28214	28.75277	65.215	57.5	0.142
1.9994	19.05	13.125	0.33953	0.71420	1.28520	28.82229	62.875	72.4	0.173
1.9994	10.80	13.600	0.31207	0.68018	1.31926	29.58522	62.400	73.7	0.181
1.9994	7.34	14.100	0.29812	0.67367	1.32577	29.73120	61.900	76.6	0.191
1.9994	6.31	13.935	0.29711	0.66353	1.33591	29.45860	62.065	74.9	0.183
1.59586	41.70	6.335	0.41242	0.41873	1.17715	26.39830	69.665	34.5	0.0834
1.59586	19.05	7.830	0.33837	0.42461	1.17127	26.26645	68.170	43.7	0.103
1.59586	10.80	8.000	0.31396	0.39925	1.19663	26.83516	68.000	43.8	0.105
1.59586	7.34	8.405	0.30008	0.40422	1.19166	26.72370	67.595	46.6	0.111
1.59586	6.31	8.070	0.29671	0.38375	1.21213	27.18275	67.930	43.7	0.106

(Cont.)

TABLE V - Cont.

n ($\times 10^{+3}$)	V_b	P_a	$\frac{V_b}{(273.15+t)}\left[+\frac{21.3}{77.15}\right]$	n_g ($\times 10^{+3}$)	Δn ($\times 10^{+3}$)	V (STP) per sample	$P_s - P_a$	$\frac{P_a}{V(P_s-P_a)}$ (10^{+4})	P_s/P_a
1.42289	41.70	4.930	0.41364	0.32682	1.09607	24.58000	71.070	28.2	0.0649
1.42289	19.05	6.200	0.33892	0.33677	1.08420	24.35690	69.800	36.4	0.0816
1.42289	10.80	6.185	0.31171	0.30898	1.11391	24.98010	69.815	35.4	0.0814
1.42289	7.34	6.505	0.30029	0.31307	1.10982	24.88390	69.495	37.0	0.0856
1.42289	6.31	6.255	0.29690	0.29763	1.12526	25.23465	69.745	35.5	0.0823
1.05750	41.70	1.875	0.41642	0.12513	0.93237	20.90897	74.125	12.1	0.0247
1.05750	19.05	2.460	0.34019	0.13412	0.92338	20.70736	73.540	16.2	0.0324
1.05750	10.80	2.125	0.31243	0.10640	0.95110	21.32900	73.875	13.5	0.0280
1.05750	7.34	2.475	0.30074	0.11929	0.93821	21.03993	73.525	16.0	0.0326
1.05750	6.31	2.180	0.29735	0.10388	0.95362	21.38551	73.820	13.8	0.0287
0.70331	41.70	0.250	0.41409	0.01659	0.68672	15.40012	75.750	2.14	0.00329
0.70331	19.05	0.690	0.27837	0.03078	0.67253	15.08189	75.310	6.07	0.00902
0.70331	10.80	0.250	0.31183	0.01249	0.69082	15.49206	75.750	2.13	0.00329
0.70331	7.34	0.645	0.30038	0.03105	0.67226	15.07584	75.355	5.68	0.00849
0.70331	6.31	0.330	0.29707	0.01571	0.68760	15.41985	75.670	2.83	0.00434
0.48798	41.70	0.070	0.41665	0.00467	0.48331	10.83852	75.930	0.85	0.000921
0.48798	19.05	0.480	0.34030	0.02617	0.46181	10.35637	75.520	6.14	0.00632
0.48798	10.80	0.200	0.31249	0.01001	0.47797	10.71876	75.800	2.46	0.00263
0.48798	7.34	0.525	0.30080	0.02530	0.46268	10.37588	75.475	6.70	0.00691
0.48798	6.31	0.190	0.29743	0.00905	0.47893	10.74029	75.810	2.33	0.00250

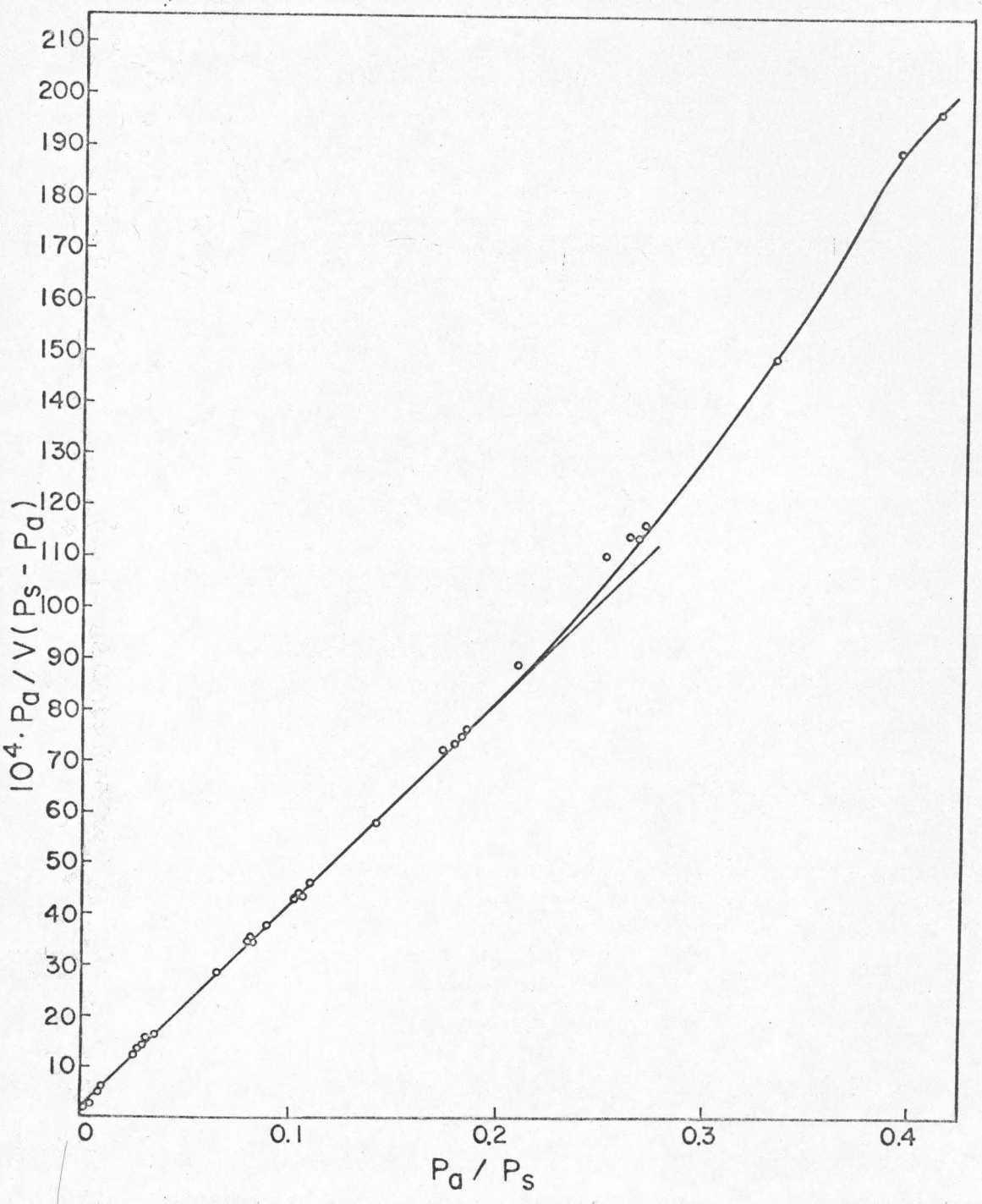

Figure 28. Nitrogen adsorption curve (B.E.T. plot).

TABLE VI

Data Pertinent to the Determination of Desorption Curve from B.E.T. Measurements
(Decimals are not significant figures except in last two columns)

n ($\times 10^{+3}$)	V_b	P_a	$\frac{V_b}{[(273.15+t)+\frac{21.3}{77.15}]}$	n_g ($\times 10^{+3}$)	Δn ($\times 10^{+3}$)	V (STP) per sample	$P_s - P_a$	$\frac{P_a}{V(P_s-P_a)}$ (10^{+4})	P_s/P_a
3.1392	41.70	24.635	0.41554	1.63673	1.50247	33.69381	51.365	142	0.324
3.1392	19.05	29.335	0.33934	1.59539	1.54381	34.62088	46.665	182	0.390
2.3858	41.70	15.345	0.41525	1.02120	1.36460	30.60199	60.655	82.7	0.202
2.3858	19.05	18.510	0.33966	1.00760	1.37820	30.90698	57.490	104	0.244
2.3858	10.80	19.395	0.31213	0.97020	1.41560	31.74570	56.605	108	0.261
2.3858	7.34	20.155	0.30058	0.97090	1.41490	31.73000	55.845	114	0.265
1.9994	41.70	10.580	0.41502	0.70370	1.29574	29.05777	65.420	55.7	0.139
1.9994	19.05	12.905	0.33957	0.70220	1.29724	29.09140	63.095	70.3	0.169
1.9994	10.80	13.620	0.31206	0.68118	1.31826	29.56279	62.380	71.9	0.179
1.9994	7.34	14.040	0.29812	0.67080	1.32864	29.79552	61.960	76.1	0.185
1.59586	41.70	6.185	0.41243	0.40881	1.18707	26.62077	69.815	33.3	0.0814
1.59586	19.05	7.660	0.33837	0.41539	1.18049	26.47321	68.340	42.3	0.101
1.59586	10.80	7.905	0.31139	0.39451	1.20137	26.94146	68.095	43.1	0.104
1.59586	7.34	8.235	0.30008	0.39604	1.19984	26.90715	67.765	45.2	0.108
1.42289	41.70	4.745	0.41364	0.31455	1.10834	24.85520	71.255	27.1	0.0624
1.42289	19.05	6.030	0.33892	0.32753	1.09536	24.56410	69.970	35.1	0.0893
1.42289	10.80	6.040	0.31171	0.30173	1.12116	25.14270	69.960	34.3	0.0895
1.42289	7.34	6.485	0.30029	0.31210	1.11079	24.91010	69.515	37.5	0.0853

(Cont.)

TABLE VI - Cont.

n $(\times 10^{+3})$	V_b	P_a	$\frac{V_b}{(273.15+t)} + \frac{21.3}{77.15}$	n_g $(\times 10^{+3})$	Δn $(\times 10^{+3})$	V (STP) per sample	$P_s - P_a$	$\frac{P_a}{V(P_s-P_a)}$ (10^{+4})	P_s/P_a
1.05750	41.70	1.610	0.41571	0.10726	0.95024	21.30972	74.390	10.1	0.0212
1.05750	19.05	2.135	0.33987	0.11629	0.94121	21.10743	73.865	13.6	0.0281
1.05750	10.80	1.870	0.31225	0.09358	0.96392	21.61649	74.130	11.6	0.0246
1.05750	7.34	2.260	0.30066	0.10890	0.94860	21.27294	73.740	14.4	0.0297
0.70331	41.70	0.190	0.41432	0.01261	0.69070	15.48937	75.810	1.62	0.00250
0.70331	19.05	0.620	0.33924	0.03370	0.66961	15.01644	75.380	5.48	0.00816
0.70331	10.80	0.180	0.31188	0.00899	0.69432	15.57055	75.820	1.52	0.00237
0.70331	7.34	0.530	0.30041	0.02551	0.67780	15.20008	75.470	4.62	0.00697
0.48798	41.70	0.110	0.41689	0.00734	0.48064	10.77865	75.890	1.34	0.00145
0.48798	19.05	0.440	0.34030	0.02399	0.46399	10.40526	75.560	5.59	0.00579
0.48798	10.80	0.155	0.31249	0.00776	0.48022	10.76923	75.845	1.90	0.00204
0.48798	7.34	0.380	0.30080	0.01831	0.46967	10.53264	75.620	4.77	0.00500

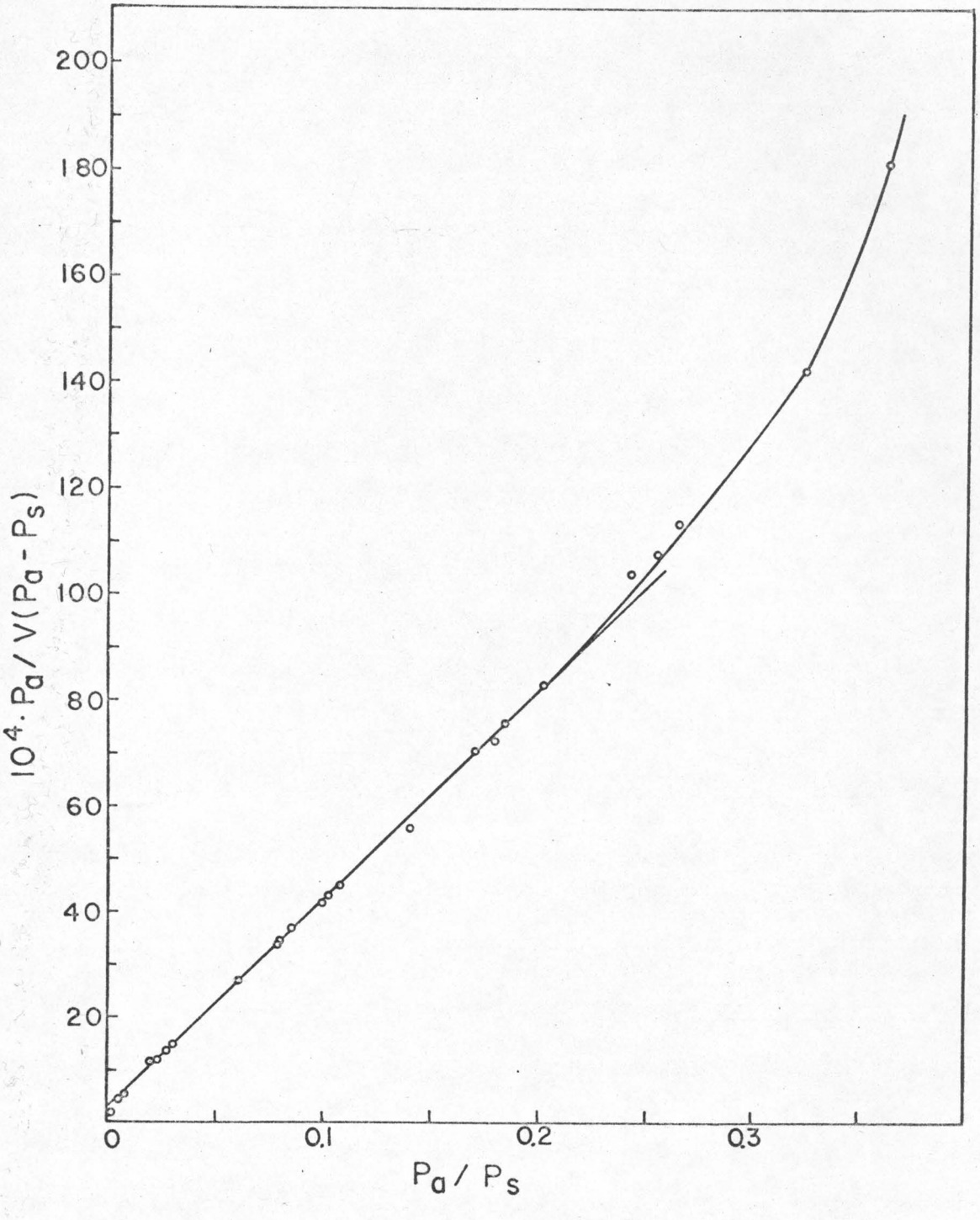

Figure 29. Nitrogen desorption curve (B.E.T. plot).

Therefore, the number of molecules of adsorbate required to cover the entire adsorbent surface with a complete unimolecular layer is $1.112 \times 10^{-3} \times 6 \times 10^{23} = 6.672 \times 10^{20}$. If the area occupied by a nitrogen molecule at -196°C is estimated to be 16.2 $\mathring{A}^2$ (75), the total surface area is equal to

$$16.2 \times 6.672 \times 10^{20} = 108.0864 \times 10^{20}\ \mathring{A}^2/\text{sample}$$
$$= 108\ m^2/\text{sample}$$

The amount of sample is equal to 1.4336 gm; therefore, the surface area of montmorillonite per unit weight is $108/1.4336 = 75\ m^2/gm$.

G. Dielectric Constant Measurement

In the apparatus described in the experimental section, two components will contribute to the measured capacitance, viz, the capacitance of the glass walls, C_g, and the capacitance of the sample contained in the cell, C_s (whether this sample be air or solution). Because of the series connection the total cell capacitance is:

$$C = \frac{C_g C_s}{C_g + C_s} \qquad \text{(Eq. 18)}$$

The dielectric constant of air is unity; if we denote by C_o the contribution to the capacitance of the air, then a sample with dielectric constant ε will contribute

$$C_s = \varepsilon C_o \qquad \text{(Eq. 19)}$$

to the capacitance. Introducing this into Eq. 18 yields the combined capacitance of glass and solution:

$$C = \frac{C_g C_o \varepsilon}{C_g + \varepsilon C_o} \qquad \text{(Eq. 20)}$$

The instrument scale is in equal units of capacitance and the point of reference is established by adjusting the needle to zero (center position) when the cell is empty. Since the dielectric constant of air is unity, it contributes to the capacitance by an amount of:

$$C = \frac{C_g C_o}{C_g + C_o} \qquad \text{(Eq. 21)}$$

If a solution of known dielectric constant, ε_1, is placed in the sample cell, its contribution to the capacitance will be

$$C_1 = \frac{C_g C_o \varepsilon_1}{C_g + \varepsilon_1 C_o} \qquad \text{(Eq. 22)}$$

Since the apparatus was adjusted to zero with air, the measured scale reading will be $C_1 - C = S_1$, i.e.,

$$S_1 = \frac{C_g C_o \varepsilon_1}{C_g + C_o \varepsilon_1} - \frac{C_g C_o}{C_g + C_o} \qquad \text{(Eq. 23)}$$

Doing likewise for a second solvent with known dielectric constant, ε_2, yields

$$S_2 = \frac{C_g C_o \varepsilon_2}{C_g + C_o \varepsilon_2} - \frac{C_g C_o}{C_g + C_o} \qquad \text{(Eq. 24)}$$

Eq. 23 and Eq. 24 constitute two equations with two unknowns. Denoting $C_g/C_o = \alpha$ for convenience, these may be solved giving the following solutions:

$$\frac{1}{\alpha} = \frac{C_o}{C_g} = \frac{S_2(\varepsilon_1 - 1) - S_1(\varepsilon_2 - 1)}{\varepsilon_1 S_1(\varepsilon_2 - 1) - \varepsilon_2 S_2(\varepsilon_1 - 1)} \qquad \text{(Eq. 25)}$$

and

$$C_g = \frac{S_1(\alpha + 1) + \varepsilon_1 S_1(\frac{1}{\alpha} + 1)}{\varepsilon_1 - 1} \qquad \text{(Eq. 26)}$$

Hence we know both C_g and C_o $(=\alpha C_g)$ and can use Eq. 23 in the form:

$$\varepsilon_x = \frac{C_g + S_x(\alpha + 1)}{C_g - S_x(\frac{1}{\alpha} + 1)} \qquad \text{(Eq. 27)}$$

to calculate the dielectric constant for a sample from the measured scale reading S_x. The dielectric constant values of various solvents obtained in this fashion compared favorably with the values in the International Critical Tables (Vol. VI), as shown in Table VII.

TABLE VII

Comparison of Dielectric Constants of Various Solvents

Solvent	Data from I.C. Table	Measured from Model V Oscillometer
Acetonitrile	34.00	36.16
Methanol	31.50	30.28
Ethanol	23.00	23.73
n-Propanol	20.00	19.44
Isobutyl alcohol	17.34	17.51
Isoamyl alcohol	15.30	15.75
n-Amyl alcohol	14.34	14.98
Isopropanol	12.42	13.41
Dichloroethane	10.36	9.32
tert-Butyl alcohol	9.90	8.42

H. Dipole Moment Determination

According to Guggenheim (76) and Minkin, et al. (77),

$$\frac{3M_2V_1}{(\varepsilon_1 + 2)^2}\left[\left(\frac{d\varepsilon}{dw_2}\right)_{w_2\to 0} - \left(\frac{dn_D^2}{dw_2}\right)_{w_2\to 0}\right] = \frac{4}{9}\pi N \frac{\mu^2}{kT} \qquad \text{(Eq.28)}$$

where

M_2: the molecular weight of solute

V_1: the molar volume of solvent

ε_1: dielectric constant of pure solvent

N: Avogadro number

k: Boltzmann constant

T: absolute temperature

μ: dipole moment of solute

ε: dielectric constant of solution

n_D: refractive index of solution

w_2: weight fraction of solute

The problem is to evaluate the quantities $\left(\frac{d\varepsilon}{dw_2}\right)_{w_2\to 0}$ and $\left(\frac{dn_D^2}{dw_2}\right)_{w_2\to 0}$. This is done by assuming both the dielectric constant of solution, ε_1, and the refractive index of the solution, n_D, (in high dilution) to be linearly dependent on the weight fraction of solute, w_2 (78), i.e.,

$$\varepsilon = \varepsilon_1 + aw_2 \qquad \text{(Eq. 29)}$$

$$n_D^2 = n_{D,1}^2 + bw_2 \qquad \text{(Eq. 30)}$$

where $n_{D,1}$ is the refractive index of pure solvent and a and b are coefficients. Equation 28 can then be written

$$\mu^2 = \frac{9}{4} \cdot \frac{kT}{\pi N} \cdot \frac{3M_2V_1}{(\varepsilon_1 + 2)^2} (a - b)$$

that is

$$\mu = \left[\frac{9}{4} \cdot \frac{kT}{\pi N} \cdot \frac{3M_2V_1}{(\varepsilon_1 + 2)^2} (a - b)\right]^{\frac{1}{2}} \quad \text{(Eq. 31)}$$

The value of μ is obtained in this form in esu units which then are converted to Debye units. The dipole moments of diazepam derivatives obtained in this fashion are shown in Table VIII.

I. Infrared Spectra of Adsorbates

The IR spectra of (a) montmorillonite, (b) diazepam adsorbed on montmorillonite, and (c) oxazepam adsorbed on montmorillonite are shown in Figure 30. It is noted that there is no substantial difference between the spectra.

J. Reflectance Spectra

The reflectance spectra are shown in Figure 31.

TABLE VIII

Calculation of Dipole Moments of Benzodiazepine Derivatives
(Decimals are not significant figures except in last column (μ))

System No.	Name of Compound*	Molecular Weight	n_D (25°C)	n_D^2 (25°C)	ε (25°C)	Density (gm/ml)	Weight of Solute (gm/100 ml)
1	Solvent**	88	1.4185	2.01214	2.46709	1.0328	-
2	Diazepam	284.76	1.4203	2.01725	2.53011	1.0347	1.0015
3	Compound b	286.76	1.4211	2.01953	2.58082	1.0350	1.0014
4	Compound c	316.4	1.4205	2.01782	2.51626	1.0357	1.0019
5	Compound d	281.26	1.4209	2.01896	2.49394	1.0356	1.0014
6	Compound e	312.30	1.4207	2.01839	2.48037	1.0333	1.0013
7	Compound f	315.76	1.4211	2.01953	2.50327	1.0355	1.0005
8	Compound g	287	1.4212	2.01981	2.55109	1.0357	1.0037

*For the nomenclature of compounds, refer to Table I.

**Solvent is 1,4-dioxane.

TABLE VIII - Cont.

System No.	Weight Fraction of Solute (10^2)	V_1 (ml/gm)	$a = \frac{\varepsilon - \varepsilon_1}{W_2}$	$b = \frac{n_D^2 - n_{D,1}^2}{W_2}$	$\frac{3M_2V_1}{(\varepsilon_1 + 2)^2}(a-b)$	μ (Debye)
1	-	0.96824	-	-	-	-
2	0.96791	0.96824	6.51094	0.52794	248.00071	3.4
3	0.96754	0.96824	11.75455	0.76379	458.77657	4.7
4	0.96737	0.96824	5.08285	0.58716	206.93164	3.2
5	0.96697	0.96824	2.77672	0.70529	84.80729	2.0
6	0.96903	0.96824	1.37044	0.64497	32.97968	1.3
7	0.96619	0.96824	3.74461	0.76486	136.95941	2.6
8	0.96910	0.96824	8.66783	0.79146	329.05121	4.0

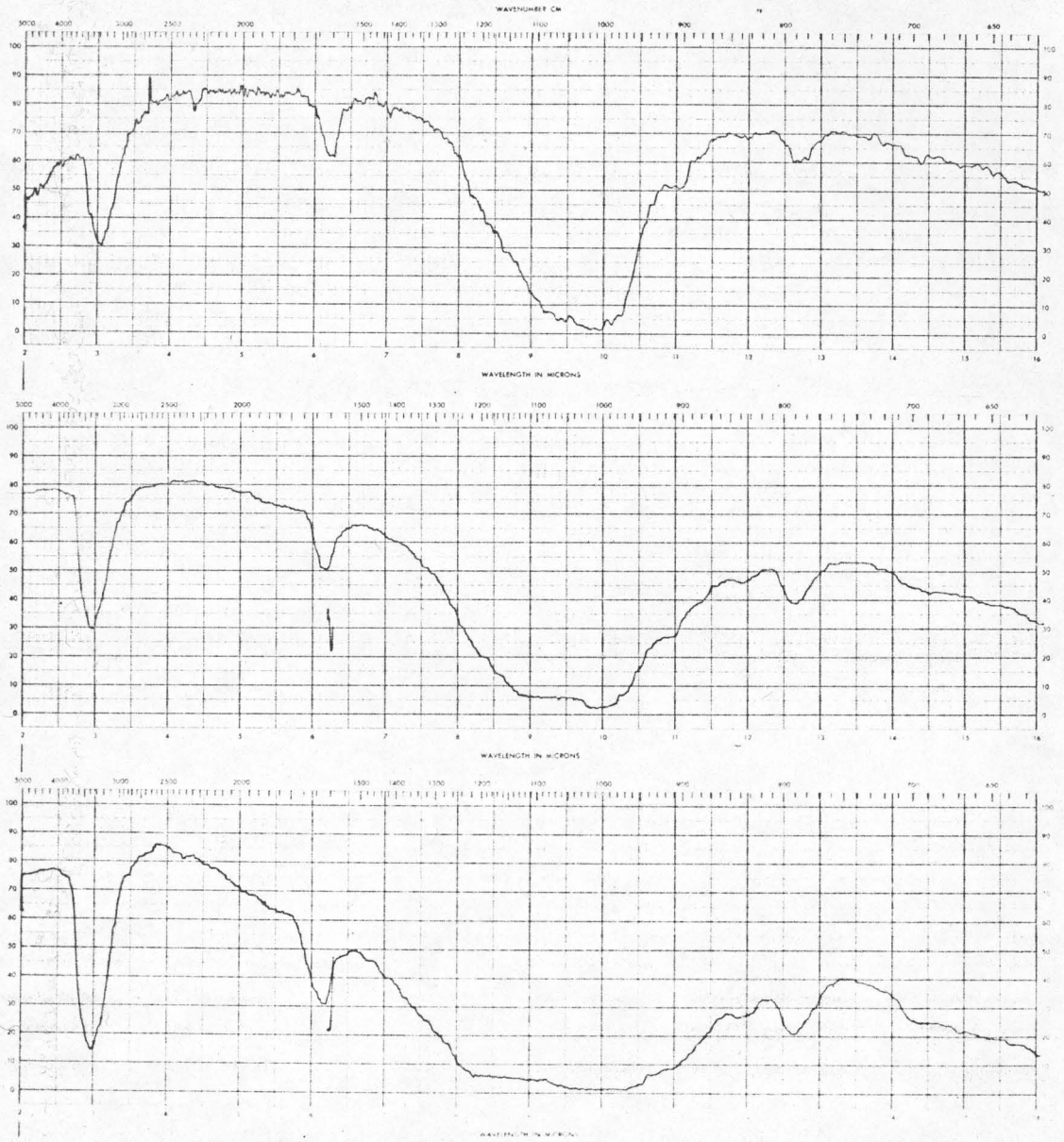

Figure 30. Infrared spectra of adsorbates.

Key: Top - montmorillonite
Center - diazepam adsorbed on montmorillonite
Bottom - oxazepam adsorbed on montmorillonite

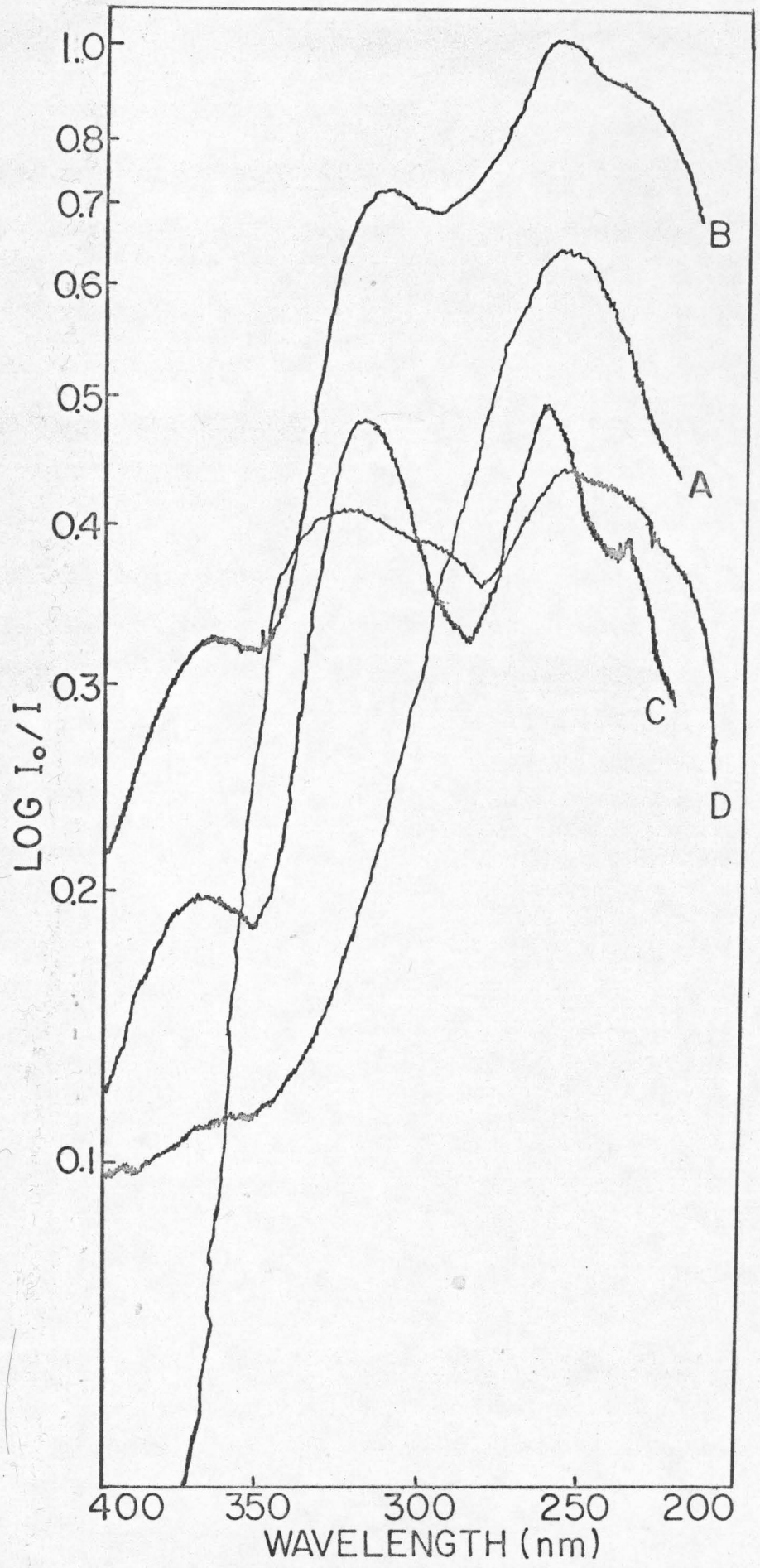

Figure 31. Reflectance spectra of adsorbate.
Key: A: montmorillonite (blank)
B: diazepam adsorbate on montmorillonite from isopropanol
C: diazepam adsorbate measured against montmorillonite plus isopropanol
D: diazepam

IV. DISCUSSION

In investigating the adsorption of various solutes on montmorillonite it became clear, at an early point in the investigation that, as a trend, the adsorption from anhydrous solvents was the stronger the smaller the dielectric constant. Prior to investigating this systematically, it was necessary to establish the order of magnitudes of the adsorption of the solvents themselves.

This (and obtaining information relative to the number of adsorption sites) was the prime purpose of conducting this set of experiments with benzoic acid as solute. If the adsorption of benzoic acid is a competition between solvent (o) and benzoic acid (b), then the surface fraction covered (θ) is given in terms of the concentrations in solution (C) by (79):

$$\theta_b = \frac{K_b C_b}{1 + K_b C_b + K_o C_o} \qquad \text{(Eq. 32)}$$

If $K_o C_o$ is negligible compared to unity, then (taking reciprocals) this equation becomes:

$$\frac{1}{\theta_b} = 1 + \frac{1}{K_b C_b} \qquad \text{(Eq. 33)}$$

If one gram of montmorillonite contains N sites in total, and the number of sites occupied per gram is n (i.e., there are n molecules adsorbed per gram), then $\theta_b = n/N$ is the fractional coverage. If (as is conventionally assumed) the number of sites N equals the saturation value of n for high values of C_b, then $N = n_\infty$ and $\theta_b = n/n_\infty$ is a dimensionless quantity. Equation 33 may then be written:

$$\frac{N}{n} = 1 + \frac{1}{K_b C_b} \qquad \text{(Eq. 34)}$$

Since this equation is dimensionless, K_b is in reciprocal concentration units; molarity is used here so this unit is M^{-1}. Eq. 34 may be written:

$$\frac{1}{n} = \frac{1}{N} + \frac{1}{K_b N} \cdot \frac{1}{C_b} \qquad \text{(Eq. 35)}$$

so that a plot of the reciprocal of the number of molecules adsorbed per gram of montmorillonite versus reciprocal concentration will yield an intercept of 1/N and an intercept/slope ratio of K_b. These considerations assume that $K_o C_o$ is negligible compared to unity. If $K_o C_o$ is not negligible, then Eq. 35 becomes:

$$\frac{1}{n} = \frac{1}{N} + \frac{[K_o C_o + 1]}{K_b N} \cdot \frac{1}{C_b} \qquad \text{(Eq. 36)}$$

For benzoic acid isotherms, the concentration of benzoic acid is low, so C_o is practically invariant; reciprocal plotting of benzoic acid adsorption data from isopropanol, therefore, still yields a straight line (Figure 6). However, the intercept to slope ratio only yields the value for K_b if the value of K_oC_o is negligible compared to unity.

Figure 6 shows that the intercept is 1.67×10^{-20}, hence $N = 6.0 \times 10^{19}$ for isopropanol. Intercept and N-values for other solvents and benzoic acid are listed in Table IX, and it is seen that these do not differ greatly from solvent to solvent; $N = 4.8 \times 10^{19}$ is the average value. From Figure 6 it is, furthermore, seen (from intercept to slope ratio) that provided K_oC_o is negligible compared to unity, $K_b = 20\ M^{-1}$.

From Eq. 35 it follows that if the concentration on the solid is expressed as C_v moles per gram then $n = 6.10^{23} \times C_v$, then

$$\frac{1}{6.10^{23} \cdot C_v} = \frac{1}{N} + \frac{1}{K_bN} \cdot \frac{1}{C_b} \qquad \text{(Eq. 37)}$$

or

$$\frac{1}{C_v} = \frac{6.10^{23}}{N} + \frac{6.10^{23}}{K_bN} \cdot \frac{1}{C_b} \qquad \text{(Eq. 38)}$$

TABLE IX

Benzoic Acid Isotherms in Various Solvents

Solvent	Intercept	Sites per Gram
Isopropanol	1.67×10^{-20}	6.0×10^{19}
Water-Isopropanol (50% w/w)	2.07×10^{-20}	4.6×10^{19}
Ethanol	2.51×10^{-20}	4.0×10^{19}
Butanol	2.34×10^{-20}	4.3×10^{19}
Methanol	2.01×10^{-20}	5.0×10^{19}
	Average:	4.8×10^{19}
	Standard Deviation:	0.8×10^{19}

so that N equals 6×10^{23} divided by the intercept and K_b emerges directly (in units of M^{-1}) as the intercept:slope ratio. The graphs (Figure 11 through Figure 27) are presented in this fashion.

As mentioned in the introduction, solvent (and water) molecules migrate into the crystal space in the montmorillonite. It is, a priori, possible that the solute molecules will behave likewise (62). If this were the case, then the total number of interstitial and surface sites should be available for adsorption. If so, the number of sites obtained from a water isotherm should equal that from a benzoic acid isotherm. It was for this reason that the amount of water removed by montmorillonite from hydroisopropanolic solutions was determined. In this case, the concentration of water in Eq. 36 is represented by C_b and C_o is the concentration of isopropanol. Since C_b in this case is not small and is varied over a large range, C_o is not invariant. If, however, K_oC_o is negligible (compared to unity), Eq. 35 should be obeyed.

A plot of the data is shown in Figure 9 and plotting according to Eq. 35 is shown in Figure 32. The linearity of the data in Figure 32 is good and the number of sites calculated is $N = 3.5 \times 10^{22}$. This is about 600 times larger than the number of sites available for benzoic acid adsorption and it may be concluded that the adsorption of the latter is strictly a surface phenomenon on the neutralized montmorillonite.

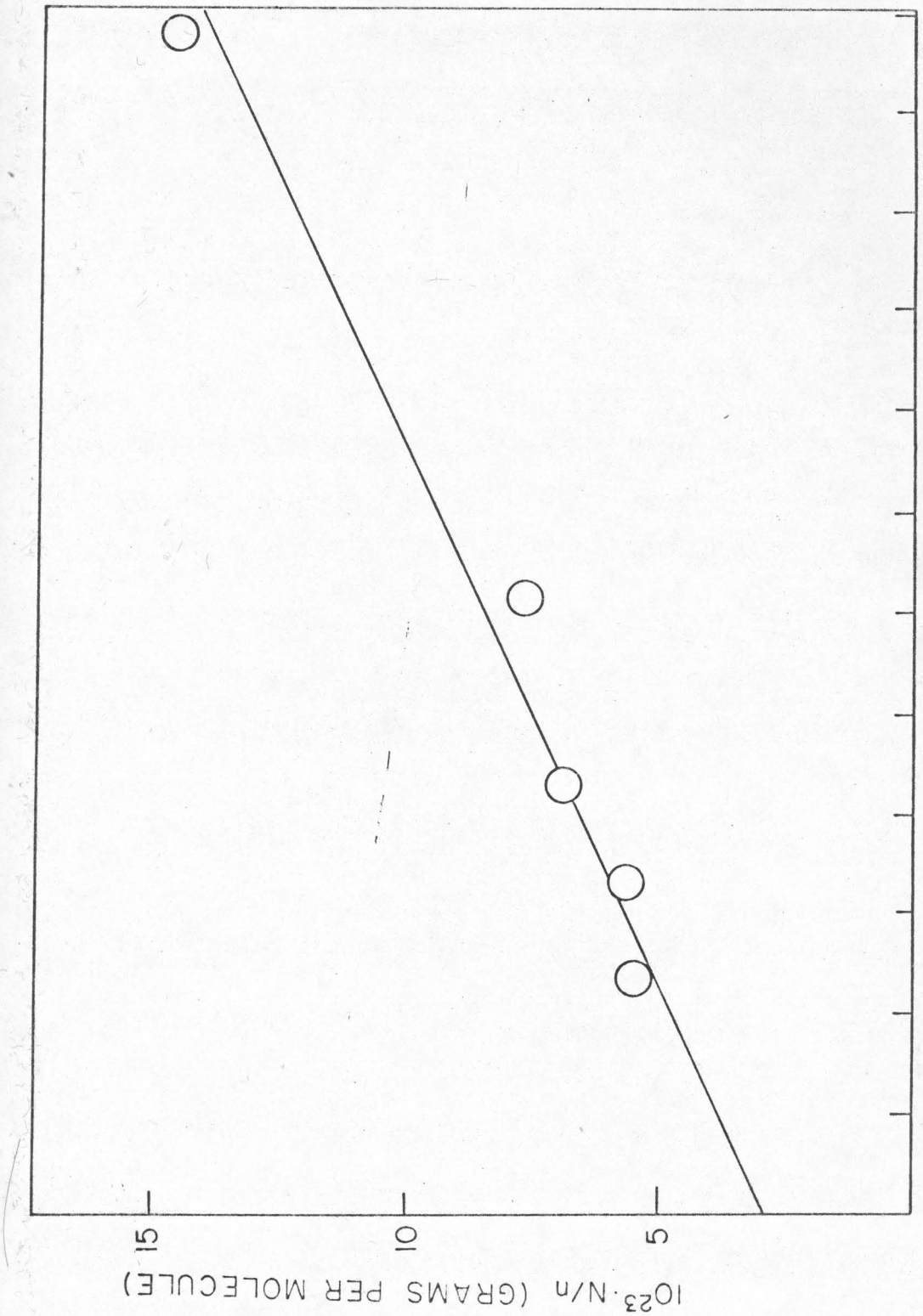

Figure 32. Langmuir plot of data from Fig. 9. The equation of the line is $1/n = 2.86 \times 10^{-23} + 9.4 \times 10^{-22}/C_{H_2O}$.

It is important to note that the number of sites available to benzoic acid adsorption does not change appreciably with water content as seen from Table IX: the number of sites calculated from the benzoic acid isotherm in 50% aqueous isopropanol equals the number obtained from anhydrous isopropanol and other solvents tested in this series.

Regarding the assumption that $K_oC_o \ll 1$, it is seen from Figure 32 that reciprocal plotting yields a straight line; in order for linearity to prevail in the water isotherm it is necessary that $K_oC_o \ll 1$ (Eq. 36). The value of $K_b = 20\ M^{-1}$, therefore, represents a realistic figure. It should be noted that in the benzoic acid isotherm, C_b is in the range 0.02-0.05 M, so $K_bC_b = 0.4 - 1$; since K_bC_b, therefore, is of the order of unity and K_oC_o is much smaller than unity, it can also be stated with acceptable credibility that $K_bC_b \gg K_oC_o$.

The manner in which this will be utilized in the following is that if K_2C_2, where the subscript 2 refers to solute, is larger than unity, then it is valid to neglect the effect of solvent adsorption in data treatment, and Eq. 35 may be used as written.

As mentioned, the general trend is for stronger adsorption from liquids with lower dielectric constants, and this would imply that the interaction is electrical in nature. To investigate this possibility a series of

compounds of the general structure given in Table I were selected. These benzodiazepines are not ionized in solution and this eliminates the possibility of ion exchange being a mode of adsorption. The compounds, however, possess dipole moments, and if the forces involved in the adsorption are electrical forces between surface ions and the solute dipoles, then forces can be formulated mathematically and the pertinent relations tested experimentally.

If it is assumed that the interaction is one between a dipole consisting of two fundamental electrical charges (e) removed from one another a distance 2d, i.e., having a dipole moment of 2 e.d. and a surface ion of charge Z (i.e., for instance minus two for a doubly negatively charged oxygen), then, at a distance x between dipole and ion, the force exerted would be:

$$f_c = -\left[\frac{Ze^2}{(x-d)^2} - \frac{Ze^2}{(x+d)^2}\right] \cdot \frac{1}{\varepsilon} \qquad \text{(Eq. 39)}$$

Repulsions are counted as being negative and attractions as being positive. ε is here the dielectric constant of the medium between ion and dipole. This preliminary model assumes that only one ion and dipole interact. More realistic corrections to this will be introduced shortly. It should be noted that Z is probably more than minus two (of smaller absolute value) for the

montmorillonite surface oxygens since (a) part of their charge is diverted by cations in the crystal interior and (b) minus two is not the effective charge in any event, because it only represents one of the resonance forms of the silicate moiety in montmorillonite (80).

When adsorbed, the dipole is an equilibrium distance r from the surface ion, so that the energy involved is:

$$E = -\frac{Ze^2}{\varepsilon}\int_{\infty}^{r}\left[\frac{1}{(x-d)^2} - \frac{1}{(x+d)^2}\right]\cdot dx \qquad \text{(Eq. 40)}$$

$$= \frac{Z2de^2}{\varepsilon(r^2 - d^2)}$$

when $d \ll r$, this reduces to:

$$E = \frac{Ze\mu}{\varepsilon r^2} \qquad \text{(Eq. 41)}$$

where μ is the dipole moment of the dipole. Up to this point the development follows the treatment by Amis (81) to some extent. As mentioned, the picture is over-simplified since it accounts for only the interaction of the dipole with one surface ion (the nearest surface ion, referred to as the contact ion in the following). A further complication is the fact that the cross-sectional area of diazepam (about 25 $\mathring{A}^2$) is too large to allow a one-to-one relationship between ion and dipole.

To take these factors into account consider the geometries of Figure 33. This is essentially Schofield's model (82); the oxygens are in a hexagonal array and 4 Å apart. It is noted that each oxygen has three nearest neighbors (denoted B) at 4 Å distance, six next-nearest neighbors (denoted C) at $4 \times \sqrt{3} = 7$ Å distance and three third-nearest neighbors (denoted D) at 8 Å distance. It is hardly plausible that there should be a one-to-one relationship between oxygen ion and organic solute dipole. The smallest area inscribed by four oxygens (BCCD) is 13.8 $Å^2$ and the largest (DBDC) is 27.7 $Å^2$ so both benzoic acid and diazepam could fit into this picture in spite of the disparity in cross section (10 versus 25 $Å^2$). It is noted that both benzoic acid (Table IX) and the benzodiazepine derivatives (Table X) give numbers of sites of comparable magnitude (of the order 10^{19} sites per g).

It is, hence, more rational to assume that the "sites" are in a quadratic array, 8 Å apart. In this visualization Z is twice the charge on the surface oxygen and there are arrays of the crystal surface where the distance between each surface ion is the minimum dictated by the lattice, viz. ℓ (8 Å) as shown in Figure 33. Then there are arrays where ions are $\ell\sqrt{2}$, $\ell\sqrt{5}$, $\ell\sqrt{10}$ .... $\ell\sqrt{m^2 + i^2}$ apart. In each array, except for i = 0 and i = 1 there are eight surface ions (N) at the same distance from the dipole. For i = 0 (Point A in Figure 34), there is one and for i = 1 there are four surface ions (N) at a

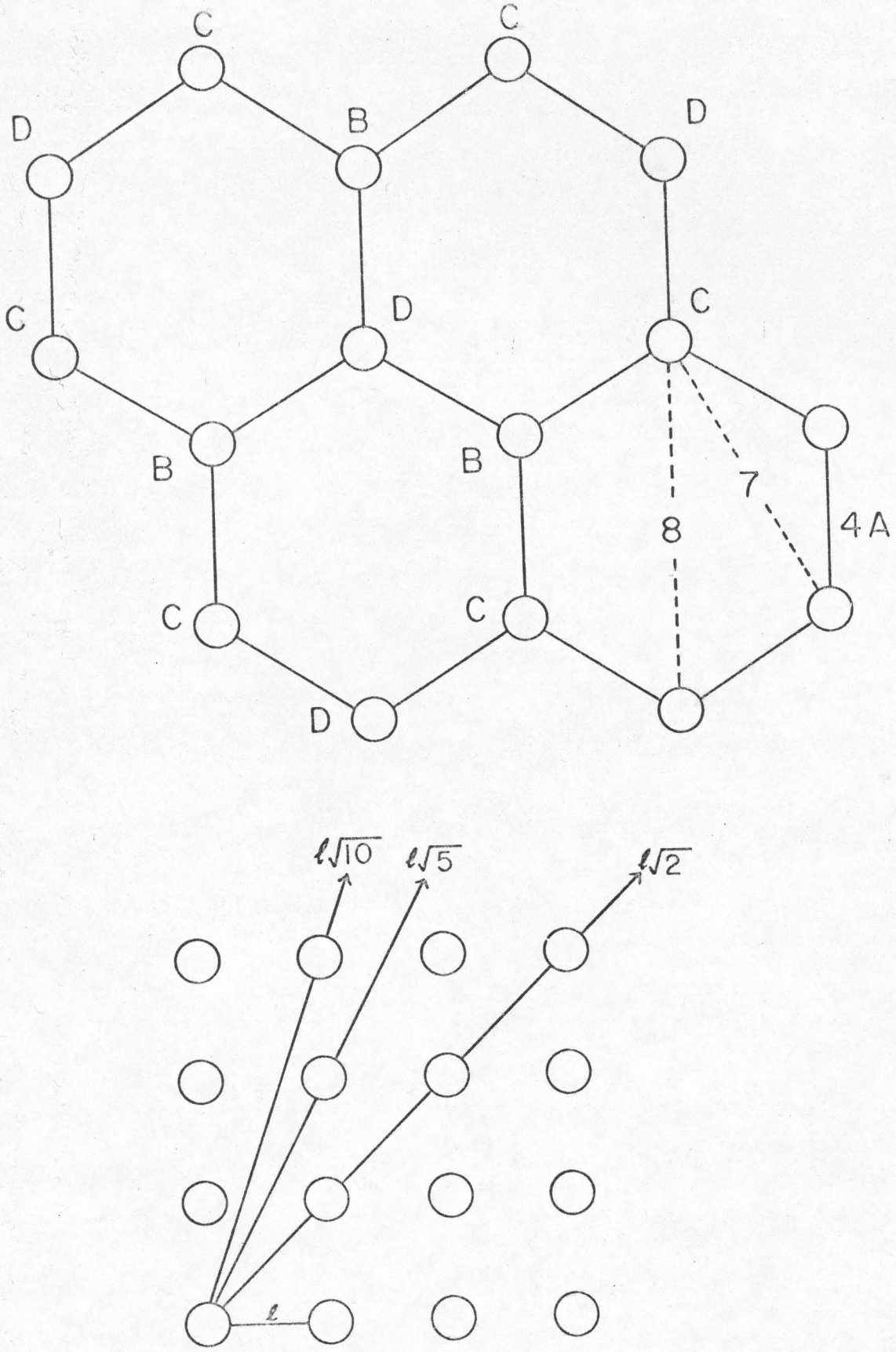

Figure 33. Geometrical drawing of montmorillonite surface.

TABLE X

Dipole Moments, Equilibrium Constants and Number of Sites of Benzodiazepine Derivative Isotherms on Montmorillonite

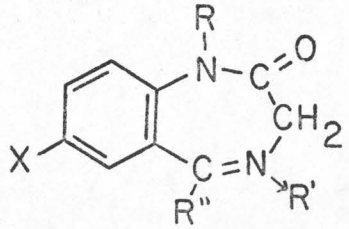

X	R	R'	R"	Dipole Moment (D)	Number of Sites*	Log K	Molecular Weight
Cl	CH_3	-	C_6H_5	3.45	5×10^{19}	4.097	285
Cl	H	O	C_6H_5	4.70	9×10^{19}	5.068	287
Br	H	-	o-C_5H_4N	3.15	7×10^{19}	4.233	316
NO_2	H	-	C_6H_5	2.02	9×10^{19}	3.187	281
NO_2	CH_3	-	o-C_6H_4F	1.26	8×10^{19}	3.067	312
NO_2	H	-	o-C_6H_4Cl	2.57	8×10^{19}	3.465	316
Cl**	H	-	C_6H_5	3.98	9×10^{19}	4.871	287

*Oxazepam, having a hydroxyl group at position 3.

**Average of these figures is 7.8×10^{19} with a standard deviation of 1.5×10^{19}.

distance b from A, a distance c from P and a distance f from Q, where P and Q are the end points of the dipole. This is depicted in Figure 34. Depending on the array, b will be a multiple of ℓ by $n \cdot \sqrt{m^2 + i^2}$ ($m = 1,2,\cdots$ and $i = 0,1,\cdots$). The force exerted by the four ions on the dipole has a resultant which is perpendicularly downwards and of the magnitude:

$$f_b' = -\frac{4}{\varepsilon} Ze^2 \left[\frac{(x - d)}{[b^2 + (x - d)^2]^{1.5}} - \frac{(x + d)}{[b^2 + (x + d)^2]^{1.5}}\right]$$

(Eq. 42)

The forces between N and P and between N and Q, of magnitude $Ze^2/\varepsilon \cdot [b^2 + (x - d)^2]$ and $Ze^2/\varepsilon \cdot [b^2 + (x + d)^2]$, respectively, have been multiplied by the cosines of the angles APN and AQN, i.e., $(x - d)/[b^2 + (x - d)^2]^{0.5}$ and $(x + d)/[b^2 + (x + d)^2]^{0.5}$ to project them on the vertical axis APQ. Attractions, again, are counted as positive (i.e., Z negative) and repulsions negative. The factor four in Eq. 42 reflects that there are four points N for each value of b.

If the dipole is moved a distance dx, then the work done is $f'_b \cdot dx$ so that the energy of one dipole as a result of its interaction with the four surface ions at a distance b from the contact ion is:

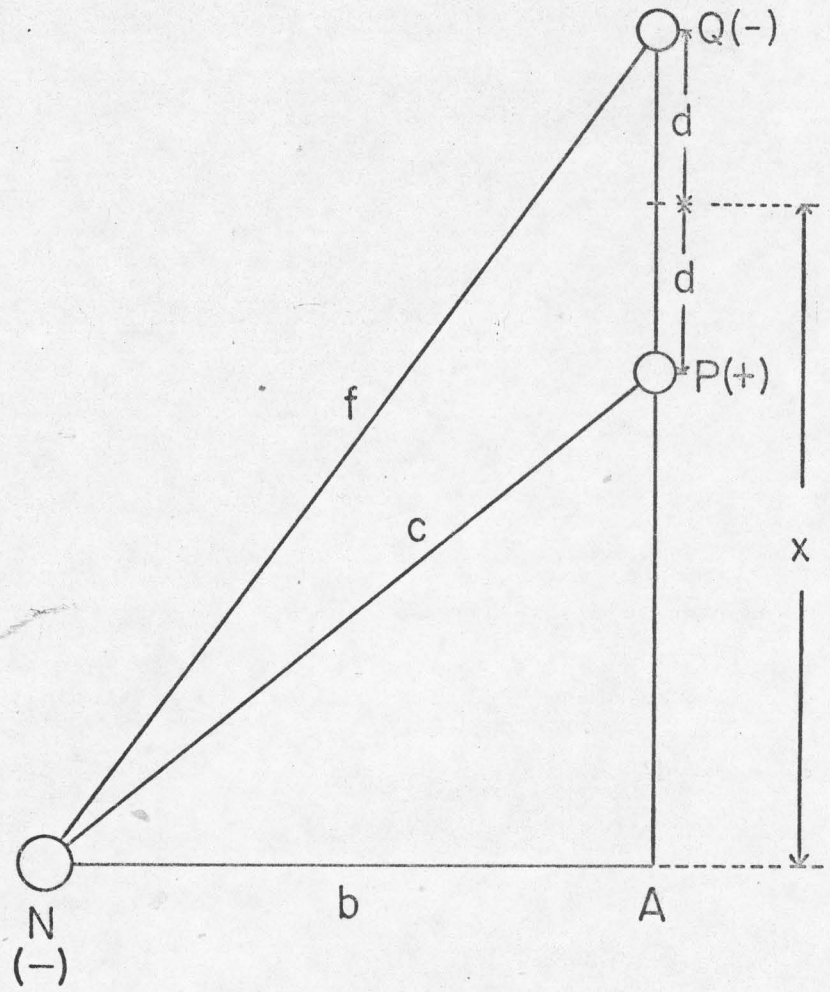

$$f^2 = b^2 + (x + d)^2$$

$$c^2 = b^2 + (x - d)^2$$

$$\cos(AQN) = (x + d)/f$$

$$\cos(APN) = (x - d)/c$$

Figure 34. Geometrical forces of surface ions on dipole.

$$E' = -\frac{4}{\varepsilon} Ze^2 \int_{\infty}^{r} \left[\frac{(x-d)}{[b^2+(x-d)^2]^{1.5}} - \frac{(x+d)}{[b^2+(x+d)^2]^{1.5}}\right] dx$$

$$= \frac{4}{\varepsilon} Ze^2 \left\{[b^2+(r-d)^2]^{-0.5} - [b^2+(r+d)^2]^{-0.5}\right\} \qquad \text{(Eq. 43)}$$

If the term $b^2 + r^2 + d^2$ is denoted a^2, then the expression in Eq. 43 can be simplified (denominators $\sqrt{a^2 \pm 2rd}$) and then, assuming 2rd to be small compared to a we may write:

$$E' \varepsilon / 4Ze^2 = \frac{1}{\sqrt{a^2 - 2rd}} - \frac{1}{\sqrt{a^2 + 2rd}} \sim$$

$$\frac{[\sqrt{a^2 + 2rd} - \sqrt{a^2 - 2rd}] \cdot [\sqrt{a^2 + 2rd} + \sqrt{a^2 - 2rd}]}{a^2 \cdot [\sqrt{a^2 + 2rd} + \sqrt{a^2 - 2rd}]} \sim$$

$$\frac{(a^2 + 2rd) - (a^2 - 2rd)}{a^2 \cdot 2\sqrt{a^2}} = \frac{4rd}{2a^3}$$

so:

$$E' = \frac{Ze^2 4}{\varepsilon} \cdot \frac{4rd}{2[b^2 + d^2 + r^2]^{1.5}} = \frac{4}{\varepsilon} \cdot \frac{rZ\mu e}{(b^2 + d^2 + r^2)^{1.5}}$$

(Eq. 44)

If $b^2 + r^2 \gg d^2$, then

$$E' = \frac{4}{\varepsilon} \cdot \frac{Z\mu er}{(b^2 + r^2)^{1.5}} \qquad \text{(Eq. 45)}$$

We have noted at an earlier point that $b = n \cdot \ell \cdot \sqrt{m^2 + i^2}$. Since ℓ can be expressed as some multiple of r, i.e., $\ell = \beta \cdot r$, we may write: $b = n \cdot \beta \cdot r \cdot \sqrt{m^2 + i^2}$ and:

$$E' = \frac{4Z\mu e}{\varepsilon r^2} \cdot \frac{1}{[1 + \beta^2 n^2 (m^2 + i^2)]^{1.5}} \qquad \text{(Eq. 46)}$$

The total energy then is:

$$E = \frac{Ze\mu}{\varepsilon r^2} \left\{ 1 + 4 \sum_{n=1}^{\infty} (1 + \beta^2 n^2)^{-1.5} + 8 \sum_{i=1}^{\infty} \sum_{m=0}^{\infty} \sum_{n=1}^{\infty} [1 + \beta^2 n^2 (m^2 + i^2)^{-1.5}] \right\} \qquad \text{(Eq. 47)}$$

The quantity in the brackets converges, and for the sake of convenience we shall denote the quantity in brackets α, i.e.:

$$\alpha = 1 + 4 \sum_{n=1}^{\infty} (1 + \beta^2 n^2)^{-1.5} + 8 \sum_{i=1}^{\infty} \sum_{m=0}^{\infty} \sum_{n=1}^{\infty} [1 + \beta^2 n^2 (m^2 + i^2)]^{-1.5} \qquad \text{(Eq. 48)}$$

so that we may write for the energy:

$$E = \frac{\alpha e\mu Z}{r^2} \cdot \frac{1}{\varepsilon} \qquad \text{(Eq. 49)}$$

It should be noted that the assumptions made to this point affect only the value of α and not the expression in Eq. 49 as a whole. As mentioned the sum represented by α converges. It converges rapidly with $\underline{i}$ and less rapidly with $\underline{n}$; as an example the value, assuming $\beta = 1$ and truncating at n = 10, m = 1 and i = 3, is 8.0.

When adsorption conditions are at equilibrium at one particular temperature T, then the equilibrium constant, K ($=k_+/k_-$) is related to energy by $E = -kT \cdot \ln K$, where $\underline{k}$ is Boltzmann's constant and where pressure-volume and entropy terms have been neglected. Inserting this in Eq. 49 gives:

$$-kT \cdot \ln K = \frac{Z\alpha\mu e}{r^2} \cdot \frac{1}{\varepsilon} \qquad \text{(Eq. 50)}$$

At any one temperature, this may be written:

$$\log K = \log K_\infty - \frac{Z\alpha\mu e}{2.3kT\ r^2} \cdot \frac{1}{\varepsilon} \qquad \text{(Eq. 51)}$$

i.e., with positive slope ($Z < 0$). K_∞ is, here, the constant at temperature T, in a medium with infinite large dielectric constant. It should be noted that the term K_∞ is not temperature independent, and that for compounds with $\mu = 0$ and solvents with large ε the assumption that G = E will fail and hence Eq. 51 is only applicable in a limited ε-range.

For this reason, it is not possible to test Eq. 51 by testing K at various temperatures. There is, however, a means by which the expression can be tested. By plotting the data in Table XI as log K versus $1/\varepsilon$, a straight line results as shown in Figure 35. Via Eq. 51, the slope and intercept give the values: $Z\alpha/r^2 = -1.44 \times 10^{15}$ and $\log K_\infty = 2.156$ at 25°C.

Eq. 51 may be re-written:

$$\log K = \log K_\infty - \frac{\alpha Ze}{2.3kT\varepsilon r^2} \cdot \mu \qquad \text{(Eq. 52)}$$

so that if several substances of varying dipole moment were tested in one solvent, the plot should be linear in μ. The fallacy in this argument is that r (and maybe also Z) may differ from compound to compound. If compounds of similar geometry were selected (as is the case here), Z (which depends on the number of oxygen molecules "occupied" by one solute molecule) would be the same, but equilibrium distances, r, would still be prone to differ from compound to compound. Whether r would increase or decrease with increasing dipole moment is not obvious *a priori*, since the increase in dipole moment from member to member in a pseudo-homologous series could be either due to an increase in charge at the dipole heads or due to an increase in distance between the heads. If the equilibrium distance for diazepam is used as a reference standard,

TABLE XI

Dielectric Constants, Equilibrium Constants ($K = k_+/k_-$) of Diazepam Isotherms and Number of Sites (N) on Montmorillonite for Various Solvents

Solvent	Dielectric Constant	log K	Number of Sites
Acetonitrile	36.2	2.86	6×10^{19}
Methyl alcohol	30.3	2.46	4×10^{19}
Ethyl alcohol	28.7	3.18	1×10^{19}
n-Propyl alcohol	19.4	3.27	6×10^{19}
Isobutyl alcohol	17.5	4.01	7×10^{19}
Isoamyl alcohol	15.8	3.95	8×10^{19}
n-Amyl alcohol	15.0	3.97	8×10^{19}
Isopropyl alcohol	13.4	4.10	5×10^{19}
Dichloroethane	9.32	4.65	9×10^{19}
Tertiary butyl alcohol	8.42	4.70	4×10^{19}
		Average:	5.8×10^{19}
		Standard Deviation:	2.4×10^{19}

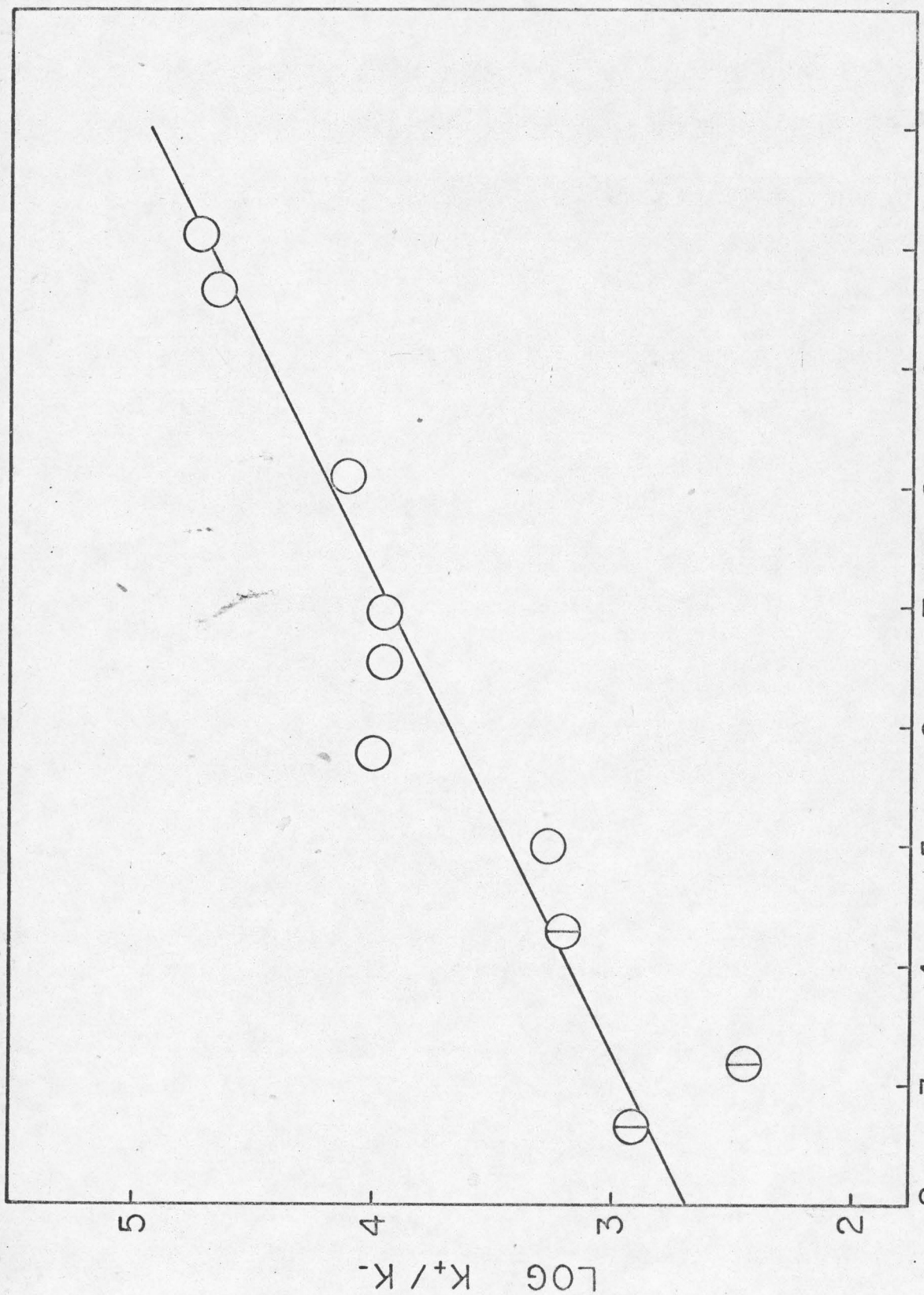

Figure 35. Log K versus reciprocal dielectric constant.

then the relation

$$r^2 = r_o^2 [1 - q(\mu - \mu_o)] \qquad \text{(Eq. 53)}$$

would qualitatively describe this change in $\underline{r}$ with dipole moment. r_o is here the equilibrium distance for diazepam. By denoting by μ' the dipole moment in Debyes, and by inserting the value $\mu_o' = 3.45$ for diazepam, Eq. 52 may be re-written:

$$\log K - \log K_\infty = \frac{Z\alpha e \cdot 10^{-18}}{2.3kT\varepsilon r_o^2} \cdot \left[\frac{\mu'}{[1 - q'(\mu' - 3.45)]}\right] \qquad \text{(Eq. 54)}$$

where q' is in D^{-1} (as opposed to q which is in cm^{-1} esu^{-1}). It is easier to treat the reciprocal of Eq. 54, i.e.,

$$\frac{1}{\log K - \log K_\infty} = -\frac{2.3kT\varepsilon r_o^2 \cdot 10^{18}}{Z\alpha e} \cdot \left[\frac{1 + 3.45q'}{\mu'} - q'\right] \qquad \text{(Eq. 55)}$$

Values of $\log K_\infty$ and $Z\alpha/r_o^2$ have been estimated at an earlier point from Figure 33. If it is assumed that $Z\alpha/r_o^2 = -1.44 \times 10^{15}$ then the coefficient to the parenthesis on the right hand side of Eq. 55 becomes 1.784, and various values for $\log K_\infty$ can be tested in the above equation. Since both the slope and the intercept give a value for q', the value of $\log K_\infty$ which gives the best

consistency between the two q'-values yields the best fit. Plots of $1/[\log K - \log K_\infty]$ versus $1/\mu'$ are shown in Figure 36. The corresponding q'-values are shown in Table XII. It is noted from the table that $\log K_\infty = 2.5$ inserted in Eq. 55 in the form ($Z\cdot\alpha/r^2 = -1.44 \times 10^{15}$):

$$\frac{1}{\log K - \log K_\infty} = 1.784 \cdot \frac{(1 + 3.45q')}{\mu'} - 1.784\ q' \qquad \text{(Eq. 56)}$$

gives a value of q' of 0.33 from the slope and 0.29 from the intercept, so that for this value of K_∞ there is good consistency. By evaluating the data by least squares fit via Eq. 55, the slope is 3.75 when $\log K_\infty = 2.5$, which, with a q'-value of 0.31 yields a value for $Z\cdot\alpha/r_o^2$ of -1.45×10^{15}, so that this (recycled) value is in good agreement with the originally assumed value. It is noted that with the assumption that one molecule of benzodiazepine occupies two oxygens (Figure 33) there would be two surface oxygens involved per adsorbed benzodiazepine molecule. This means that $Z < 4$; for $Z = 4$ and $\alpha = 8$, a value of $r = 15$ Å can be calculated, and if $Z = 2$ and $\alpha = 8$ then a value of $r = 10$ Å results. Since $\ell = 7\text{-}8$ Å, this is not compatible with the previous estimation of $\beta = 1$. The numerical calculations above, of course, are based on guesses of the magnitudes of β and Z. To arrive at a reasonable and self-consistent set of values the following may be

Figure 36. $1/(\log K - \log K_\infty)$ versus Reciprocal Dipole Moment.

Key:

Line A: $\log K_\infty = 3.0$, slope = 4.55, intercept = -0.535

Line B: $\log K_\infty = 2.5$, slope = 3.75, intercept = -0.52

Line C: $\log K_\infty = 2.0$, slope = 1.95, intercept = -0.1

Line D: $\log K_\infty = 1.5$, slope = 1.10, intercept = 0.045

Line E: $\log K_\infty = 1.0$, slope = 0.90, intercept = 0.045

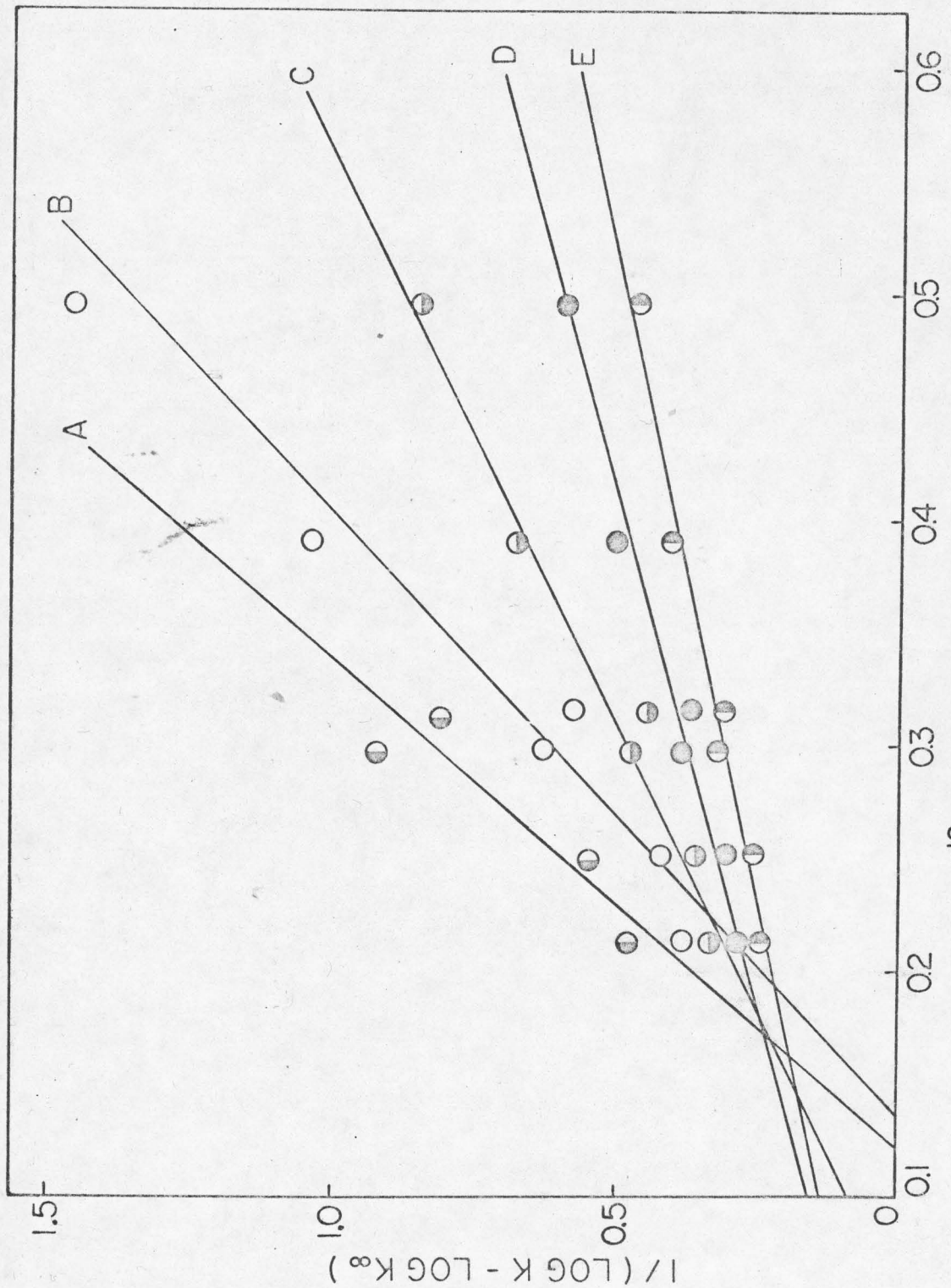
A
B
C
D
E
1.5
1.0
0.5
0
0.1
0.2
0.3
0.4
0.5
0.6
1/(LOG K - LOG K∞)
10⁻¹⁸ x (RECIPROCAL DIPOLE MOMENT)

TABLE XII

Estimation of Best q-Value in Equation 56

log K_∞	q-Value from Slope	q-Value from Intercept	Average q	$Z\alpha/r^2$
1.0	- 0.14	- 0.025	- 0.082	0.50×10^{15}
1.5	- 0.11	- 0.025	- 0.068	0.54×10^{15}
2.0	+ 0.027	+ 0.056	+ 0.042	0.81×10^{15}
2.5	+ 0.33	+ 0.29	+ 0.31	1.45×10^{15}
3.0	+ 0.45	+ 0.24	+ 0.38	1.16×10^{15}

considered. It is noted that α is a function of β and to gauge the effect of one on the other, calculations have been made and tabulated in the following fashion: It follows from Eq. 48 and Eq. 56 that $r/\sqrt{(-Z)} = (\alpha/1.45 \times 10^{15})^{0.5}$ and $\ell/\sqrt{(-Z)} = \beta\,(\alpha/1.45 \times 10^{15})^{0.5}$, where $(-Z) > 0$. These values have been calculated for a series of β-values, truncating at $n = 10$ and $i = 3$ (leaving the last terms less than 0.1% of the leading term). The values are listed in Table XIII. It will be noticed that $\ell/\sqrt{(-Z)}$ is fairly independent of β and from the average value (7.6×10^{-8}), it appears that $\sqrt{(-Z)}$ lies between $7 \times 10^{-8}/7.6 \times 10^{-8}$ and $8 \times 10^{-8}/7.6 \times 10^{-8}$, i.e., $(-Z)$ is about unity. As mentioned earlier, the actual value of $(-Z)$ is less than 4, but how much less cannot be stated *a priori*. The fact that $\ell/\sqrt{(-Z)}$ appears to be non-variant with β is a result of α being a function of β and lends some measure of credence to the calculated value of $(-Z)$. The actual value of r cannot be pinpointed but, as seen in Table XIII, it appears to be of the right order of magnitude.

Although not pointed out earlier, it should be mentioned that in this study desorption was found to be too rapid to measure by conventional means. Column chromatography was also found unsuitable and this and the fact that r cannot be pinpointed makes it impossible to check whether the adsorption described here adheres to the

TABLE XIII

Value of $\frac{r}{\sqrt{(-Z)}}$ and $\frac{\ell}{\sqrt{(-Z)}}$ for Various Values of β*

β	α	$\frac{r}{\sqrt{(-Z)}} = [\frac{\alpha}{1.45 \times 10^{15}}]^{0.5}$	$\frac{\ell}{\sqrt{(-Z)}} = \beta[\frac{\alpha}{1.45 \times 10^{15}}]^{0.5}$
0.7	11.9	9.1×10^{-8}	6.3×10^{-8}
0.8	10.3	8.5×10^{-8}	6.8×10^{-8}
1.0	8.0	7.4×10^{-8}	7.4×10^{-8}
1.4	5.8	6.3×10^{-8}	8.9×10^{-8}
			Average: 7.6×10^{-8} cm (or 7.6 Å)

*Note that (-Z) is positive.

theories of Haque, et al. (83,84).

Nitrogen adsorption data are shown in Figure 37 and Figure 38. As mentioned, porosity is negligible since the adsorption and desorption curves are found to be experimentally indistinguishable (Figure 38). From the B.E.T. data it is noted that the area is 75 m^2/g or 75×10^{20} $Å^2/g$ of montmorillonite. The cross section of a nitrogen molecule is conventionally assumed to be 16.2 $Å^2$ (75) and, using this figure, there should be 4.6×10^{20} sites. Assuming one molecule of benzodiazepine to occupy the area of one hexagon there would be two sites for each sorbed benzodiazepine molecule, so that the number of sites available in this fashion is 2.3×10^{20}. This is within an order of magnitude of the number of sites found in adsorption from liquids (Tables X and XI) and the data therefore within the limitations of the B.E.T. method (85), support previous arguments. That the figure should be less for the benzodiazepine molecule might be expected, since with the assumed model, the solute molecules would adsorb in the described fashion on the platelet surfaces, not on the edges. It should be noted, that since nitrogen adsorbs on the surface only, not by intercalation (86). This is in support of the previous arguments regarding adsorption of solute from liquids being confined to the surface.

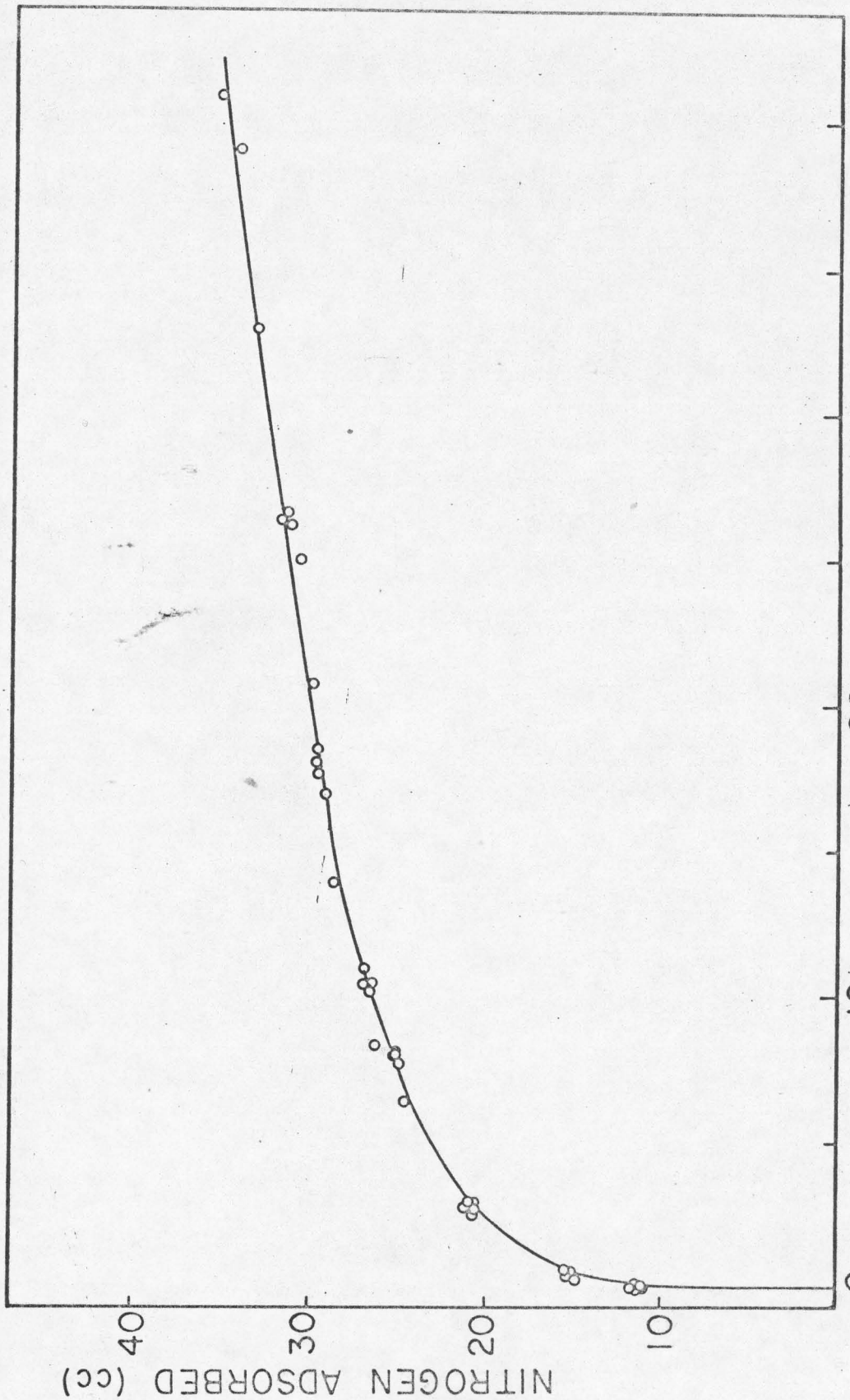

Figure 37. Nitrogen adsorbed on montmorillonite as a function of pressure.

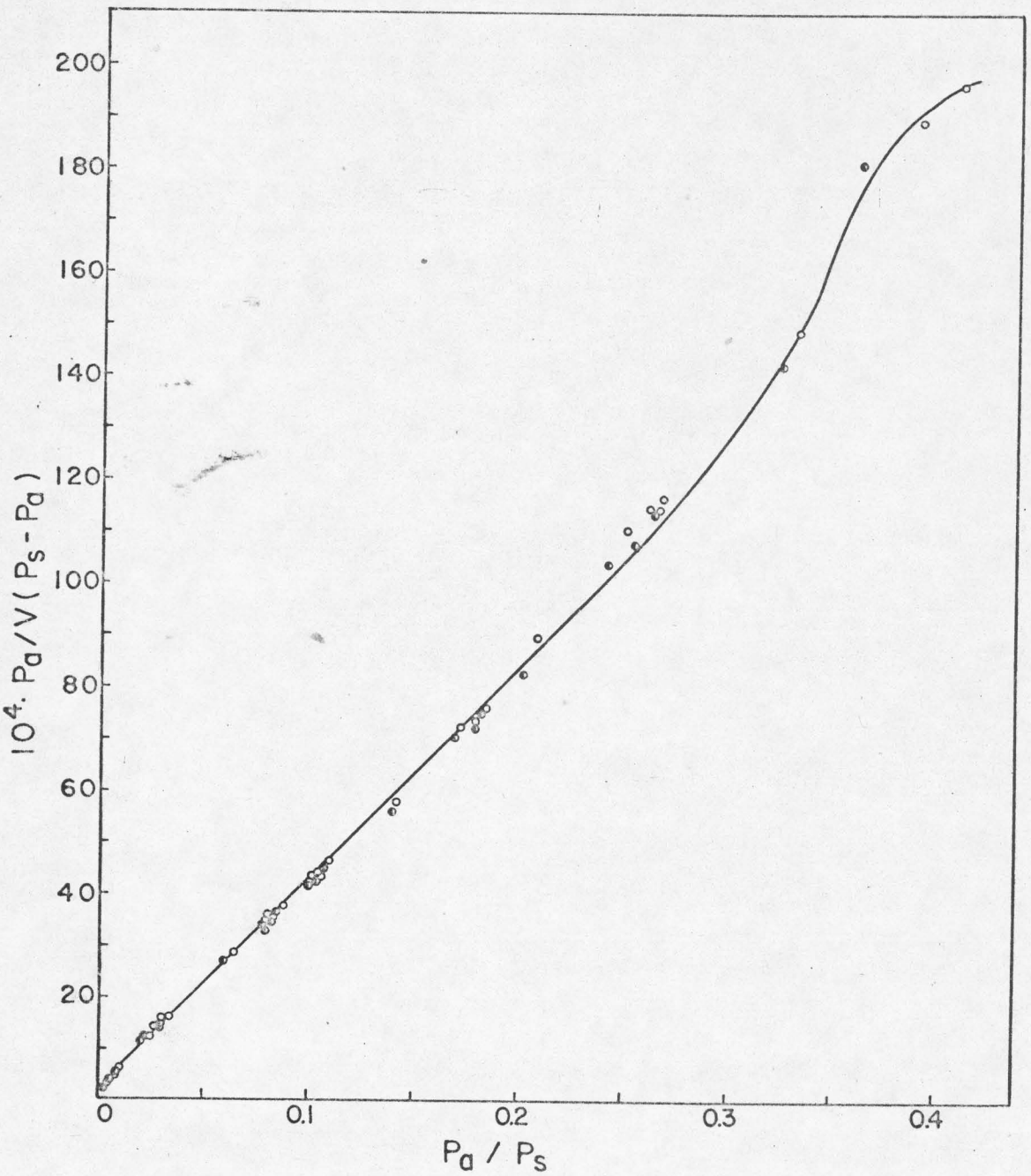

Figure 38. B.E.T. nitrogen isotherm of montmorillonite (1.4336 gm sample). Open circles are adsorption and closed circles desorption points.

Consistent values have, therefore, been arrived at by two different procedures with respect to the type of isotherm and the equilibrium value at infinite dielectric constant (or the value of $Z\alpha/r_o^2$). A consistent relation has been found between dipole moment and equilibrium distance. The number of sites have been found to be comparable by two different approaches, and these values do not conflict with the numbers obtained from B.E.T. measurements. This latter point, furthermore, substantiates the concept that the solutes are adsorbed on the surface only. All these facts are based on a model whereby the solute molecule, which is not ionized, but which possesses a dipole moment, is bound to the surface oxygen ions by ion-dipole interaction, and it therefore seems reasonable to postulate that the data support such a model.

The above facts are the general conclusions of this work. It should be pointed out that phenomena regarding solvation of montmorillonite have also been deduced and these are described shortly below: It has been mentioned in the aforegoing that isotherms, in general, have been of the Langmuir type; most of the solvents tested have had dielectric constants of less than 20, and the data are generated in conventional fashion as pointed out in the experimental section and the section on results. It has also been pointed out that solvents of high dielectric constant (36.2, 30.3, 28.7) penetrate the montmorillonite

lattice, and form solvent layers between the silicate layers. In the solvents of higher dielectric constant, reciprocal linearity is lost. Examples of this are lines A in Figures 11, 12, and 13. The distance (j Å) between silicate layers has been given by Mering (26) to be 9.3 Å; the increase caused by one solvent layer (Δ j) has been reported by MacEwan and Talib-Uddin (62) to be 3.4 Å for the three solvents tested. The data can be treated with the assumption that n layers of solvent are formed between each silicate layer, and that these solvent layers have the same density, ρ g/cc, as the bulk density. If each montmorillonite particle has a cross-sectional area A and height j, then m such particles would have a volume of m A j = w/d before addition of solvent. w is here the weight of the m particles and d is the absolute density of montmorillonite. After addition of solvent, n layers each of thickness Δj will be formed between each silicate layer, so that the swell volume will be

$$\frac{w}{d} \cdot \left[\frac{9.3 + n\Delta j}{9.3}\right]$$

The number of layers is assumed to be large so that edge effects are negligible. This in turn means that

$$\frac{w}{d} \cdot \left[\frac{9.3 + n\Delta j}{9.3} - 1\right] = \frac{wn\Delta j}{(9.3d)} \text{ cc}$$

of solvent no longer are in the external phase.

The amount of solute adsorbed is obtained by adding 100 cc of a solution of molarity C_o (i.e., 0.1 C_o moles of solute) to w g. or w/d cc of montmorillonite, and then determining the molarity, M, of the solute after adsorption equilibrium has been established. The total amount of moles present in the external phase is, however, not $\frac{M}{1000}$ x 100, since 100 cc external phase are no longer present but rather $\frac{M}{1000}$ [100 - $\frac{wn\,\Delta i}{9.3d}$] moles.

By inserting various values of n, a situation is reached where the plot is linear. To evaluate the point of best linearity, least squares fits have been calculated and the residual sums of squares:

$$s_{yx}^2 = \Sigma (y_i - \tilde{y}_i)^2/(\nu - 2)$$

have been plotted in Figure 39. ν is here the number of determinations, y_i is the observed quantity ($1/C_m$, where C_m is the (adjusted) concentration on the montmorillonite) and $\tilde{y}_i$ is the quantity calculated by inserting x_i ($1/C_s$, where C_s is concentration in solution) into the least squares equation. It would appear that 12-13 layers are involved in the acetonitrile intercalation, 6 layers in the case of ethanol and 6 layers in the case of methanol.

The computations above assume that the density of the "liquid" between the silicate layers is the same as that of the bulk liquid. This, of course, is not necessarily likely; in the cited cases the error

introduced by this assumption is, however, not serious. If there are attached to each lattice point one solvent molecule per layer, then it can be shown geometrically that each solvent molecule occupies* 23 $\mathring{A}^2$ and hence a volume of 23 x 3.4 = 78 $\mathring{A}^3$, i.e., in the case of acetonitrile one mole (41 g) occupy $78 \times 10^{-24} \times 6 \times 10^{23}$ = 46.8 cc. This is equivalent to a density of 0.875 g/cc as opposed to 0.78 g/cc for bulk acetonitrile. The number of layers is, therefore, $\frac{0.78}{0.875} \times 12.5 = 11$ rather than 12-13. For methanol and ethanol the spacings are about the same as for acetonitrile (51) (and the available surface at each lattice point also remains the same) so the densities of the solvents in the crystal are $\frac{32}{46.8} = 0.68$ and $\frac{46}{46.8} = 0.97$ g/cc, respectively, as opposed to bulk densities of 0.80 and 0.79 g/cc. The adjusted number of layers is, therefore, 7 for methanol and 5 for ethanol. It is interesting to note that in the liquid-solid equilibria the rule of the number of layers being the larger the larger the dielectric constant is even more predominant than in vapor-solid equilibria.

It should be noted (cross-hatched circles in Figure 35) that the data fall in line with isotherms from solvents of smaller dielectric constants, and that the number of sites calculated (Table XIV) is in line with the remaining

---

*Based on lattice parameters of Figure 33 (26).

Figure 39. Residual sums of squares for least squares fits of data allowing for various numbers of layers of intercalation.

Legend:

A: acetonitrile (right ordinate)

B: methanol (left scale)

C: ethanol (left scale)

$10^3 \times S^2_{y,x}$ (RESIDUAL SUM OF SQUARES)
7
6
5
4
3
2
1
0
A
B
C
0
2
4
6
8
10
12
14
16
18
LAYERS OF SOLVENT
$10^2 \times S^2_{y,x}$ (RESIDUAL SUM OF SQUARES)

TABLE XIV

Comparison of Parameters Obtained in Solvation of Montmorillonite with Conventionally Obtained Parameter Values

Solvent	Number of Sites	Number of Layers*	Log k_+/k_- Figure 35 (Theoretical)	Log k_+/k_- This Work
Acetonitrile	6×10^{19}	11	2.38	2.86
Methanol	4×10^{19}	7	2.96	2.40
Ethanol	1×10^{19}	5	3.23	3.18
Reference 6 (Average)	7×10^{19}			

*Density adjustment is accounted for in this column.

data from other solvents and derivatives. Comparisons are listed in Table XIV.

The value of the described approach is not only that of establishing the number of layers of solvent in the montmorillonite but, from an experimental point of view, it is important since it points out the necessity of volume adjustment in establishing adsorption isotherms in solutions where solvent intercalation into the adsorbing species is a possibility.

It may be worthwhile, as a last point, to examine the possible contribution of Van der Waals forces. Such forces have been shown to be the sole contributors to adsorption of sulfonic acids onto cellulose (87). The main criterion is that K is proportional to the molecular weight of the substance being adsorbed. It can be seen from Table X that this is not the case here. Van der Waals forces, of course, will contribute some, but negligibly in comparison to the mentioned electrical interactions.

BIBLIOGRAPHY

1. Taylor, G. A. and Thon, N., J. Amer. Chem. Soc., 74, 4169 (1952).

2. Cornet, I., J. Chem. Phys., 11, 217 (1943).

3. Harkins, W. D. and Jura, G., J. Amer. Chem. Soc., 66, 1362 (1944).

4. Haines, B. A. and Martin, A. N., J. Pharm. Sci., 50, 756 (1961).

5. Wai, K. N., DeKay, H. G. and Banker, G. S., J. Pharm. Sci., 55, 1244 (1966).

6. Evcim, Nur and Barr, Martin, J. Amer. Pharm. Assoc., 44, 570 (1955).

7. Slabaugh, W. H. and Siegel, R. H., J. Phys. Chem., 60, 1105 (1956).

8. Zografi, G. and Mattocks, A., J. Pharm. Sci., 52, 1103 (1963).

9. Smith, R. N., Lesnini, D. and Mooi, J., J. Phys. Chem., 60, 1063 (1956).

10. Brunauer, S., Emmett, P. H. and Teller, E., J. Amer. Chem. Soc., 60, 309 (1938).

11. Sorby, D. L. and Liu, G., J. Pharm. Sci., 55, 504 (1966).

12. Sorby, D. L., Plein, E. M. and Benmaman, J. D., J. Pharm. Sci., 55, 785 (1966).

13. Sorby, D. L. and Plein, E. M., J. Pharm. Sci., 50, 355 (1961).

14. Kennedy, P., Petronio, M. and Geisser, H., J. Phys. Chem., 74, 102 (1970).

15. Linstron, F. T., Haque, R. and Coshow, W. R., J. Phys. Chem., 74, 495 (1970).

16. Breuer, M. M., J. Colloid Interface Sci., 24, 477 (1967).

17. Thakkar, A. L., Wilham, W. L. and Zografi, G. J. Pharm. Sci., 59, 1466 (1970).

18. Murray, D. J., Healt, T. W. and Fuerstenau, D. W., Adsorption from Aqueous Solution, American Chemical Society, Washington, D.C., 1968, p. 74.

19. Zentner, M., U.S. Pat. 3,337,402 (1967), (C.A. 94016t, 1967).

20. Zentner, M., U.S. Pat. 3,337,403 (1967), (C.A. 94017u, 1967).

21. Zentner, M., U.S. Pat. 3,248,290 (1961), (C.A. p6875c, 1961).

22. Zentner, M., U.S. Pat. 3,140,978 (1961), (C.A. p6874d, 1961).

23. Rubin, S. H., Private communication.

24. Margenau, H., Rev. Mod. Phys., 11, 1 (1939).

25. Ross, S. and Oliver, J. P., Solid Surfaces and the Gas-Solid Interface, American Chemical Society, Washington, D.C., 1961, p. 309.

26. Mering, J., Colloques Intern. Centre Nat. Rech. Sci., 10, 189 (1948).

27. Tarnoff, B. J., J. Soc. Cosmetic Chemists, 2, 250 (1951).

28. Veegum Technological Bulletin, No. 44, R. T. Vanderbilt Co., New York, N.Y.

29. Pauling, L., Proc. Natl. Acad. Sci., 16, 123 (1930).

30. Hoffmann, U., Endrell, K. and Wilm, D., Zeits. f. Krist., 86, 340 (1933).

31. Hoffmann, U., Endrell, K. and Wilm, D., Zeits. f. Krist., 47, 539 (1934).

32. Marshall, C. E., Zeits. f. Krist., 91, 433 (1935).

33. Wai, K. N. and Banker, G. S., J. Pharm. Sci., 55, 1215 (1966).

34. Schofield, R. K., J. Soil Sci., 1, 1 (1949).

35. Caillere, S., Henin, S. and Mering, J., Compt. Rendue, 224, 842 (1947).

36. Caillere, S. and Henin, S., Compt. Rendue, 224, 53 (1947).

37. Wilson, C. O. and Soine, T. O., Roger's Inorganic Pharmaceutical Chemistry, Lea and Febiger, Philadelphia, Pa., 1957, p. 473.

38. MacEwan, M. B. and Pratt, M. I., Trans. Faraday Soc., 53, 535 (1957).

39. Bush, D. C., Jenkins, R. E. and McCaleb, S. B., Clays and Clay Minerals, Vol. 26, Pergamon Press, New York, N.Y., 1966, p. 407.

40. Wurster, D. E. and Polli, G. P., J. Pharm. Sci., 53, 311 (1964).

41. Norrish, K., Disc. Faraday Soc., 18, 120 (1954).

42. Slabaugh, W. H. and Hiltner, P. A., J. Phys. Chem., 72, 4295 (1968).

43. Van Olphen, H., Disc. Faraday Soc., 11, 82 (1951).

44. Packter, A., Kolloid Z., 150, 60 (1957).

45. Van Olphen, H., Natl. Acad. Sci.-Natl. Research Council Publication, No. 256, 204 (1956).

46. Levy, G., J. Pharm. Sci., 51, 947 (1962).

47. Wood, J., Catacalus, G. and Lieberman, S., J. Pharm. Sci., 52, 354 (1963).

48. Broughton, G. and Squires, L., J. Phys. Chem., 40, 1041 (1936).

49. Houwinak, R., Elasticity, Plasticity and Structure of Matter, 2nd ed., Dover Publications, N.Y., 1958, p. 14.

50. McVean, D. E. and Mattocks, A. M., J. Pharm. Sci., 50, 785 (1961).

51. MacEwan, D. M. C., Colloques Intern. Centre Rech. Sci., 10, 21 (1948).

52. Bradley, W. F., Grim, R. E. and Clark, G. L., J. Krist., 97, 216 (1937).

53. Jordan, J. W., J. Phys. Chem., 53, 294 (1949).

54. Hendricks, S. B. and Jefferson, M. E., Am. Mineral, 23, 863 (1938).

55. Andrews, D. E., Schmidt, P. W. and Van Olphen, H., Clays and Clay Minerals, Vol. 27, Pergamon Press, New York, N.Y., 1967, p. 321.

56. Granquist, W. T. and Kennedy, J. V., Clays and Clay Minerals, Vol. 27, Pergamon Press, New York, N.Y., 1967, p. 103.

57. Norrish, K. and Rausell-Colom, J. A., Clays and Clay Minerals, Vol. 10, Pergamon Press, New York, N.Y., 1963, p. 123.

58. Hoffmann, U. and Hausdorf, A., Z. Krist., 104, 265 (1942).

59. Barrer, R. M. and Kelsey, K. E., Trans. Faraday Soc., 57, 625 (1961).

60. Bradley, W. F., J. Amer. Chem. Soc., 67, 975 (1945).

61. MacEwan, D. M. C., Nature, 162, 195 (1948).

62. MacEwan, D. M. C. and Talib-Uddin, O., Colloques Intern. Centre Nat. Rech. Sci., 10, 24 (1948).

63. Adamson, A. and Ling, I., Adv. Chem., 33, 51 (1961).

64. Weaver, C. E., Bull. Geol. Soc. Amer., 64, 921 (1953).

65. Vogel, A. I., A Textbook of Practical Organic Chemistry, 3rd ed., John Wiley and Sons, Inc., New York, N.Y., 1966.

66. Carstensen, J. T. and Su, K. S. E., J. Pharm. Sci., 59, 666 (1970).

67. Carstensen, J. T. and Su, K. S. E., J. Pharm. Sci., 59, 671 (1970).

68. Connors, K. A., A Textbook of Pharmaceutical Analysis, John Wiley and Sons, Inc., New York, N.Y., 1967, p. 698.

69. Sherrick, P. H., Karr, R., Edward, F. E. and Dawe, G. A., Manual of Chemical Oscillometry, E. H. Sargent, Chicago, Illinois, 1954.

70. Smyth, C. P., Physical Methods of Organic Chemistry, Vol. 2, Interscience, New York, N.Y., 1946, p. 998-1009.

71. Bender, P., University of Wisconsin, Madison, Wisconsin.

72. Hill, N. E., Vaughan, W. E., Price, A. H., and Davies, M., Dielectric Properties and Molecular Behaviour, Van Nostrand, New York, N.Y., 1969, p. 175-180.

73. Hertl, W. and Hair, M. L., J. Phys. Chem., 72, 4676 (1968).

74. Brunaver, S., Emmett, P. H. and Teller, E., J. Amer. Chem. Soc., 62, 1732 (1940).

75. Eggers, D. F., Gregory, N. W., Halsey, G. D. and Rabinovitch, B. S., Physical Chemistry, John Wiley and Sons, Inc., New York, N.Y., 1964, p. 729.

76. Guggenheim, E. A., Trans. Faraday Soc., 47, 573 (1951).

77. Minkin, V. I., Osipor, O. A., and Zhdanov, Y. A., Dipole Moment in Organic Chemistry: Physical Methods in Organic Chemistry, Plenum Publishing Corporation, New York, N.Y., 1970.

78. Hedestrand, Z., Physik. Chem., B2, 428 (1929).

79. Carstensen, J. T., Osadoa, M. and Rubin, S. H., J. Pharm. Sci., 58, 549 (1969).

80. Evans, R. C., An Introduction to Crystal Chemistry, Cambridge University Press, 1966.

81. Amis, E. S., Solvent Effects on Reaction Rates and Mechanisms, Academic Press, New York, N.Y., 1966, p. 41.

82. Schofield, R. K., J. Soil Sci., 1, 1 (1949).

83. Lindstron, F. T., Haque, R. and Coshow, W. R., J. Phys. Chem., 74, 495 (1970).

84. Haque, R. and Sexton, R., J. Colloid Interface Sci., 25, 818 (1968).

85. Garner, W. E., Chemistry of the Solid State, Butterworths, London, 1955.

86. Mooney, R. W., Keenan, A. G. and Wood, L. A., J. Amer. Chem. Soc., 74, 1367 (1952).

87. Giles, C., Jain, S. and Hassan, A., Chem. Ind., 629 (1955).

PUBLICATIONS

(1) Carstensen, J. T. and Su, Kenneth S. E., "Sedimentation Kinetics of Flocculated Suspensions. I: Initial Sedimentation Region," J. Pharm. Sci., 59, 666 (1970). [reprint included here]

(2) Carstensen, J. T. and Su, Kenneth S. E., "Sedimentation Kinetics of Flocculated Suspensions. II: Sedimentation below the Critical Height," J. Pharm. Sci., 59, 671 (1970). [reprint included here]

(3) Carstensen, J. T. and Su, Kenneth S. E., "Nature of Bonding in Montmorillonite Adsorbates. I: Surface Adsorption," J. Pharm. Sci., 60, 733 (1971). [Xerox copy included here]

(4) Su, Kenneth S. E. and Carstensen, J. T., "Nature of Bonding in Montmorillonite Adsorbates. II: The Bonding as an Ion-Dipole Interaction," Submitted to J. Pharm. Sci. for publication.

(5) Carstensen, J. T. and Su, Kenneth S. E., "Solvation of Montmorillonite," Submitted to J. Pharm. Sci. for publication.

(6) Carstensen, J. T., Su, Kenneth S. E., Maddrell, Paul, Johnson, James B. and Newmark, Harold N., "Thermodynamic and Kinetic Aspects of Parenteral Benzodiazepines," Accepted for publication in Bull. Parenteral Drug Assoc., 1971.

(7) Carstensen, J. T. and Su, Kenneth S. E., "Some Statistical Aspects of Arrhenius Plotting," Accepted for publication in Bull. Parenteral Drug Assoc., 1971.

VITAE

KENNETH SHYAN-ELL SU was born on November 26, 1941 in Taiwan, China. He attended the Taipei Medical College, Department of Pharmacy, from 1961 to 1965 at which time he received his Bachelor of Science degree in Pharmacy. He attended graduate school at Columbia University from 1966 to 1967 and attended the University of Wisconsin from 1967 where he was granted his Master of Science degree in Pharmaceutics in 1969.